Design of Organoboron Solid Electrolytes/Solid Electrolyte Interface for Enhanced Performance of Lithium Ion Secondary Batteries

Prerna Joshi

Japan Advanced Institute of Science and Technology

Doctoral Dissertation

Design of Organoboron Solid Electrolytes/Solid Electrolyte Interface for Enhanced Performance of Lithium Ion Secondary Batteries

Prerna Joshi

Supervisor :Noriyoshi Matsumi

School of Materials Science

Japan Advanced Institute of Science and Technology

June 2016

Design of Organoboron Solid Electrolytes/Solid Electrolyte Interface for Enhanced Performance of Lithium Ion Secondary Batteries

Abstract

Lithium ion batteries (LiBs) in the current day are the most competitive energy storage media amongst all conventional sources of energy storage due to their high energy density and high power. The constant use of conventional electrolytes such as organic carbonate solvents mixed with lithium salts, have resulted into high performance of these batteries. In spite of having impressive ionic conductivity and practical usage at ambient temperature, these organic liquid electrolytes are known to be unsafe because of their high flammability, spilling and reactivity with lithium. Hence, Solid Polymer Electrolytes (SPEs) come up as excellent alternative to these electrolytes. Though, they suffer from demerits such as poor ionic conductivity, low mechanical strength, their low flammability and ease of processability prove to be advantageous in compared to organic liquid electrolytes. These polymer electrolytes undergo polymer segmental motion which is the mode of ion conduction in these systems.

Conduction mechanisms in SPEs of Li ion batteries have always been a concern due to their theoretical limitation in conductivity value. Electrolyte, being one of the most important component of a Li ion battery must have properties such as good electronic insulator and ionic conductor, wide electrochemical window, high mechanical and thermal stability and the most important intrinsic parameters i.e. *ionic conductivity (σ_i)* and the *cation transference number (t_{Li}^+)* which ultimately is the outcome of the ion conduction mechanism responsible in the electrolytic system. Lithium ion super conductors, anion doped π-conjugated systems and lithium alkoxide based MOFs are some of the electrolytic systems reported in literature that showed an altered ion conductive mechanism other than polymer segmental motion.

Unceasing research on electrolytes to improve the conductive properties stimulated our interest towards designing novel electrolytes and study their ion conduction mechanisms. Such systems will not only result in improved ionic

conductivity and cation transference number but will also enhance the capacity of the battery by forming a stable and tunable SEI (Solid Electrolyte Interface: Interface allowing Li^+ ions to be transported through the film during the successive intercalation and deintercalation processes) . The formation of thin but stable SEI prevents further electrolyte reduction at the electrode and protects it from solvent co-intercalation. The study of chemical and morphological characteristics of the surface films can provide an idea about the ionic conduction, that is, primary requirements of the reduction products in a functional SEI layer are Li^+ ion conductivity and electronic insulation. This interface which allows Li^+ ions to be transported through the film during the subsequent intercalation and deintercalation processes, can be achieved either by the use of *a)* electrolytes with highly ordered structures or *b)* by highly conducting electron rich conjugated polymers and self-polymerizing them over anode for better SEI characteristics.

Hence, in this research theme, we have synthesized various low molecular weight solid organoboron electrolytes as highly ordered structures for interfacial studies at carbon electrode and studied the utilization of organoboron containing conducting polymers to reduce the interfacial resistance at SEI over Carbon electrode by using charge discharge analysis and Dynamic Electrochemical Impedance Spectroscopy (DEIS).

Preface

The present dissertation is submitted for the Degree of Doctor of Philosophy at Japan Advanced Institute of Science and Technology, Japan. The dissertation is consolidation of results of the works on the topic "Design of Organoboron Solid Electrolytes/Solid Electrolyte Interface for Enhanced Performance of Lithium Ion Secondary Batteries" under the direction of *Prof. Noriyoshi Matsumi* at the School of Materials Sciences, Japan Advanced Institute of Science and Technology during July 2013-June 2016.

Lithium-ion batteries is currently the leader among the existing energy storage technologies due to its various attractive features. However, as a means of improvement of its electrolyte system and study the electrode-electrolyte interface in order to enhance the performance of the batteries various kinds of research approaches are being investigated. The author's main focus is to deal with the design of low molecular weight electrolytes that possess a different ion conducting mechanism than the already existing polymer electrolytes and can be applied as efficient electrolytes for lithium-ion batteries.

The work presented in this thesis covers the synthesis and characterization of novel low molecular weight organoboron electrolytes along with their performance parameters as observed in lithium-ion batteries. Also their real time application in Li ion batteries have been studied. To the best of my knowledge, the work is original and no part of the thesis has been plagiarized.

School of Materials Science   Prerna Joshi

Japan Advanced Institute of Science and Technology

June 2016

Acknowledgement

Firstly, the author expresses her sincere gratitude to the supervisor *Prof. Noriyoshi Matsumi,* School of Materials Science, Japan Advanced Institute of Science and Technology, for his kind guidance, valuable suggestions and heartfelt encouragements throughout this work. I am thankful to him for his patience, motivation, and immense knowledge. His guidance helped me in all the time of research and writing of this thesis.

I would also like to thank the members of my Review committee *Prof. Masayuki Yamaguchi* (JAIST)*, Assoc. Prof. Yuki Nagao* (JAIST)*, Prof. Tomoki Ogoshi* (Kanazawa University, Kanazawa)*, Assoc. Prof. Kazuaki Matsumura* (JAIST), who have spent their valuable time to read my manuscript, for their insightful comments and remarks to enhance the quality of this dissertation from various perspectives.

The author is thankful to *Dr. Rajalakshmi Natarajan,* Senior Scientist, CFCT, IITM-Research Park, Chennai, India and *Prof. Sundara Ramaprabhu*, AENL, Department of Physics, IITM, Chennai, India for giving her an opportunity to join their team as an intern and carry out experiments at, India during for her 3 months minor research. Furthermore, the author wishes to express her special thanks to *Dr. Rajalakshmi* and *Prof. Ramaprabhu* and their lab members for their warm support and valuable suggestions during the author's stay in India.

The author also takes an opportunity to thank *Assistant Prof. Raman Vedarajan* for his guidance and encouragement at a professional and personal level. I am also grateful to other laboratory members, for their valuable inputs, cooperation and stimulating discussions, for the all the time we were working together before deadlines, and for all the fun we have had throughout my time at JAIST.

The author expresses her heartfelt gratitude to her parents and dear ones, for their relentless encouragement and support at difficult times. Finally, the author expresses her humble gratitude to the Almighty for all the good things.

School of Materials Science   Prerna Joshi
Japan Advanced Institute of Science and Technology
June 2016

List of Figures

List of Tables

Table of Contents

Chapter 1

Introduction to Lithium Ion Batteries

1.1 General Introduction

A battery is a device made up of unit called electrochemical cell in which chemical energy gets converted into electric energy through a specific electrochemical reaction befitting the type of cell. The chemical energy stored in the materials used as the components of the battery is converted into electrical energy as output through specific reduction-oxidation (redox) reaction. Depending upon the type of reduction-oxidation reaction, battery can be primary (irreversible redox/non-rechargeable) or can be secondary (reversible redox/rechargeable). This kind of reduction oxidation reaction involves the transfer of electrons between two materials via an electric circuit. Batteries are used to store energy and are capable of having higher energy conversion efficiencies.

As a general classification of batteries, batteries can be grouped broadly into two categories: Primary and secondary batteries. **Primary batteries** are batteries that can produce current when assembled. These batteries produce higher energy densities as compared to the rechargeable batteries, however, can be used only for once and are then, discarded. Primary batteries show advantages such as simple and easy to use, can be shaped and sized according to the application, good shelf life and reasonable energy density. In these batteries, the chemical reactions are not reversible and hence, the active materials do not recover back to their original forms and they cannot be recharged. However, this does not happen in the case of secondary

batteries. **Secondary batteries** or the rechargeable batteries have to be charged before they are used first. They can be charged or recharged several times by applying electric current depending on the stability of the materials used in the cells. The reaction occurring in these batteries are reversible reactions and hence, can be used for more than single cycle of charge-discharge. The first example of a rechargeable battery is lead-acid battery. Lead acid batteries are highly durable and have long life but its demand in the market gradually reduced because of its high cost, requirements of maintenance and lower specific energy. Table 1.1 shows some of the examples of primary and secondary batteries based on the electrolytes used.

Table 1.1 Types of primary and secondary batteries

	Aqueous electrolyte battery	Non aqueous electrolyte battery (high energy, high capacity, high voltage)
Primary battery	Manganese dry cell Alkaline dry cell	Metallic lithium battery
Secondary battery	Lead-acid battery Ni-Cd battery Ni-MH battery	**Lithium ion battery**

Lithium ion batteries comes under the category of secondary batteries or the rechargeable batteries. Besides lithium ion batteries, there are other classes of lithium batteries as well that serves under the category of secondary batteries for example, lithium metal batteries, lithium air batteries, and lithium sulphur batteries. Lithium metal batteries use lithium metal as the negative electrode and are more unsafe than the primary lithium batteries. Search for high-energy density batteries led to the discovery of lithium metal as an efficient anode material for energy-storage purposes.

In general, an electrochemical cell consists of three primary components:

1. **The negative electrode or the anode**: the electrode at which oxidation occurs, or the one which provides electrons to the external circuit;

2. **The positive electrode or the cathode**: the electrode at which reduction occurs, or the one which accepts electrons from the external circuit.

3. **The ionic conductor or electrolyte**: ion conducting media between the two electrodes. It also acts as the separator between the electrodes preventing them from internal short-circuiting.

The materials used as cathode or anode materials must provide a high cell potential and should be lighter in weight as well. Besides these two essential properties, there are factors such as reactivity with other cell components, electrode polarization and high cost, which affect the practical application of the electrodes. The electrolyte must be ionically conductive but not electronically conductive. Combinations of various salts and liquids (aqueous and non-aqueous) can be used as electrolytic system in a battery. Non aqueous electrolytes like organic solvents and molten salts show higher cell potential as compared to the aqueous electrolytes showing at 1.5 V, equivalent to the potential for the electrolysis of water (1.23 V). Therefore, aqueous electrolytes have a limitation in the capacity. However, in the case of non-aqueous electrolytes, since the obtained potential per cell is equal to or more than 3 V, the possibility of achieving higher capacities are enhanced.

1.2 History and Evolution of Lithium Ion Batteries

The research in the field on lithium batteries started in the 1950s. With the introduction of

lithium metal as an active anode material, several primary lithium batteries with high energy densities were developed and commercialized by 1970s. Lithium is the lightest (M=6.94 gmol^{-1} and specific gravity ρ=0.53 gcm^{-3}) of all metals and is the most electropositive element (-3.04 V vs Standard Hydrogen Electrode). Hence, it can be used to design storage systems with high energy density[1] and can provide much high specific capacity (3860 mAh/g) (Handbook of batteries, Mc Graw Hill, 2001). Further, lithium metal has high electrochemical equivalence and high conductivity which adds up to its features for using it as an electrode material. Unfortunately, lithium metal could not be used with water and hence, its application required a complete shift from aqueous to more stable common non-aqueous solutions or organic solvents.

1970s was the decade of primary lithium batteries that commercialized the use of manganese oxide cathode (MnO_2), iron sulfides (FeS_2) and copper oxide (CuO). However, these were primary batteries and hence, the search and development of batteries that can be recharged for certain number of cycles was also started. Over this period only, certain inorganic compounds, later termed as the "*intercalation compounds*" were found to react with alkali salts in a reversible manner. This crucial discovery of intercalation compounds paved way for proceeding towards the development of high energy rechargeable lithium batteries. The practicality of an intercalation electrode for a rechargeable lithium battery was demonstrated in 1976 by Whittingham using Li_xTiS_2 /Li cell in which TiS_2 was used as the intercalating cathode and Li metal as anode.   However, lower cell potential and difficulty of using non aqueous solutions with lithium metal electrode motivated towards the search for a new intercalation electrode that can provide higher cell potential as compared to the TiS_2. And hence,

came the contribution of Li_xMO_2 (specifically $LiCoO_2$; M=Ni, Mn, Co), reported by Goodenough *et al.* in 1980. Using lithium over sodium and oxides over sulphides proved to be a beneficial idea in the search of the intercalation cathode materials for lithium rechargeable batteries.

Another important demerit of using Li metal as anode with liquid electrolytes was dendritic growth over lithium as the metal was replated during several charge-discharge cycles changing the morphology of lithium metal electrode. Formation of dendrite leads to substantial loss of lithium and solution species because of surface reactions and repairing of surface films[2]. This will result in complete consumption of the electrolyte material and connect positive and negative electrode, resulting in short-circuiting and hence, failure of the battery[3-5] (Fig. 1.1). Replacing lithium metal anode was one possible solution and substitution using aluminum alloys solved the safety issues, however, the capacities reduced to low values when compared with lithium metal electrode. To evade the safety issues arising from lithium metal anode, several attempts were made in two alternative directions: 1) changing the lithium metal electrode with a second insertion material or intercalating compound and 2) changing the organic solvent or solvent compositions used as electrolytes. The concept was experimentally tested in lab by Murphy and Scrosati *et al.* using two insertion electrodes and cycling lithium ions between them. This successful experiment led to substantial research and development of rechargeable battery systems based upon intercalation and deintercalation using both host electrodes and removal of lithium metal anode completely. This concept led to the development of the presently called "**Li ion technology**", also termed as the "*rocking chair technology*" as the two-way movement of lithium ions occur between anode and cathode via the electrolyte

during charge-discharge processes.

Continuous efforts were taken in the direction of developing a second insertion material with higher potential. However, it took almost a decade to implement the concept of Li ion battery because of delay in finalizing the most suitable negative material. Steele in 1973 had suggested graphite and layered sulphide TiS_2 as the second insertion material or the host material that can intercalate lithium ions. Though metal suphides were less oxidizing than metal oxides, the quest went on till the discovery of carbon as highly reversible, low voltage Li intercalation material.
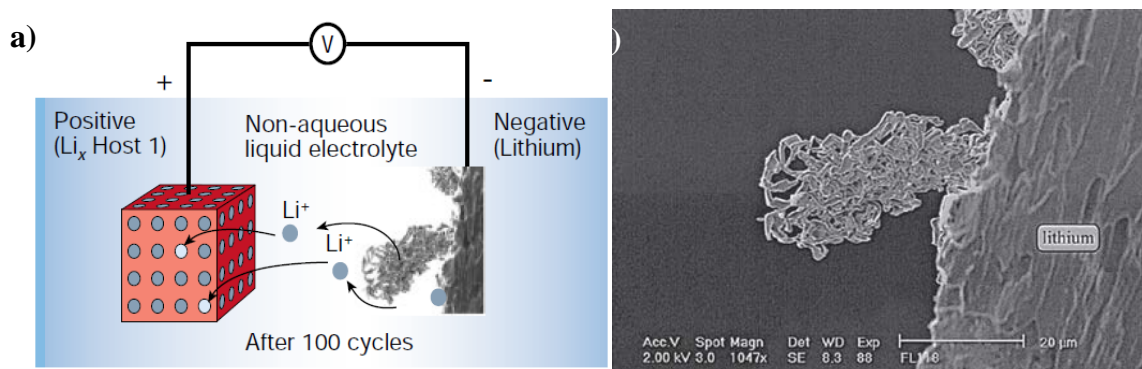
Fig. 1.1 a) Rechargeable Li-metal battery (dendrite growth at the Li surface) (adapted from[1]1) ; b) Lithium dendrite formation on the surface of bellcore-type $LiMn_2O_4$/Li battery after first charge at 1C (adapted from 4)

Finally in 1991, Sony Corporation came with the first Li ion rechargeable battery using C/$LiCoO_2$ which showed an open circuit potential of 4.2 V and an operational potential of 3.6 V (3 time of alkaline systems) and gravimetric energy densities of 120-150 Wh/kg (2 times higher than Ni-Cd systems) (Fig. 1.2). Since then, the research has not ended, in looking for better electrode materials, for better electrolytic systems, on morphological studies after

cycling, on study of the underlying electrochemical reactions etc., all of which aiming for enhancement of performance of the Li ion batteries.
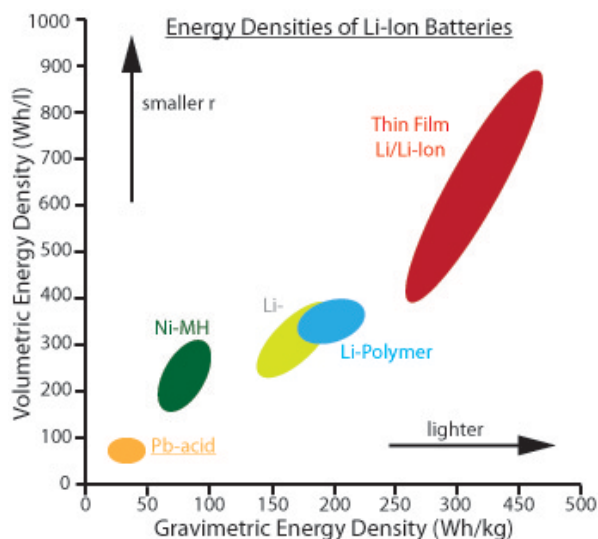
Fig. 1.2 Comparison of energy densities of different kind of batteries

1.3 Component Materials of a Lithium Ion Battery

The smallest working unit in a battery is an electrochemical cell. Although, there are several number of components that contribute to the efficient performance of a lithium ion cell such as anode, cathode, electrolyte, binder used for electrode preparation, back contact to tap electrical contact, separators determining the distance between the electrodes and the casing of the cell, however, as discussed earlier, in general, anodes and cathodes for the batteries have to be chosen in a way such that they result in high cell potential and high capacity after fabrication of cell. The maximum energy that can be obtained from a cell is based on the type of active materials, activity of the materials used and on the amount of the active material used in the cell.

1.3.1 Anode Materials

Practically, while choosing anodes, certain properties have to be kept in mind: efficiency as a reducing agent, high coulombic output (Ah/ g), good conductivity, stability, ease of fabrication, and low cost. Technically, any electrode with a very low potential vs Li/Li$^+$ can work as negative electrode material. Practically, metals are used as effective anodes, however, in case of lithium batteries, use of lithium metal resulted in dendrite formation and hence, were regarded unsafe to be used as anode for lithium ion batteries. Further, carbonaceous materials as lithium intercalation materials became very popular after the commercialization of Sony's first Li ion battery using host materials as electrodes. Carbonaceous materials could solve the lithium dendritic problem but compromise was done in terms of the capacities. For example, graphitic carbon shows a theoretical capacity of 372 mAh/g[6] which is only a tenth of the original capacity of lithium anode (3829 mAh/g).

"The theoretical capacity of any electrode material is determined by the amount of active materials in the cell. It is total quantity of electricity obtained from the active materials in the electrochemical cell and is defined in terms of Ampere hours."-Handbook of Batteries. It is calculated from the equivalent weight of the reactants. Theoretically, 1 gram-equivalent weight of material should deliver 96,487 C or 26.8 Ah (3600 C=1 Ah). In lithium ion battery, it is the maximum intercalation level of 1 mole of Li$^+$ per mole of the active electrode material. Table 1.2 lists the theoretical capacities of various anodes used in different kinds of the batteries.

Table 1.2 Theoretical capacities and other characteristics of anode materials

Material	Atomic or molecular weight, g	Standard reduction potential at 25°C, V	Valence change	Melting point, °C	Density, g/cm³	Electrochemical equivalents		
						Ah/g	g/Ah	Ah/cm³‡
Anode materials								
H₂	2.01	0 −0.83†	2	—	—	26.59	0.037	
Li	6.94	−3.01	1	180	0.54	3.86	0.259	2.06
Na	23.0	−2.71	1	98	0.97	1.16	0.858	1.14
Mg	24.3	−2.38 −2.69†	2	650	1.74	2.20	0.454	3.8
Al	26.9	−1.66	3	659	2.69	2.98	0.335	8.1
Ca	40.1	−2.84 −2.35†	2	851	1.54	1.34	0.748	2.06
Fe	55.8	−0.44 −0.88†	2	1528	7.85	0.96	1.04	7.5
Zn	65.4	−0.76 −1.25†	2	419	7.14	0.82	1.22	5.8
Cd	112.4	−0.40 −0.81†	2	321	8.65	0.48	2.10	4.1
Pb	207.2	−0.13	2	327	11.34	0.26	3.87	2.9
(Li)C₆[(1)]	72.06	~−2.8	1	—	2.25	0.37	2.68	0.84
MH[(2)]	116.2	−0.83†	2	—	—	0.45	2.21	—
CH₃OH	32.04	—	6	—	—	5.02	0.20	—

Anode materials for lithium ion battery can be broadly classified into six categories:

a) Graphite based

b) Group IV alloys

c) Conversion electrodes

d) Other alloy materials

e) Nanostructured carbon

a) *Graphite based anode materials*[7-15] are currently used in the commercial lithium ion batteries. They are known to show highly reversible charge discharge capacities. The lithiation process occurs in different stages of intercalation and deintercalation between the

graphene planes from the diluted stage of Li_xC_6 to LiC_6 which is the basis of its theoretical capacity of 372 mAh/g. Extensive studies have been carried on the morphological characteristics and interface formation onto the graphite anodes.

b) The search for novel materials showing better performance led to the introduction of *alloy anodes* based on Sn[16] and Si. Si anodes being one popular among the anode materials exhibits the largest theoretical gravimetric capacity of 3579 mAh/g representing the $Li_{15}Si_4$ phase[17-19]. However, volume expansion due to Li^+ ion intercalation during charge discharge cycles at higher current rates lead to high capacity loss and mars the overall performance of the anodes.

c) The use of oxide anodes had also been proposed and they were termed as *conversion electrodes*, as they were synthesized by the conversion of transition metal oxides (Fig. 1.3). Their forms changes from crystalline to amorphous during lithium insertion and show a very high capacity, but a large capacity fade is observed on subsequent charge discharge cycles.
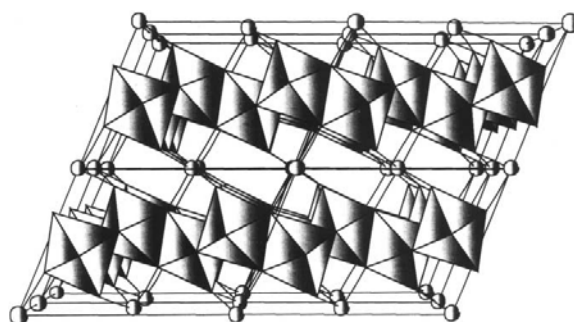
Fig. 1.3 Structure of brannerite (MnV_2O_6); Mn is represented by circles and vanadium is located at the centre of each octahedron (Adapted from 10)

d) Recently, graphene as emerged as a very efficient anode material under one of the forms of nanostructured carbon. It exhibits very high capacity (744 mAh/g) but suffer from highly irreversible capacity loss. Nanostructured carbon materials do not show high reversible delithiation capacity due to high surface area, nanopore accumulation and functional groups on the surface[11, 20-22].

1.3.2 Cathode Materials

Cathode material for a battery must be an efficient oxidizing agent with high stability when in contact with the electrolyte and should demonstrate a useful working potential. Most common cathode materials are metal oxides. Further, in the case of lithium ion batteries, lithiated metal oxides are used as active cathode materials. For any material to be employed as a lithium ion battery cathode material, there are certain prerequisites:

1. The material should show high free energy of reaction with lithium ion and the reaction with lithium must occur at high potential vs. Li/Li^+ to achieve high cell potential and high energy density.

2. The material should be able to incorporate large quantities of lithium ion reversibly without any structural change to enable high capacity, permit long cycle life, high coulombic efficiency and high energy efficiency.

3. The material should exhibit good electronic conductivity and high lithium ion mobility in order to complete the process of charge discharge at high rate.

4. The material should also not react with the electrolyte or other components of the cell.

5. The material should be prepared from inexpensive reagents.

Cathode intercalation materials started with the novel work by Whittingham who first proposed the use of TiS_2 as the host material for non-aqueous secondary batteries. After this discovery, a variety of positive electrode materials were reported, some of which are commercially available now or then. Broadly classified into three groups, they can be:

a) Layered transition metal oxides

b) Spinel oxides

c) Polyanion type electrodes

a) The first *layered transition metal oxides* reported by Goodenough *et al.*, was $LiCoO_2$ that offered a high theoretical capacity (274 mAh/g) and a cell voltage of 3.9 V (Fig. 1.4). They are oxides with the general formula $LiMO_2$ (M=V, Cr, Co or Mn) crystallized in a layered structure in which lithium ions and metal ions occupy interstitial sites in an octahedral manner, facilitating movement of lithium ions in and out of the matrix[23, 24].
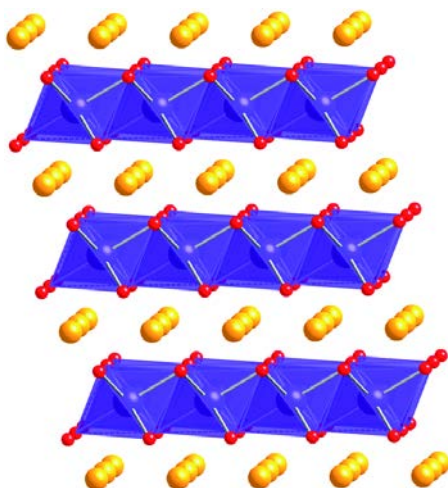
Fig. 1.4 Structure of $LiCoO_2$ (adapted from 25)

b) ***Spinel cathodes*** have a 3 dimensional framework or tunneled structure based on λ-MnO$_2$. These are the cathodes that have a spinel structure. In spinel cathodes, Mn centered oxygen fills half of the octahedral sites whereas lithium fills 1/8th of the tetrahedral sites within the λ-MnO$_2$ structure (Handbook of batteries, Mc Graw Hill, 2001). These cathodes offer safety, durability, cost effectiveness and intrinsic rate capability that arise from the chemically stable Mn^{3+}/Mn^{4+} couple. The best example of these types of cathode materials is LiMn$_2$O$_4$[1, 26] (Fig. 1.5). LiMn$_2$O$_4$ spinel is a lithium intercalation cathode material whose composition can be varied over the range Li$_x$Mn$_2$O$_4$, $0<x<2$[27].

λ-MnO$_2$ LiMn$_2$O$_4$
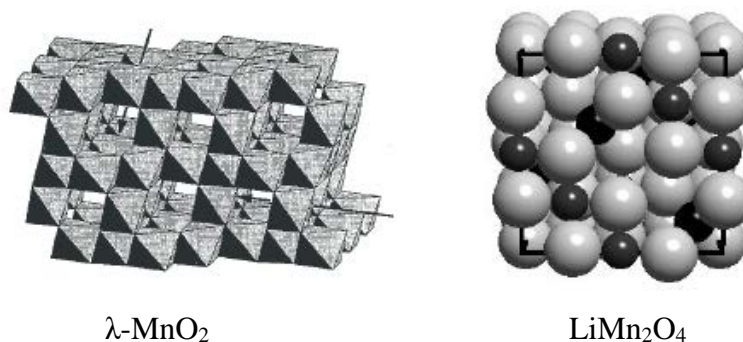
Fig. 1.5 The idealized structure of λ-MnO$_2$ and LiMn$_2$O$_4$ spinel (adapted from Handbook of batteries, Mc Graw Hill, 2001).

c) ***Polyanion based materials*** refer to phosphor-olivines and lithium metal orthosilicates. They are tetrahedral polyanion structure units (XO$_4$)$^{n-}$ along with metal oxide polyhedrals. These materials are known to show high thermal stability than layered transition metal oxides and are regarded as the most promising cathode materials. Examples are lithium iron phosphate (LiFePO$_4$) that has a slightly distorted hexagonal closed packed geometry, lithium iron/manganese silicate (Li$_2$MSiO$_4$, M=Fe, Mn or combinations) that holds two lithium ions per unit of material and has a theoretical capacity of 333 mAh/g. However,

these electrodes suffer from low electronic conductivity, slow reaction kinetics and poor cycle life caused by loss of crystallinity during cycling.[9]

1.3.3 Electrolytes

An electrolyte is a substance that separates into anions and cations when dissolved into a solvent. Electrically, such a solution is neutral in nature. The cations and anions of the electrolyte move to their respective electrodes when a potential is applied between the electrodes which produces current. Electrolytes play an important decisive role in the performance of any battery as they are the medium of conduction of ions between the two electrodes. In order to be used as an effective Li ion battery electrolyte, a substance must meet some of the important requirements:

1. High thermal, chemical and electrochemical stability.
2. The material should exhibit high solubility in different organic solvents.
3. High ionic conductivity indicating high ionic mobility is an important characteristic needed for an electrolytic material.
4. The material should also be able to passivate the electrode surfaces finely so that it can lead to reduction of irreversible capacity loss i.e., it must result in a solid, stable, thin and conductive Solid Electrolyte Interface (SEI, will be discussed in detail in section 1.6)
5. And finally, it should be cost effective and less toxic.

Replacement of lithium metal anode by host material ensured the safety issues arising from the anode materials of the battery, however, to assure cycle life along with safety, electrolyte

system also had to be carefully chosen and optimized. The first proper organic electrolyte was selected based on solutions of $LiAsF_6$ in aliphatic ethers such as 2-methyltetrahydrofuran which obeyed almost all of the pre-requisites.
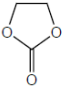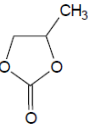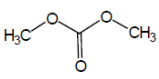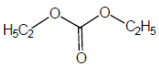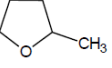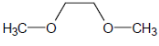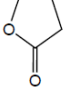
Depending on the cell design and purpose, electrolytes can be classified under four different aspects:

a)   Liquid Electrolytes

b)   Gel Electrolytes

c)   Polymer Electrolytes

d)   Solid State Electrolytes

a) Liquid Electrolytes:

In lithium ion rechargeable batteries, since average cell potential remains beyond 3V, an aqueous electrolyte cannot be employed as it will decompose by the time it reaches this potential. Hence, organic carbonate solvents with dissolved lithium salts were considered to be the effective candidates for an electrolytic system[28]. The discovery of mixtures of organic carbonate solvents as electrolytes and the lithium salt, lithium hexaflourophosphate, $LiPF_6$ for lithium ion battery was a breakthrough. Table 1.3 lists the structure and properties of some organic solvents used in lithium ion batteries.

Table 1.3 Structure and properties of organic solvents for lithium ion batteries

Solvent name and abbrev.	Stuctural fomula	Melting point (°C)	Boiling point (°C)
Ethylene carbonate, **EC**		39-40	248
Propylene carbonate, **PC**		-49	240
Dimethyl carbonate, **DMC**		4.6	91
Diethyl carbonate, **DEC**		-43	126
2-Methyl-tetra hydrofuran, **2Me-THF**		-137	79
Dimethoxy ethane, **DME**		-58	85
γ-Butyro lactone, **γ-BL**		-43	204

Ionic conductivity of any material is reflected by the mobility of the ions present and the total number of mobile ions. Cyclic carbonate esters like PC (propylene carbonate) and EC (ethylene carbonate) have high dielectric constants, however, their viscosities are high due to interaction between molecules and hence, results in deviation of electric charge. Whereas, chain like esters have low viscosities and dielectric constants, they do not create much restrictions for the mobility of lithium ions. For easy movement of lithium ions, electrolyte solutions must have lower viscosities. Moreover, too high dielectric constant also is a drawback as it imparts a high degree of ionic dissociation in the neighbouring molecule. Hence, commonly, mixtures of these two kinds of solvents are used for obtaining the desirable set of properties and are commercially available. Since, the reduction of

electrolyte at the anode is inevitable, solvents that can form a stable and a conductive SEI must be used. EC is one of those magic solvents which when used either as pure or as an additive in a solvent, leads to highly reversible behavior of lithiation.

Second important component of the liquid electrolyte is the lithium salt used. It can be lithium hexaflourophosphate ($LiPF_6$), lithium hexaflouroarsenate ($LiAsF_6$), lithium methylsulphonate ($LiCF_3SO_3$), lithium bis(triflouromethylsulphonyl)imide ($LiN(SO_2CF_3)_2$)/LiTFSI, lithium perchlorate ($LiClO_4$), lithium tetraflouroborate ($LiBF_4$) and the recently introduced lithium bis(oxalato)borate (LiBOB). There are certain other salts as well which were being synthesized over the course of time and were studied for the application in lithium ion battery. These salts also have certain specific features that are required before employing it for battery purposes[29]. **1)** The salt must be highly chemically and thermally stable and should inherently possess high ionic conductivity when dissolved in various solutions. **2)** The salt should yield into reduction products that can form a conductive SEI instead of a resistive SEI over anodes. **3)** Both the ions of the salt should remain inactive towards other cell components of the battery, nontoxic and stable against thermally induced reactions in the cell. **4)** And most importantly, the salt should have high solubility and high degree of dissociation in the organic solvent used as electrolyte resulting into solvated ions of high mobility. Irrespective of the Li salt used, the salt must enable the process of ion diffusion between the electrolyte and electrode effectively.

The salt used most commonly in commercial cells is $LiPF_6$. $LiPF_6$ is a salt of strong acid. It exhibits high ionic conductivity, high anodic stability upto (5.1 V) and forms stable

SEI layer with very low interfacial resistance. Other salts like lithium trifluoromethanesulphonate (LiTf) and LiTFSI are being designed specifically with a larger anion size for use in polymer electrolytes. Greater anion size results in weaker coordination and hence, higher dissociation nature increases the lithium cation mobility and further result in increased transference number[29]. Fig. 1.6 shows the structure of different types of Li salts that are being developed for Li ion battery.
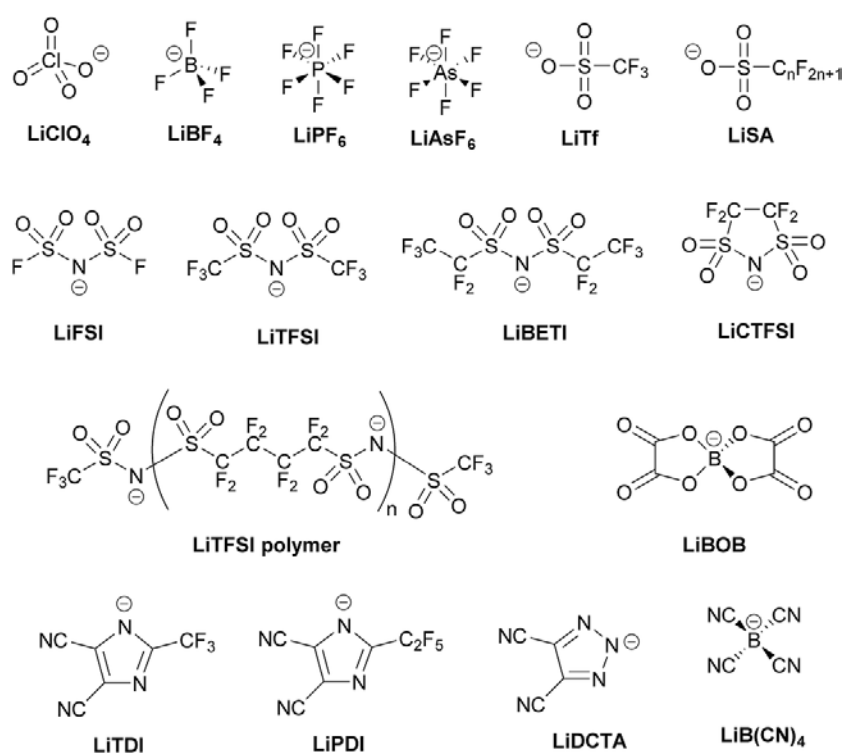
Fig. 1.6 Structure of different types of Li salts (adapted from 30)

Among safer liquid electrolytes, ionic liquids are also considered as one of the alternatives to the conventional liquid electrolytes. Ionic liquids are molten salts composed of cations and anions discretely and are characterized by weak interactions due to the presence of large cation and charge delocalized anion. Ionic liquids show various

advantages and interesting properties as compared to the conventional organic carbonate solvents. Properties like viscosity, high ionic conductivity, high chemical, thermal and electrochemical stability, non-flammability, non-volatility and high solubility and affinity with variety of compounds are specific to ionic liquids and marks their safety[31-37]. Fig. 1.7 shows the properties and common cations and anions used as ionic liquids.
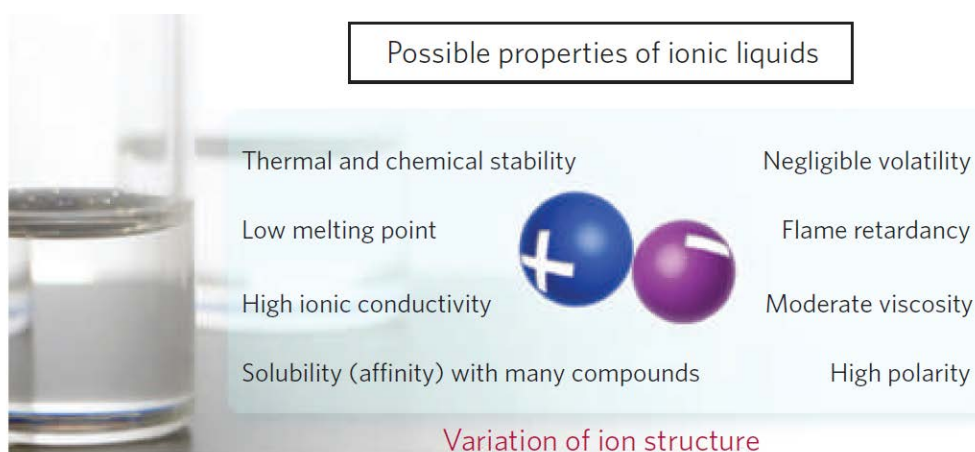
Fig. 1.7 Properties of ionic liquids

b) Gel Electrolytes:

A gel is a state of matter that is neither completely solid nor completely liquid. A polymeric gel is a system that has a polymer network swollen with a solvent, i.e., the solvent is absorbed by the polymer gel and not vice-versa (Fig. 1.8). Gel electrolytes are typically films of polyvinyledenediflouride-hexaflourophosphate (PVDF-HFP)[37], a lithium salt and a carbonate solvent. Since the liquid electrolyte is absorbed within the polymer, it prevents leakage of the electrolyte from the battery unlike liquid electrolytes. Gels always possess the properties of both solids and liquids. Like solids, they are cohesive and like liquids, they facilitate diffusion of ions[38].
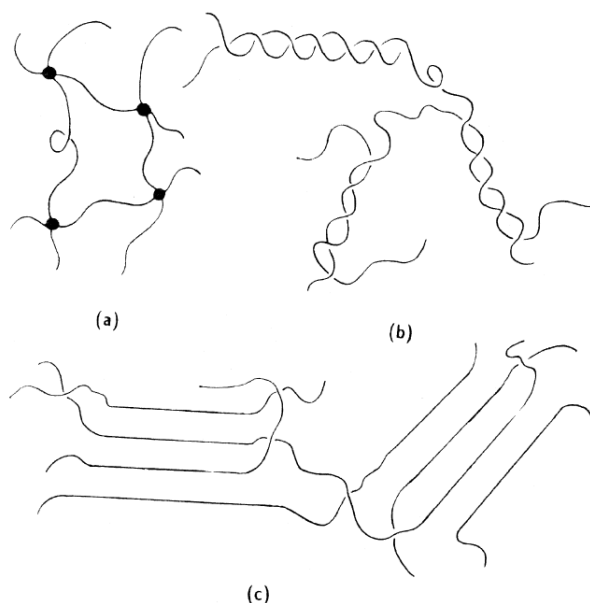
Fig. 1.8 Diagrammatic representation of gels a) chemical gel network, b) physical

gel network and c) fringed micelles (adapted from 38)

c) **Polymer Electrolytes:**

Polymer electrolyte is a solvent free liquid/solid material where salts are dissolved in a high molecular weight polymer to form an ionically conducting phase. Polymers like polyethylene oxide (PEO) and polyethylene glycol (PEG) along with the combination of Li salts are used as polymer electrolytes (Table 1.4). They were designed with an aim of developing an all-solid state electrolyte to ensure the development of a safe lithium ion battery. Suppression of dendrite growth, reduced reactivity with liquid electrolyte, enhanced endurance to varying electrode volume during cycling, improved safety, better shape flexibility are some of the key features of polymer electrolytes[30, 38-40]. In the case of polymer electrolytes, the mobility of ion is governed by polymer segmental motion (Fig.

1.9) and hence, these polymer electrolytes though having several safety traits show lower conductivities within the range of 10^{-4} to 10^{-5} Scm^{-1}.

○ = Lithium
● = Oxygen
~●~ = PEO Chain
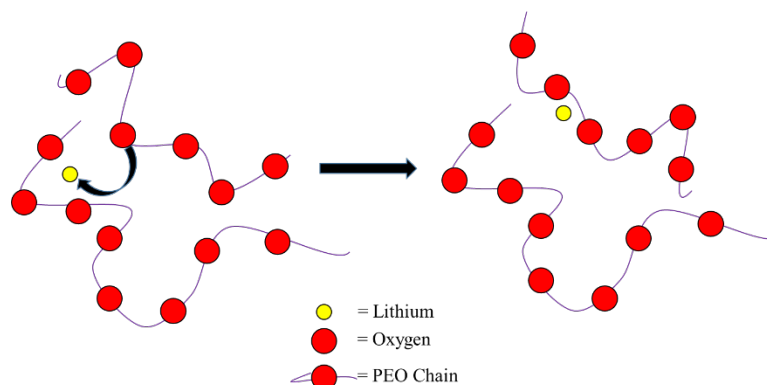
Fig. 1.9 Lithium ion conduction mechanism via polymer segmental motion in PEO –Li salt complex

Table 1.4 Polymer hosts, their structural formulae and physical properties

Polymer host	Repeat unit	Glass transition Temperature, T_g (ºC)	Melting Point, T_m (ºC)
Poly(ethylene oxide)	-(CH$_2$CH$_2$O)$_n$-	-64	65
Poly(propylene oxide)	-(CH (-CH$_3$)CH$_2$O)$_n$-	-60	-^{a}
Poly(bis(methoxy ethoxyethoxide)-phosphazene	-[N=P(-O(CH$_2$CH$_2$O)$_2$CH$_3$]$_n$-	-83	-^{a}
Poly(dimethylsiloxane)	-[SiO(CH$_3$)$_2$]$_n$	-127	-40
Poly(acrylonitrile)	-(CH$_2$CH(-CN))$_n$-	125	317
Poly(methyl methacrylate)	-(CH$_2$C(-CH$_3$)(-COOCH$_3$))$_n$-	105	-^{a}
Poly(vinyl chloride)	-(CH$_2$CHCl)$_n$-	82	-^{a}
Poly(vinyledene fluoride)	-(CH$_2$CF$_2$)$_n$-	-40	171

^{a} Amorphous Polymer

d) Solid State Electrolytes:

Solid state materials that are ionically conductive come under the category of solid state electrolytes. Due to safety problems arising from liquid electrolytes and insufficient conductivities obtained from gel/polymer electrolytes, solid electrolytes were thought to be an interesting alternative to the conventional electrolytes. Compared to liquid counterparts, these solid electrolytes solve the problem of flammability of the liquid organic solvents and further, can be processed for sleek and better battery designs[38, 41, 42]. Moreover, it will also allow the use of lithium metal as anode providing high capacity to the battery. Various solid state electrolytes were designed keeping this in mind starting from a PEO based solid state electrolyte[30]. However, the electrolyte was not as conductive as required. Broadly, solid electrolytes can be categorized as gelled polymers, solvent free polymers, inorganic crystalline compounds and inorganic glasses[43]. Table 1.5 lists some of the examples of solid state electrolytes and their ionic conductivities.

Table 1.5 Ionic conductivity of solid state electrolytes (polymeric) (adapted from[43] 43)

Type	Ionic Conductivity (Scm^{-1})
Wet polymer	8.46×10^{-8} (LiPF$_6$ 5wt% in PVdF)
	2.34×10^{-6} (LiPF$_6$ 10 wt% in PVdF)
	2.70×10^{-4} (LiPF$_6$ 20 wt% in PVdF)
Gel-polymer	9.4×10^{-8} (at 30 ∘C) (ST-BD (60:40) swollen by electrolyte)
	~10^{-4}: EMITFSI (at 30 ∘C) (PEO–PMA (7:3) swollen by ionic liquid or ionic liquid based electrolyte)

	~10^{-2} (EMITFSI + LiTFSI) (at 30 ∘C)
Li-ion conducting polymer	8.0×10^{-8} (PEO (polymer): host material)
	1.0×10^{-8} (SiO$_2$ (inorganic filler; plasticizer) and LiBF$_4$ (Li salt) are added to PEO)
Plastic crystal	1×10^{-4} (4%), 5×10^{-5} (15%) (LiBF$_4$ Succinonitrile doped by Li salts)

1.3.4 Charge Discharge Mechanism

The process of charge-discharge in a lithium ion battery is based on the intercalation and deintercalation of lithium ions. A lithium ion battery can be charged at a particular current rate with an external DC power source. Intercalation process is a topotactic reaction in which ions are added or removed from the host without causing any significant structural change to the host. The cathode being a metal oxide has a layered structure and the anode generally being carbonaceous materials, also have layered graphene planes and hence, both the electrodes act as the host material in the case of lithium ion battery.

When all the lithium is present at the cathode, that is the discharged state and they are assembled as such. Charging is intercalation of Li$^+$ ions in the anode accomplished by movement of Li$^+$ ions from the cathode to the anode under the influence of an electric field (Fig. 1.10). The Li$^+$ ions migrate between the electrodes through the electrolyte while the electrons flow through the external circuit. The battery is considered to be fully charged when all the active sites of the anode are intercalated with Li$^+$ ions. In contrast, while discharging, Li$^+$ ions get deintercalated from the anode and move back to the original position in cathode. When all the ions reach cathode, the battery is considered to be completely discharged and

requires charging again. Technically, intercalation and deintercalation of all Li^+ ions is the ideal case, however, this does not happen in real cases. There is always some amount of irreversible capacity loss resulting due to incomplete intercalation of Li^+ ions.
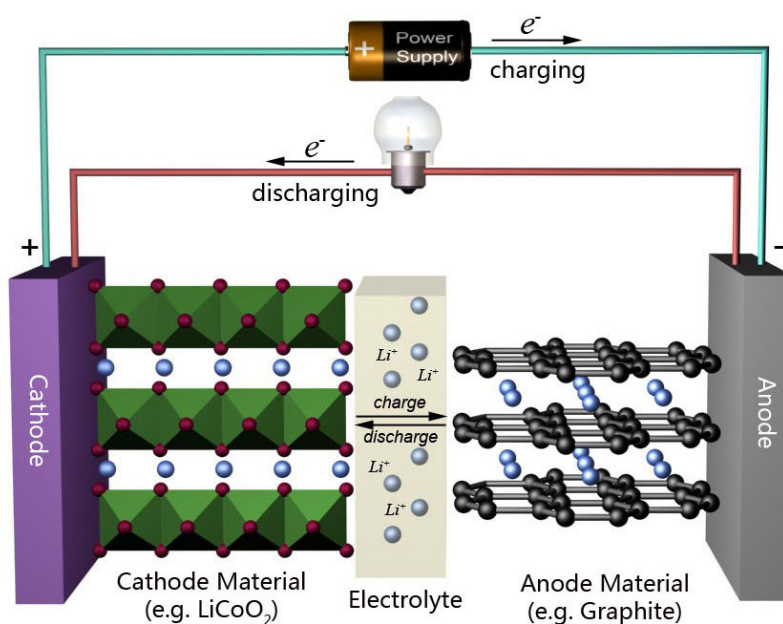
Fig. **1.10** Schematic representation of charge-discharge process in a lithium ion battery

(adapted from research.chem.psu.edu)

1.4 Electrolyte Bulk Properties and Analysis Techniques

The designing, functioning and formation of interfaces at electrodes are all attributed to the bulk properties of electrolytes. Moresoever, the bulk properties also play a major role in the overall performance of the battery. Electrolyte to be used in a battery must have several advantageous properties as told earlier such as thermal and mechanical strength, electrochemical stability and ease of manufacturing into different shapes and sizes. Further, there are certain intrinsic parameters which define an electrolyte completely such as viscosity, conductivity and transference number. A detailed description of the factors influencing these

parameters and the techniques to quantitatively determine these values will be provided in the following section.

1.4.1 Ionic Diffusion

Diffusion is the process of movement of entities (here, ions) from a region of higher concentration to lower concentration. Diffusion can occur only when a concentration gradient is developed. This is one of the dominant mass transport process in batteries which determine the charge-discharge rate, actual capacity and cycling stability. Diffusion can be analyzed by the basic Fick's law which defines the amount of flux transferred through a surface at a distance x in time t. The general expression of Fick's law of diffusion is given by:

$$q = D \, \frac{\delta C}{\delta x}$$

where, q is the net flux transferred, D is the diffusion coefficient (m^2/s) and C is the concentration. Fick's second law of diffusion gives the rate of change of concentration with time. To understand the diffusion process, it is important to have a clear idea of the structure of the material in which Li^+ ion diffusion is taking place.

1.4.2 Ionic Conductivity

Ionic conductivity is the key property of an electrolyte as it determines the mobility and the availability of the ions for the continuing electrochemical reactions at the surfaces of electrodes. Hence, the ionic conductivity of an electrolyte is responsible for determination of the total power output obtained from the cell[44]. Conductivity, in general, is the reciprocal of resistivity. It is generally given by the equation,

$$\sigma_i = \Sigma n e \mu$$

where, σ_i is the ionic conductivity, n is the carrier ion number, e is the electric charge and μ is

the mobility of the carrier ions. Ionic conductivity increases with an increase in the number of dissociated free ions and the mobility of these dissociated ions. In order to achieve sufficient capacity, the ionic conductivity of the electrolyte must be high, else Li^+ ions produced at one electrode will not be properly transported between the electrodes resulting into lower capacities. Ionic conductivity of an electrolyte is highly dependent on the ion conduction mechanism that is responsible for the migration of ions from one electrode to another. The detailed ion conduction mechanisms are discussed in the next section (Section 1.5).

1.4.2.1 Technique for Identification

Ionic conductivity can be measured using a conductivity meter, however, more common is the method in which first the solution resistance of the electrolyte is obtained and then the conductivity is calculated by using the formula,

Ionic conductivity = distance between the electrodes/(solution resistance × area of the electrode).

To calculate the solution resistance of the electrolyte, recently electrochemical impedance spectroscopy has emerged as a very powerful and effective tool. It is employed in the investigation of mechanisms in electrochemical reactions, in the measurement of transport properties of materials and very widely in the study of passive surfaces. Fig. 1.11 gives a brief idea about key features of EIS technique.
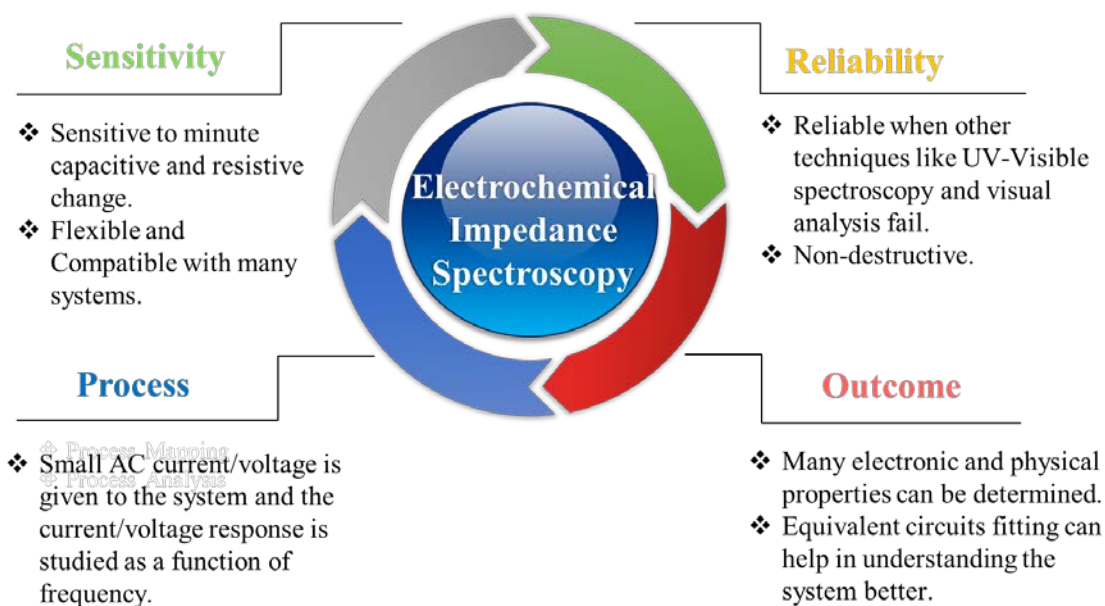
Fig. 1.11 Key features of Electrochemical Impedance Spectroscopy (EIS)

Ionic conductivity of an electrolyte is generally calculated by measuring the impedance profiles over a wide range of temperatures (30-60ºC or 30-90ºC). The relationship between ionic conductivity and temperature is studied with the help of various models. The different models that determine the type of electrolytes are:

a) Arrhenius model

b) VFT (Vogel-Fulcher-Tammann) model

c) WLF (Williams-Landel-Ferry) model

a) *Arrhenius model*

The Arrhenius equation, named after Svante Arrhenius, can be represented by the equation (eq.) 1,

$$\sigma = Ae^{(-Ea/\kappa T)} \text{ or } \sigma = \sigma_o\, e^{(-Ea/\kappa T)} \dots\dots\dots\dots\dots\dots\dots① $$

where σ_o or A is the pre-exponential factor (Scm^{-1})[45], E_a refers to the activation energy (eV or K), κ is Boltzmann constant ($1.38064852 \times 10^{-23}$ m^2 kg s^{-2} K^{-1}) and T is the temperature (K) at which experiment is performed. A linear plot when obtained for log σ vs 1000/T is referred to as typical Arrhenius profile, whereas, a non-linear plot indicates a change in the state of material within that temperature range.

b) *VFT (Vogel-Fulcher-Tammann) model*

The most empirical and commonly used relationship to study the temperature dependence of ionic conductivity is given by the VFT equation, eq. 2:

$$\sigma = A/T^{1/2}\ e^{\ (-B/R(T-T_o))} \ldots\ldots\ldots\ldots\ldots\ldots\ldots\ldots\ldots\ldots ②$$

where, A is the carrier ion number (Scm^{-1}K$^{1/2}$), B refers to the pseudo-activation energy (eV or K), R is gas constant (8.3144598 J mol^{-1} K^{-1}), T is the absolute temperature (K) while T_o is the ideal glass transition temperature (K, in this case 150 K) , ideally lower than the experimental glass transition temperature by 50-60 K. Though VFT model is just an approximation, as its temperature dependence specifically cannot be explained by the conventional modifications of Arrhenius law, it has been used to characterize a wide variety of materials and almost nearly precise values for these parameters were obtained. Various other models proposed were not favored over the VFT model due to its precise fitting compared to the other models[46].

c) *WLF (Williams-Landel-Ferry) model*

The William Landel Ferry model is a variation of VFT law in which $T-T_o$ is replaced by free volume. This is theoretically justified but since the data in this expression does not fit well,

this model is not very widely used[46] .

In general, Arrhenius and VFT models are more commonly employed to study the temperature-conductivity relationships.

1.4.3 Lithium Ion Transference Number

Lithium ion transference number is an important measure of the maximum limiting current that can be drawn from the cell and the cyclability of the cell. For instance, in an electrolyte composed of a single anion and cation, the transport number is given by the number of Faradays of charge carried by a particular type of ion across a plane for every one Faraday of charge that flows across the plane and is given by eq. 3:

$$t^+ = \frac{i^+}{i^+ + i^-} \dots\dots\dots\dots\dots\dots\dots\dots\dots\dots\dots\dots\dots\dots\text{③}$$

where, i^+ and i^- are the currents carried by the cations and anions respectively (A) and t^+ is the transport number of the cation.

However, in reality, while measuring transference number, along with the transport number of cations/anions, the number of associated solvent molecules is also measured that induces resistance[43]. Hence, transference number is used to measure the actual number of ions travelling in an electrolyte. The transference number is calculated by the Bruce-Vincent-Evans formula, eq. 4:

$$t_{Li}^+ = i_f(V - i_o R_o)/i_o(V - i_f R_f) \dots\dots\dots\dots\dots\dots\dots\dots\dots\dots\dots\text{④}$$

where, t_{Li}^+ is the Li^+ transference number, V is the potential applied across the cell (V), R_o and R_f are the initial and steady-state resistances of the passivating layers (Ω), and i_o and i_f are the

initial and steady-state currents (A). Transference number is a dimensionless parameter which notifies about the participation of a specific charge species present in the electrolyte to the overall charge transport across the cell.

1.4.3.1 <u>Bruce-Vincent-Evans formula to measure t_{Li}^{+}</u>

Several sophisticated techniques can precisely determine the Li ion transference number of the electrolyte, the most preferable, convenient and nearly accurate method was developed by Bruce-Vincent-Evans. The technique adapts a combination of Electrochemical Impedance Spectroscopy (EIS) and DC Polarization methods. The analysis employs sandwiching the electrolyte between two identical Li metal electrodes, one being the reference and counter electrode and the second as the working electrode. Charge-transfer resistance before polarization (R_o) is measured at very low amplitudes and then, a small constant potential (V) is applied between the electrodes which results in gradual decrease in the observed initial current (i_o) with time until a steady state value (i_f) is observed. Fig. 1.12 explains the fall in current which occurs due to the development of concentration gradient across the cell. The experiment is followed by measuring the charge-transfer resistance after polarization (R_f). The values thus obtained are substituted in the Bruce-Vincent-Evans equation to get the Li$^+$ transference number, t_{Li}^{+}.

Concentration gradient across the cell-

Reduces and stops net motion of anions

EMF acting in the opposite direction reduces the migration current of cations and anions

Increasing the motion of the cations in the direction of the field to compensate for the reduction in the migration current.
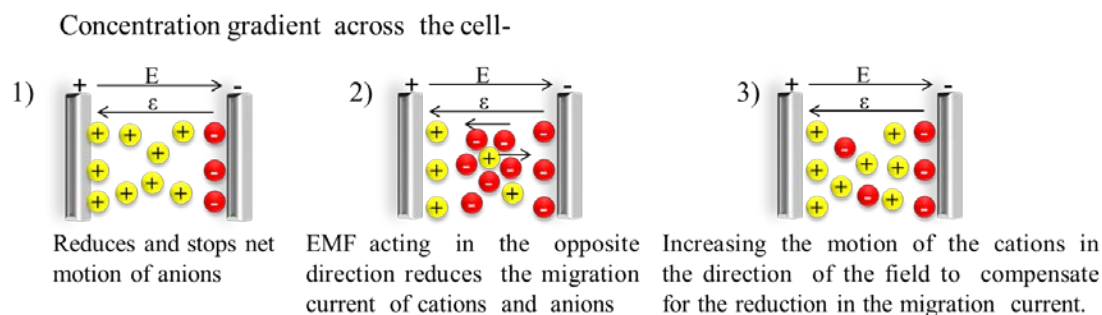
Fig. 1.12 Schematic representation for the fall in current during DC polarization method

1.4.4 Potential Window

The potential window, technically termed as the electrochemical stability of a material is the range of potential under which it does not undergo any electrochemical degradation or it works as a stable electrolyte. The electrolyte must possess a stable potential window range of 4.0 V. Table 1.6 lists the oxidative potential of the commonly used solvents vs. Li/Li$^+$.

Table 1.6 Physicochemical properties of the electrolytic solvents vs. Li/Li$^+$

Solvent	T_m (°C)	T_b (°C)	Dielectric constant	Viscosity (cP)	Donor number (DN)	Acceptor number (AN)	E_{ox}[b] (V versus Li/Li$^+$)
Ethylene carbonate (EC)	39	248	89.6	1.86[a]	16.4	—	6.2
Propylene carbonate (PC)	−49.2	241.7	64.4	2.53	15.1	18.3	6.6
Dimethyl carbonate (DMC)	0.5	90	3.11	0.59	—	—	6.7
Diethyl carbonate (DEC)	−43	126.8	2.81	0.75	—	—	6.7
Ethylmethyl carbonate (EMC)	−55	108	2.96	0.65	—	—	6.7
1,2-Dimethoxyethane (DME)	−58	84.7	7.2	0.46	24.0	—	5.1
γ-Butyrolactone (GBL)	−42	206	39.1	1.75	—	—	8.2
Tetrahydrofuran	−108.5	65	7.3	0.46	20.0	8.0	5.2
1,3-Dioxolane (DOL)	−95	78	6.8	0.58	—	—	5.2
Diethylether (DEE)	−116.2	34.6	4.3	0.22	19.2	3.9	—
Methyl formate (MF)	−99	31.5	8.5	0.33	—	—	5.4
Methyl propionate (MP)	−88	79	6.2	0.43	—	—	6.4
Sulfolane (S)	28.9	287.3	42.5	9.87	14.8	19.3	—
Dimethylsulfoxide (DMSO)	18.4	189	46.5	1.99	29.8	19.3	—
Acetonitrile (AN)	−45.7	81.8	38	0.35	14.1	18.9	—

a) Measured at 40°C.
b) E_{ox}: Oxidative potential (scan rate: 5 mV/s; reference electrode: Li).

1.4.4.1 <u>Techniques for analysis</u>

In general, linear sweep voltammetry is the method to determine the electrochemical stability of any electrolyte. Linear Sweep Voltammetry is used calculate the potential window of the electrolyte. Potential is scanned across a working electrode at a constant rate and the resulting current is observed. Any rapid increase or decrease in the value of current indicates decomposition or degradation of the electrolyte. It can be done in a two electrode cell which uses working electrode as platinum (Pt), carbon (C) or stainless steel and the reference electrode can be Li metal or Ag/AgCl.

1.4.5 Interfacial Characteristics

The electrode-electrolyte interface plays a major role in the cycle life and performance of a lithium ion battery. The electrolyte chosen must be able to form a stable and conductive interface on the electrode surface thereby helping in facile Li^+ ion intercalation/deintercalation. Interfacial reactions of electrode/electrolytes differ depending on the nature of the electrodes and electrolytes. A more detailed description for the interfaces is given in section 1.6.

1.5 Ion Conduction Mechanisms in Electrolytic Systems

As already mentioned, an electrolyte must have high ionic conductivity i.e. the tendency of ions to move fast and easily between the two electrodes. Many parameters governs the conductivity of an electrolyte such as viscosity, solvation of ions, concentration of salt used, degree of dissociation of ion pairs and interaction with the solvent. Till now, only organic liquid electrolytes are known to show ionic conductivity as high as 1.1-11.7 Scm^{-1}, however several reasons direct towards developing new alternatives. The efficient functioning of an electrolyte

in a commercial battery system requires a minimal ionic conductivity of 10^{-3} Scm^{-1} at room temperature (theoretically, 10^{-4} Scm^{-1})[43]. The shuttling rate of ions between the two electrodes also depends on the conduction mechanism through which it is transported between the two electrodes. These ion conduction mechanisms are dependent on the structure of the electrolyte material used.

Depending on the electrolytic system, the ion conduction mechanisms are explained below:

1.5.1 Organic Liquid Electrolytes

Addition of Li salt in to a solvent leads to immediate dissociation into Li$^+$ cation and the corresponding anion. The degree of dissociation depends on the dielectric constant of the solvent that is a measure of its solvating ability. Since, the Li$^+$ ion is surrounded by the solvent molecules, solvation occurs and thereby the transfer of Li$^+$ ion from one electrode to another (Fig. 1.13). Ionic conduction is favored by large size of the anion and low viscosity of the solvent. Greater the size of anion, greater the distribution of negative charge and lower the tendency to form ion pairs. Since a single solvent can rarely show high dielectric constant and low viscosity, mixtures of solvents are used in the case of organic liquid electrolytes for Li ion secondary battery.
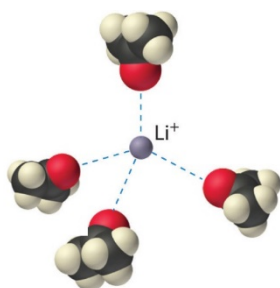
Fig. 1.13 Solvation of Li$^+$ ion by solvent (here, acetone)

1.5.2. Polymer Electrolytes

Ion conduction in polymers such as PEO, PEG electrolytes occur via polymer segmental motion (Fig. 1.14). Segmental motion of polymer chains that results into simultaneous making and breaking of cation-oxygen interactions provides free space for ions to diffuse under the influence of electric field and promote ionic motion and hence, enhance Li^+ ion conduction. Ion conduction in polymer electrolytes is highly dependent on the movement of the polymer host. Ions can move only if the polymer chains undergo large amplitude motions. These segmental motions can be inter polymer or intra polymer segmental motions *i.e.* the ionic jumps can occur between two polymer chains or within the fragments of single polymer chain respectively. An important factor that plays a major role here is the glass transition temperature[47]. Cation mobility is highly restricted by the glass transition temperature of the polymer. Below the glass transition temperature, such segmental motion does not take place, and ionic conductivity of the electrolyte drops to very low values resulting into a theoretical limitation in the ionic conductivity of the polymer electrolytes[48].
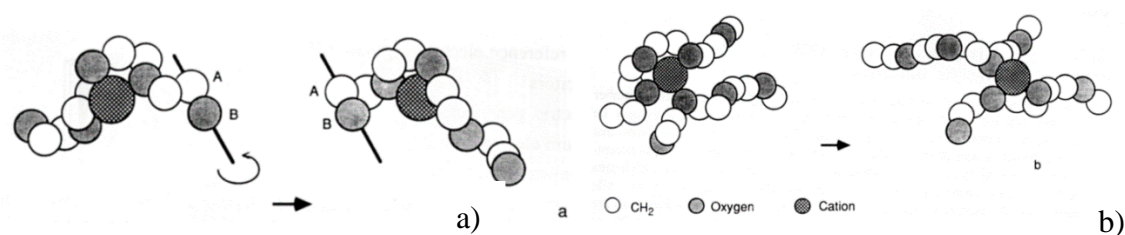
Fig. 1.14 a) Intra polymer segmental motion   b) Inter polymer segmental motion

1.5.3 Solid State Electrolytes

Although designed as an alternative to liquid electrolyte, solid state electrolyte have lower ionic conductivity as compared to their liquid counterparts. In the case of solid state electrolytes, only one ionic species is predominantly the charge carrier. The ion conduction mechanism in

different kind of solid state electrolytes is known to occur by various different ion conduction mechanisms. In inorganic crystalline compounds, ion conduction is known to occur by ion hopping to energetically favorable sites, assisted by motion of the surrounding ions. Reports on other crystalline compounds claim forming 1D, 2D and 3D channels or tunnels that facilitates ion conduction[49].

Continuous efforts have been done in order to increase the ionic conductivity of the solid state electrolytes considering crystalline, glassy and polymeric electrolytes and to understand the ion conduction mechanism in detail. Despite all these efforts till now, only lithium nitride, Li_3N, discovered in 1977 is known to possess the highest ionic conductivity at room temperature (6 x 10^{-3} Scm^{-1}). Recently, a research group have designed a lithium superionic conductor $Li_{10}GeP_2S_{12}$ having a 3D framework structure that shows ionic conductivity in the range of 10^{-2} Scm^{-1}. Ion conduction in this solid state electrolyte is found to be occurring via the 1D channels formed with LiS_6 octahedra and $(Ge_{0.5}P_{0.5})$ S_4 tetrahedra connected by a common edge (Fig. 1.15).
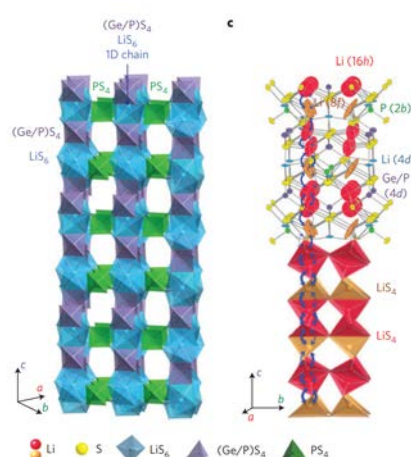
Fig. 1.15 a) Framework structure of $Li_{10}GeP_2S_{12}$. b) Conduction pathways of lithium ions.

1.6 Interface: Introduction

Since 1991, when Li ion battery was commercialized, there had been lots of advancements and research on the high performance electrode materials and safer electrolytes[1, 50-52]. A high research interest in this arena is diverted mainly towards the improvement of capacity of these batteries[9, 10, 53]. Further, this field attracts attention towards the control and optimization of interfaces at electrode surfaces. Surface films on electrodes is a very common and important phenomenon that controls their electrochemical behavior[24]. When a fresh active metal is dipped in a polar solution, its components get reduced on the active surface of the metal to form a surface film of insoluble metal salts on the metal electrode. This happens because of the difference in the redox potentials of the active metal and the solution species. Classically, the surface film formed on the metal surface should conduct the electrode's metal ions with a transference number close to unity. The thicker the film, less conductive it becomes.

An "Interface" is a term used to define a boundary formed between two different phases of matter. An interfacial region has discontinuity in both chemical and electric potentials, significant changes in structure, chemistry and dynamics. These altered characteristics determine the maximum mass and charge transfer process across the interfaces[54].

1.6.1 Solid Electrolyte Interface (SEI)

Metallic lithium has an inherent redox potential of -3.1 V (vs SHE)[1] where no solvent or no salt is stable, i.e. they decompose reductively on the surface of metallic lithium to form a passivation film and increase the stability of the metallic lithium in non-aqueous electrolytes. The passivation film formed onto the surface of the electrode by the reduction products of the

electrolytes is Solid Electrolyte Interface (SEI)[54, 55]. This SEI film is a conductor of ions and insulator for electrons[56]. If SEI layer does not block electrons, it will result into continuous decomposition of electrolyte on the electrode surface, consuming lithium and decreasing the capacity of the battery. And if Li$^+$ ions cannot pass through, the interfacial resistance increases as the thickness of SEI increases or its chemistry or morphology changes[57]. The extent and reversibility of Li intercalation depends on the nature of the host material, i.e. its structure, morphology, texture, grain-size and crystalline properties[8, 14, 58].

The protective SEI film formed on the electrode surface plays a vital role in determining the battery performance, cycle life, self-discharge rate, safety, coulombic efficiency and capacity loss[59]. Poor performance of lithium ion batteries at both high and low temperatures is due to the instability and lower conduction ability of the SEI films. The electrochemical reactions at SEI film occurs via 3 stages,

a) Charge transfer between electrolyte and interface,

b) Ion migration through the interface and

c) Charge transfer between interface and electrode.

As a result, great amount of research and reviews have been produced on the formation of SEI over anode (specifically, carbonaceous materials) as by choosing the appropriate carbon material, optimization can be done. Although, the process of Li intercalation and deintercalation in cathodes involves Li migration through surface films in a similar fashion like the carbon anodes[60], SEI formed on cathode surfaces[61] has gathered very less attention and the surface chemistry on cathode surfaces is not clearly understood.

The interfacial behavior of electrolytes with the electrode from the view point of electrolyte, an understanding of their electrochemical decomposition is necessary. Since Li salts are an inevitable part of the electrolytes used in the batteries, the nature of the anions in Li salt reflects the composition and stability of the SEI layer[62]. Li^+ ions in the electrolyte solution get solvated easily and hence, the mobility of solvated Li^+ ions is lower than that of the anions in the solution such as AsF_6^-, PF_6^-, ClO_4^-, BF_4^-, and $N(SO_2CF_3)_2^-$ (Fig. 1.16). These anions reach the surface of the electrode faster than the Li^+ ions and get reduce at the surface of the anode at the potential near to the potential of Li/Li^{+}[63].
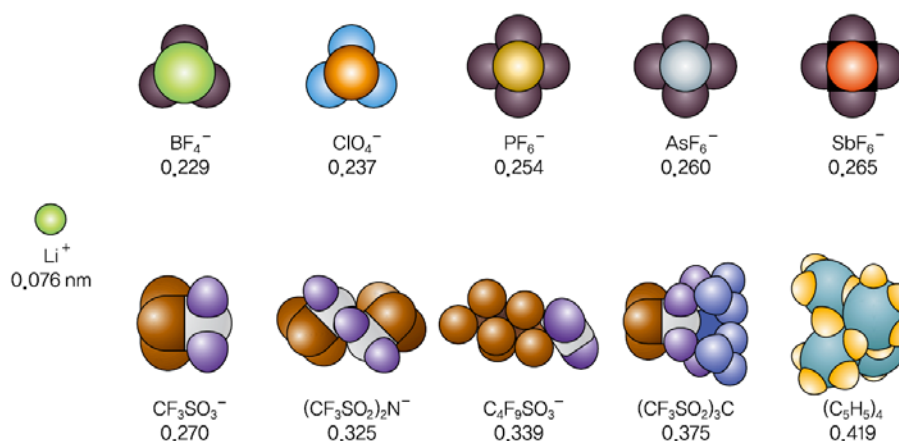
Fig. 1.16 Model structures of various Li salt anions and their ionic radii (adapted from 63)

In case of organic solvents such as alkyl carbonates, decomposition takes place within the range of discharge potential. Primary requirement of forming an SEI is the conduction of Li^+ ions and insulation of electrons and the preferred choice for this is alkyl carbonate solvents. The SEI layer formed by using the alkyl carbonates and Li salts is composed mainly of the insoluble inorganic or semi-inorganic Li salts including Li_2O, LiF, Li_2CO_3, RCO_2Li, alkoxides, and nonconducting polymers[59]. Decomposition reactions of the alkyl carbonates reductively

occurs by the ring opening reaction by one electron transfer (Fig. 1.17). Along with one electron transfer reaction, chain reactions also occur at the surface resulting into high molecular weight compounds.
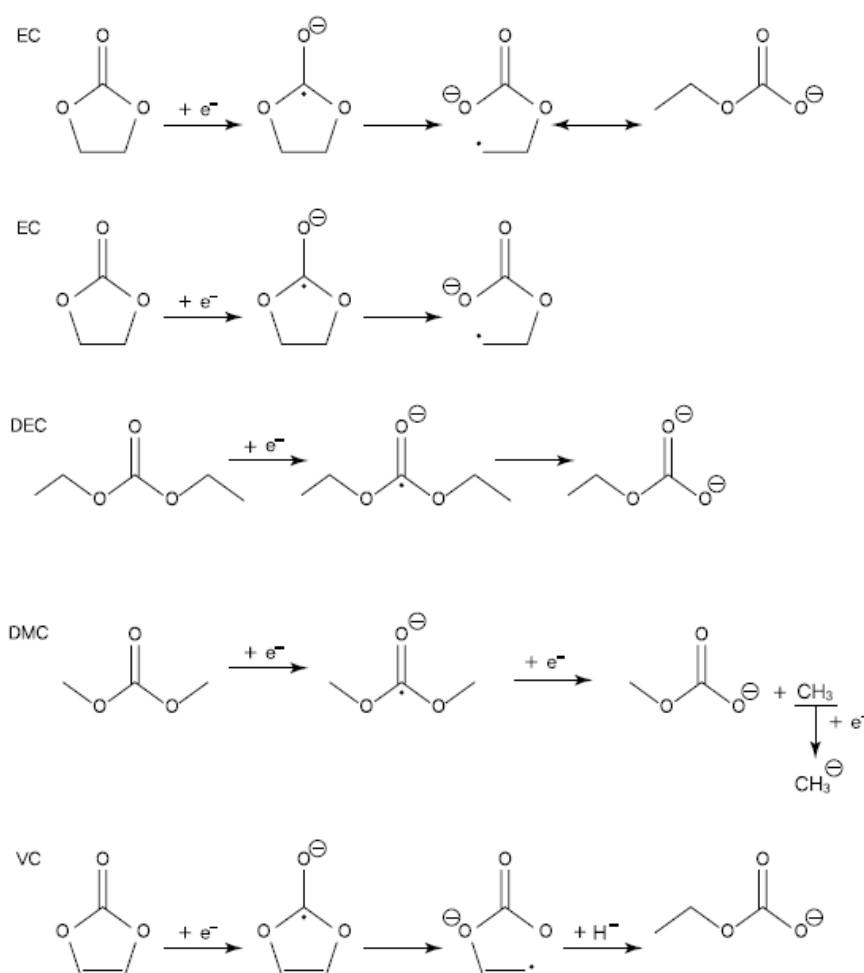
Fig. 1.17 Ring opening reaction of alkyl carbonate solvents via single electron transfer

For example, the main product of EC decomposition is $(CH_2OCO_2Li)_2$, and other derivatives include lithiumalkyl bicarbonates, $(CH_2CH_2OCO_2Li)_2$, $LiO(CH_2)_2CO_2(CH_2)_2OCO_2Li$, $Li(CH_2)_2OCO_2Li$ and Li_2CO_3.[64] Fig. 1.18 shows the possible reduction mechanism of EC.
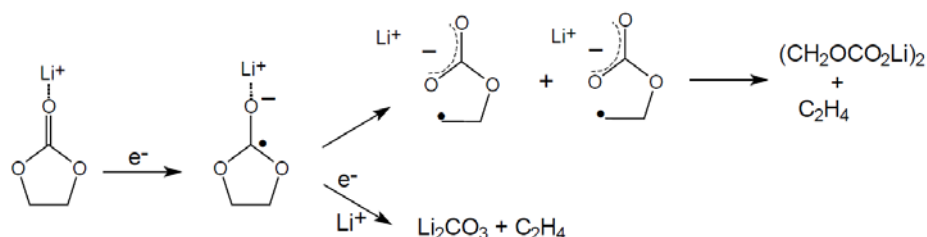
Fig. 1.18 Possible reduction mechanism of EC (adapted from 64)

1.6.2 Characterization and Analysis of SEI Layer

Understanding the formation mechanisms, composition, morphology, stability and nature of the SEI on the electrode/electrolyte interface is important for Li ion batteries. The formation conditions, storage conditions, voltage range significantly affect the SEI composition[7]. Many researchers have focused in this route of research dealing with the identification and understanding of the interfacial layer. Several *ex-situ* and *in-situ* techniques have been developed and used to determine the actual nature of the SEI layer.

There are various spectroscopic techniques that can provide surface structure of the electrodes after passivation. These can be *ex-situ/in-situ* Fourier Transform Infrared Spectroscopy (FTIR)[6], Raman Spectroscopy, Secondary Ion Mass Spectrometry (SIMS), X-ray Photoelectron Spectroscopy (XPS)[57, 65], Extended X-ray Absorption Fine Structure (EXAFS) and X-ray Diffraction (XRD)[66] for identification of surface species. Techniques such as Energy-dispersive X-ray Spectroscopy (EDAX), Scanning Electron Microscopy (SEM)[57], Transmission Electron Microscopy (TEM)[55], Atomic-force Microscopy (AFM)[67, 68] and solid state Nuclear Magnetic Resonance Spectroscopy (NMR) also are useful but they do not provide

specific information like the former ones. Techniques such as SIMS, XPS and Atomic Emission Spectroscopy (AES) were also proposed but they destroy the electrode's surfaces during the analysis. In the case of *in-situ* techniques, the surface films are identified under controlled potential while the electrode is in solution. Besides, all these techniques, EIS serves as an excellent tool for studying the nature and properties of the host electrodes. The impedance profiles can provide a large amount of information on the stabilization and failure of certain insertion electrodes. Different time constants are obtained for different electrochemical processes during charging process or intercalation into anode. Fig. 1.19 gives a brief interpretation of the impedance spectra obtained while charging process in graphite.
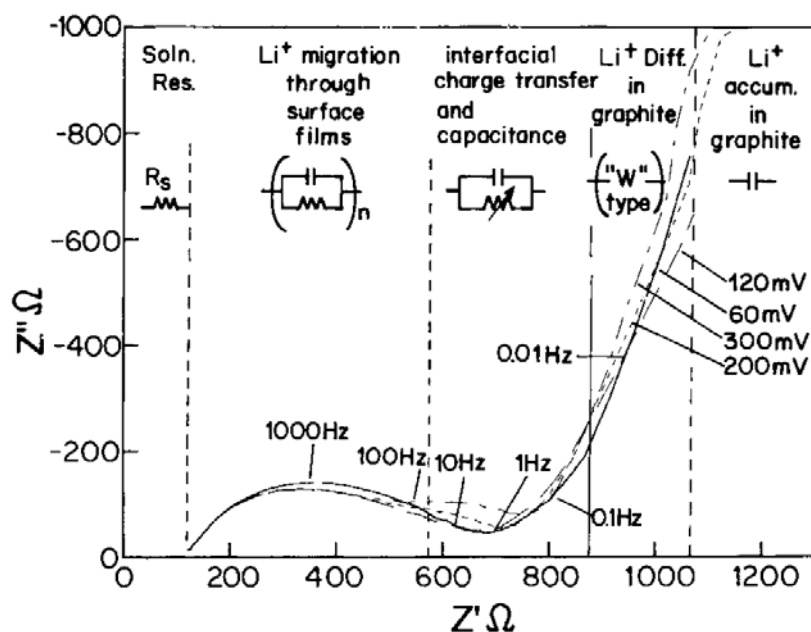
Fig. 1.19 Typical impedance spectrum measured for a graphite electrode at equilibrium potentials (adapted from 6)

1.6.3 SEI on Carbon Electrodes

Since early times, graphitic carbon materials are known to intercalate with lithium and are

being widely used in commercial Li batteries. As already told, lithium with a potential of -3.1 V serves as perfect electrode for formation of SEI layer. However, dendritic formation with non-aqueous electrolytes, unsafe operating characteristics, and poor plating efficiencies marks its disadvantages to be used as an effective anode material[12]. As an alternative, graphitic carbon serves the role of a high performance anode material, as its intercalation potential (0.20-0.02 V vs Li/Li$^+$) is close to that of Li metal, so it is assumed that like lithium metal, there must be passivation surface film formed onto the graphitic anodes on coming in contact with the organic liquid electrolytes[54].

Carbon exhibits ionic conductivity as well as electronic conductivity and has a tendency to incorporate a large number of Li ions. It can be structurally modified from highly crystalline graphites to highly disordered amorphous carbons[58]. Li ion intercalation into graphitic carbon lattices is a sequential process that involves phase transition between intercalation stages, the reason it has gained interest of researchers worldwide[6]. The study of the interesting electrochemistry of lithiation of graphite anodes can provide answers to the serious problems related to Li ion batteries concerning its safety, capacity of the electrode and the overall performance. The reason we focused on graphite as the anode material is that **a)** graphite has a high storage capacity, as Li$^+$ ion intercalate into the Van der Waals gaps above and below a graphite hexagon providing lithiated graphite with a stoichiometry of Li$_x$C$_6$ (x≤1) and **b)** it shows a flat potential profile near the redox potential of Li/Li$^+$ during charge-discharge process[12].
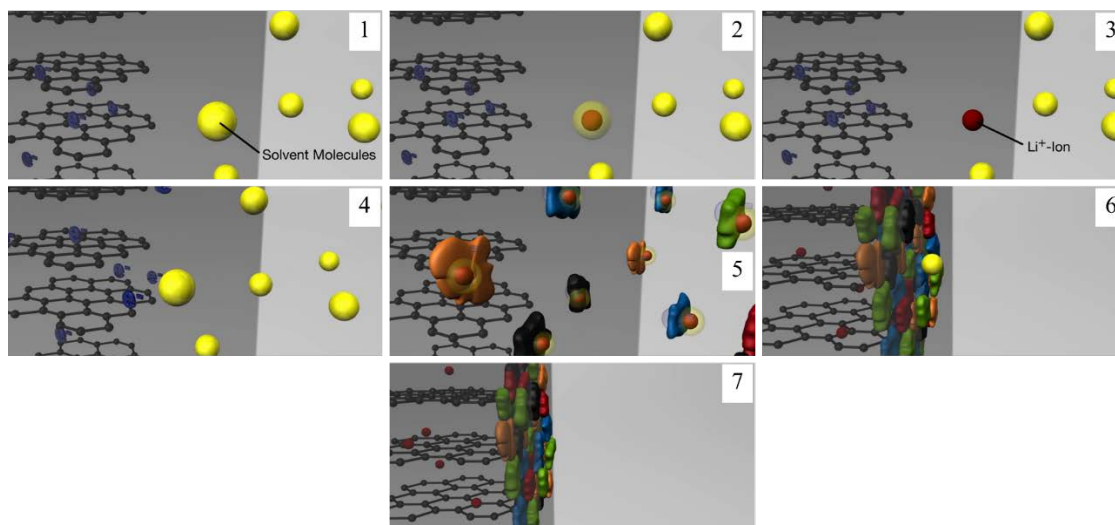
Fig 1.20 Sequence of images (1-7) corresponding to the formation of SEI layer onto graphite (*1-3: Electrolyte solvent molecules containing Li$^+$ ions travelling to graphite electrode, 4-5: electrons from graphite interact with the electrolyte solvent molecules forming their reduction products, 6-7: The reduced electrolyte products form a layer on the surface of the graphite anode allowing only Li$^+$ ions to pass through*)

The exact mechanism of the formation of SEI film is as follows:

Lithium batteries when assembled using a transition metal oxide cathode and graphitic anode are in discharged state. During the first charging cycle, organic liquid electrolytes present as the combination of solvents and salts, get reduced at the surface of the anode at a potential (1.5V-0.7 V vs Li/Li$^+$)[69], forming a passivation film on the anode surface. This surface film, termed as the Solid Electrolyte Interface (SEI) is composed of variety of salt and solvent reduction products and is a conductor of Li ions. Fig 1.20 shows a set of images corresponding to the formation of SEI layer onto graphite. It does not allow solvent molecules or electrons to pass through. This SEI film formed should be thin but stable for maintaining the passivation of the electrode. In this context, the choice of electrolyte plays a major role in the SEI layer

formation. Fig. 1.21 shows a first charge-discharge profile of a graphite electrode in 1 M $LiBF_4$ in EC/DMC solution, displaying a plateau at 0.7 V corresponding to the reduction of electrolyte and a plateau near 0.1 V corresponding to Li^+ ion intercalation.
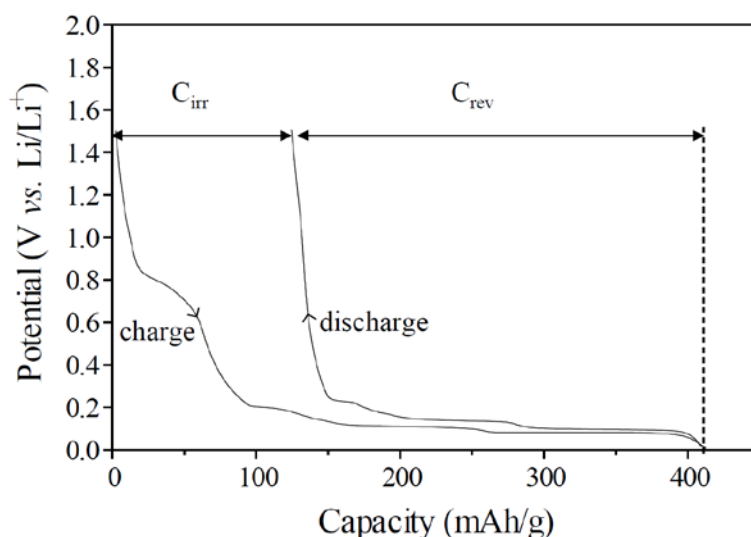
Fig. 1.21 First charge discharge cycle of graphite electrode in 1M $LiBF_4$, EC/DMC solution

SEI layer formation onto carbon anodes takes place via set of reactions that define the stages of Li^+ intercalation, as explained by D. Aurbach[6],

$$C_6 + 0.083\ Li^+ + 0.083e^- \rightleftharpoons Li_{0.083}C_6$$

$$Li_{0.083}C_6 + 0.083\ Li^+ + 0.083e^- \rightleftharpoons Li_{0.166}C_6$$

$$Li_{0.166}C_6 + 0.056\ Li^+ + 0.056e^- \rightleftharpoons Li_{0.222}C_6$$

$$Li_{0.222}C_6 + 0.278\ Li^+ + 0.278e^- \rightleftharpoons Li_{0.5}C_6$$

$$Li_{0.5}C_6 + 0.5\ Li^+ + 0.5e^- \rightleftharpoons LiC_6$$
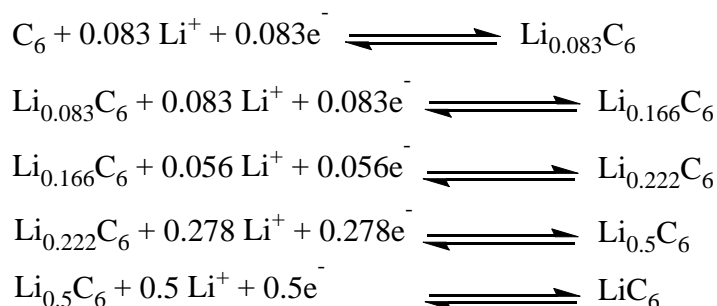
Under ambient conditions, maximum one lithium per six carbons can be intercalated corresponding to a theoretical capacity of 372 mAh/g. These different stages are usually

referred to as Stage I, stage II, stage III and stage IV. Fig. 1.22 shows different stages and structure of fully lithiated graphite.
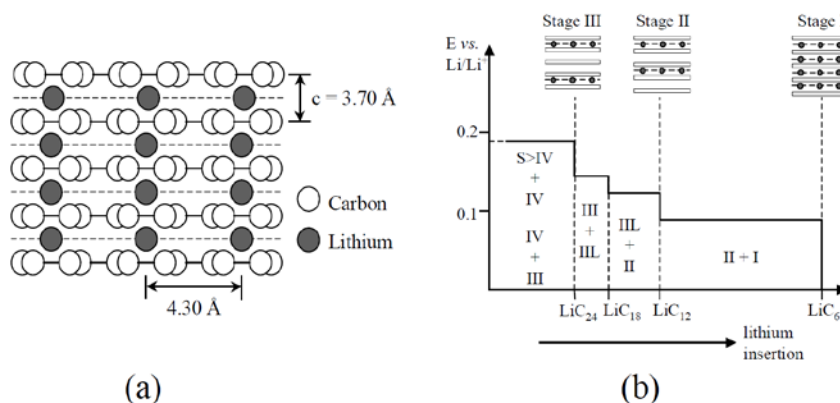
Fig. 1.22 a) Structure of LiC_6 and b) schematic potential profile of stages of Li intercalation (adapted from [13]13).

The findings on Li intercalation chemistry on carbonaceous anodes provide certain conclusions:

1. Li^+ ion intercalation in graphite occurs at low potentials reaching a stoichiometric composition of LiC_6.

2. Less ordered the carbon is, wider is the intercalation potential range.

3. The formation of SEI on carbon after the first charging cycle is similar to that on lithium metal anode.

Based on the type of carbon, type of electrolyte, and the selected active additive used, the performance, stability towards Li^+ ion intercalation and cycle life of the graphite depends.

1.7 Organoboron Compounds in Lithium Ion Batteries

Enormous amount of research analyzing the compatibility of electrolytes for Li ion

batteries as wholesome are available in literature. Solid state electrolytes with high ionic conductivity and high Li cation transference number have been designed by several research groups focusing on the safety and manufacturing aspect of LiBs. Solvent-free comb shaped poly (ethylene oxide) (PEO) polymer electrolytes show ionic conductivity around 10^{-4} Scm^{-1}. In order to obtain high ionic conductivity and high cation transference number, immobilizing the corresponding anion of the Li salt used has been considered as an effective approach. Incorporation of Lewis acidic boron with empty p-orbitals to electrolyte has shown significant immobilization of anion. Boron has a tendency to trap the anion and allows Li$^+$ ions to move freely.

1.7.1 Incorporation of Boron in Electrolytes

Research on incorporation of boron in electrolytes started in 1995 by Barthel *et al.*, with the design of a new lithium salt containing boron chelate complexes of aromatic, aliphatic diols or carboxylic acids as anions. These class of compounds were thermally, chemically and electrochemically stable, however the potential window was not sufficiently high for application in lithium ion secondary batteries[70]. Following this, Angell in 1996 reported boric esters of glycol (BEG solvents) as an alternative to the conventional organic carbonate solvents. The purpose was to design a Li$^+$ ion conducting surface film which can avoid co-intercalation of solvent molecules into graphite thereby reducing the irreversible capacity loss[71]. Subsequently in 1998, boron based anion receptors were introduced as electrolyte additives[72, 73] for LiBs. The research on polymer electrolytes also gained interest parallely and several reports by various research groups based on boron incorporation in polymer electrolytes for Li ion battery applications highlighted the scientific arena. Mehta *et al.*, in 1997, introduced anion

trapping in polymer electrolytes containing networks of boroxine rings[39, 74-76] and Angel in 2001 reported purely cation conducting polymeric electrolytes based on phenylboronic acid and discussed its ion conductive properties[77]. Matsumi *et al.*, in 2002 reported linear organoboron polymeric electrolytes based on PEO with an improved transference number of an immobilized anion electrolyte as compared to the salt-dissolved systems[78]. This continued with introduction of boric ester type electrolytes with improved electrochemical properties due to effective anion trapping[79] and organoboron π-conjugated systems to obtain high conductivity based on an ion conduction mechanism other than polymer segmental motion[80].
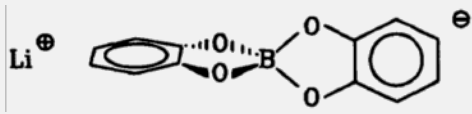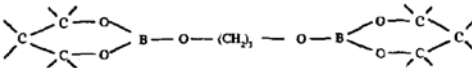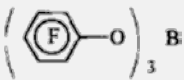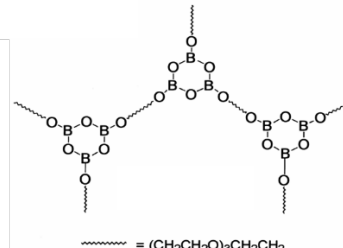
In order to further improve the conductivities, single cation conducting[81] organoboron electrolytes were proposed in the form of zwitter ionic molten salts and imidazolium type complex[82] and their conductive properties were discussed in detail. Furthermore, other organoboron electrolytes were designed via synthetic routes other than boration polymerization[83] *i.e.,* hydroboration polymerization[84], *in-situ* sol gel reaction[85], condensation reaction[86] etc., and varied anion trapping moieties other than mesitylborane[79] such as 9-borabicyclo [3.3.1]nonane (9-BBN)[84, 87], lithium mesitylhydroborate[88] for Li ion battery purpose. However, most of the work was solely concentrated on polymeric electrolytes and their modification to improve the ion conducting properties. Study on organic non-polymeric electrolytes was still untouched.
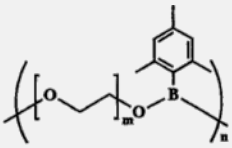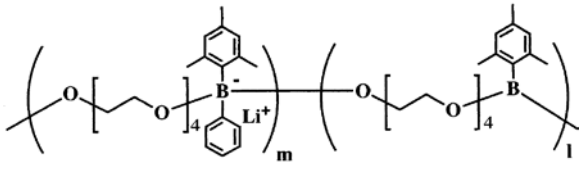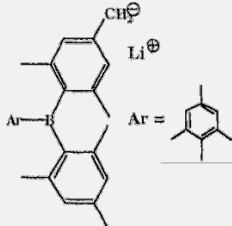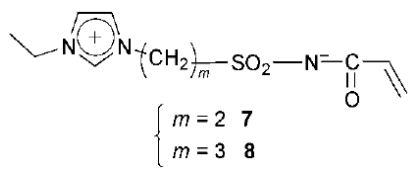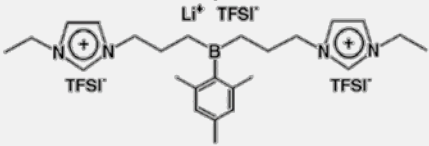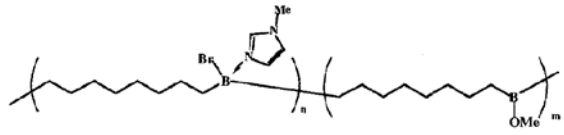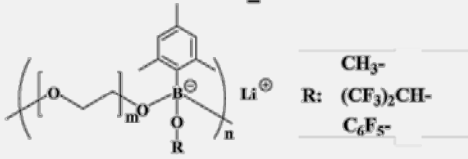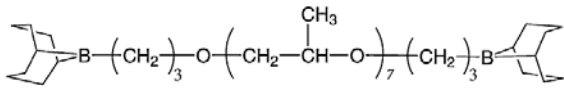
Another class of solid state electrolytes was simultaneously evolving and had gathered significant interest by now. This consisted of plastic crystals, organic liquid crystals and coordination polymers[89-93]. These class of electrolytes showed solid state non-polymeric

electrolytes with improved conducting properties, however, there are no reports focused on the incorporation of boron into these systems.

Table 1.7 summarizes the details of some of the electrolytes containing boron so far mentioned in the literature concerning their structure, ionic conductivity (σ_i)/ transference number, (t_{Li}^+) and references and Fig. 1.23 briefly shows the research on Li$^+$ ion transference numbers of various electrolytes from the year 2002 to 2015.

Table 1.7 List of boron based organic electrolytes, their structure, ionic conductivity (σ_i)/ transference number, (t_{Li}^+) and reference number

#	Structure/ name	σ_i / t_{Li}^+	Reference
1.	Lithium bis[1,2-benzenediolato(2-)-O,O']borate.	-/-	[70]
2.	BEG solvents (BEG-1)	10^{-4} Scm^{-1}/-	[71]
3.		10^{-3} Scm^{-1}/-	[72]
4.	= (CH$_2$CH$_2$O)$_3$CH$_2$CH$_2$	10^{-8}-10^{-5} Scm^{-1}/-	[76]

No.	Structure	Conductivity / t_{Li^+}	Ref.
5.		10^{-5} Scm^{-1}/ 0.35-0.39	[78]
6.		-/0.82-0.78	[79]
7.	Ar =	10^{-8} Scm^{-1}/-	[80]
8.	$m = 2$ **7** $m = 3$ **8**	10^{-5} Scm^{-1}/-	-
9.		-/0.67	[82]
10.		10^{-5} Scm^{-1}/ 0.47	[81]
11.	R: CH$_3$- (CF$_3$)$_2$CH- C$_6$F$_5$-	10^{-6}-10^{-5} Scm^{-1}/-	[88]
12.		10^{-7} Scm^{-1}/ 0.57	[84]

13.		10^{-5} Sm^{-1}/ 0.69	[94]94
14.		10^{-5} Scm^{-1}/ 0.87	[95]95
15.		10^{-4}-10^{-3} Scm^{-1}/0.16	[96]96
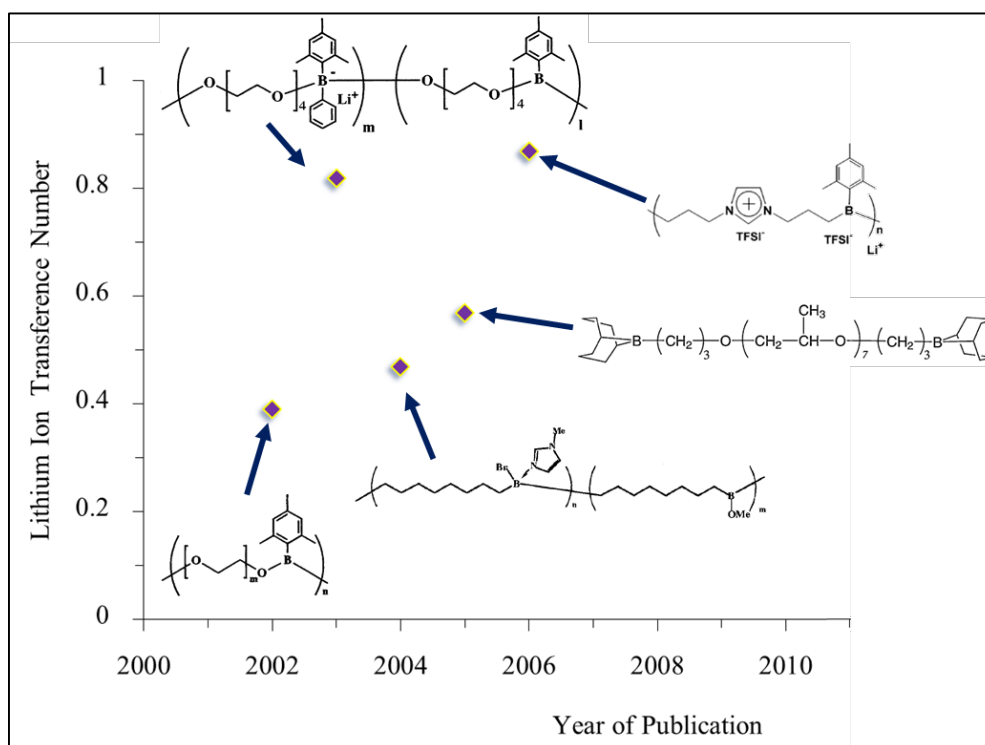
Fig. 1.23 Improvement in Li ion transference number over the period of years

1.7.2 Role of Organoboron Compounds in Carbon Electrodes

Besides electrolytes, recently, there had been several reports on boron incorporation into electrodes that resulted in enhanced capacity for lithium ion secondary batteries. Boron doping has been studied in different kinds of carbon materials ranging from graphene sheets to carbon nanotubes (CNTs)[11, 97-99] and have been studied in detail[98, 99]. Boron doping was first done on graphene for study of hydrogen adsorption[100], however it was later extended to carbon nanotubes for battery applications as the maximum capacity of CNTs that can be achieved was upto 500 mAh/g[101]. Boron doping into carbon nanotubes showed large Li adsorption energies, specifically at the favorable sites[99] and capacities 20% higher than that of graphite[102]. This method of boron doping was then extended on to single layer of graphite or graphene.

Boron enters the carbon lattice substituting carbon at one of the trigonal sites. Due to electron deficient outer shell, boron acts as an electron acceptor and produce oxidation-resistant material[103]. Doping with boron causes a shift in the Fermi level to the conduction band and modifies the electronic structure of carbon[104] by introducing defects that can be mono-vacant, di-vacant in the graphene matrix improving Li diffusion in two ways, (i) through and (ii) over (across) the graphene plane. Hence, boron doping results in high reversible capacity and improved coulombic efficiency[105]. This interesting approach has motivated various scientists in the direction of studying the effect of boron doping into graphene or graphitic materials. In 1998, Tamaki *et al.*, reported boron doped carbon fibers[106] as anode materials for lithium batteries showing capacities as high as 360 mAh/g. In 2000, Kim *et al.*, reported the structural and electrochemical properties of three different kinds of boron-doped carbon materials (powders, spheres and fibres)[107].
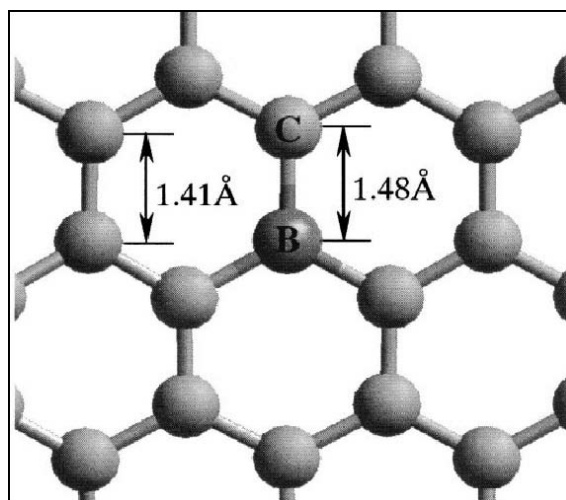
Fig. 1.24 Schematic representation of a graphene plane showing the difference in bond length between B–C and C–C bond (adapted from 108)

In the case of boron doped anodes, the voltage profiles are observed at 40 mV higher potential than natural graphite anodes. The discharging profiles of boron doped samples shows a plateau at 1.3 V corresponding to lithium insertion[11]. Boron doping helps in formation of a chemical bond between boron and carbon and the bond length of C-B bond is higher than that of C-C bond (Fig. 1.24) which facilitates the reaction of Li^+ ions with carbon leading to an intercalated graphite of $Li_{1.16}(B_{0.17}C_{0.83})_6$ compared to LiC_6 in case of graphites[108]. After establishing the doping of boron into anode materials for almost a decade, in 2011, the study of graphitized boron-doped carbon foams was produced, which focused on the influence of boron source and relationship between the amounts of boron substituted into the carbon layers[109]. Boron doped graphene (Fig. 1.25) sheets exhibit excellent properties such as improved electrical conductivity, high thermal stability of the doped graphene, better electrode/electrolyte wettability, increased interlayer distance, allowing faster Li^+ absorption.

Increased electron transport and high diffusion of Li$^+$ ions confirm the use of boron doped materials as high capacity and high power anode materials for lithium ion secondary batteries[110].
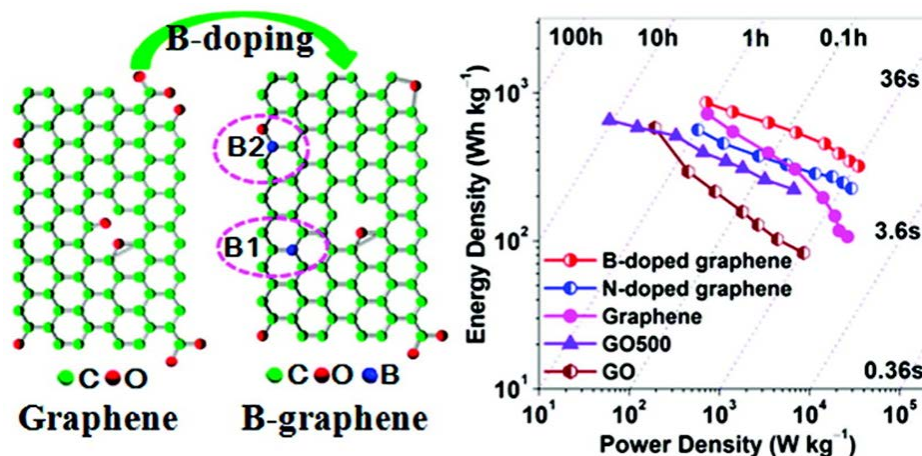
Fig. 1.25 Doping of boron into graphene and Ragone plot for graphene, graphene oxide and doped graphene (adapted from 110)

However, though boron doping results in high capacities than natural graphites, it also shows degradation in charging capacities after the 1st cycle. This can be related to presence of boron in form of boron carbides, B$_4$C, occupying the active site for lithium insertion[11].

1.7.3 Boron incorporation in Tailored Solid Electrolyte Interface (SEI)

In the case of SEI, boron incorporation has not been carried out so far. Modifications have been done on the carbon electrodes on the using conducting polymers. Conducting polymers such polythiophene[111] and polypyrrole have also contributed in this regard. Surface modification have been done onto graphitized materials via electropolymerization of thiophene and pyrrole and the electrochemical properties of the electrode then, have been widely studied. Besides other methods, surface modification via electropolymerization can be controlled by reaction potentials and time and the SEI formed in such cases are thin with lower interfacial

resistance. The polymerized layer formed onto the anodes leads to higher reversibility of lithitaion and delithiation.

1.8 Research Outlook

Abovementioned work inspires us to work towards incorporation of boron onto electrode surface and in electrolyte systems. In this research work, we aim to use this attractive approach of synthesizing single ion conducting electrolytes by anion-trapping effect of boron in three different ways.

1. Since polymer segmental motion in polymer electrolytes limits the ionic conductivity values to 10^{-3}-10^{-5} Scm^{-1}, electrolytes with increased ionic conductivity with ion conduction mechanism different than polymer electrolytes are needed. The research work deals with synthesizing low molecular weight organoboron electrolytes which does not polymerize *i.e.* single ion conducting organic cyclic electrolytes bearing boron moieties as mesitylborane. The main purpose of the work is to study the ion conduction properties of these cyclic electrolytes and their interfacial characteristics with graphitic anodes.

2. Tuning the electrode-electrolyte interfacial layer into a thin, stable and a conductive passivation film onto anodes is essential for improved performance of a battery. In this research work, we have also explored the area of chelated boron compounds in order to tune the SEI on the graphitic anodes. Chelated boron compounds such as lithium bis(oxalato)borate, LiBOB[112-116] and lithium difluoro(oxalato)borate, LiDFOB[117-120] have inherent ability to form SEI layer even in very low concentrations of the solvents used.

Such compounds result in the opening of an oxalate ring after single electron transfer reaction and initiate a polymerization reaction to form a passivation layer onto the anode (Fig. 1.25)[121].
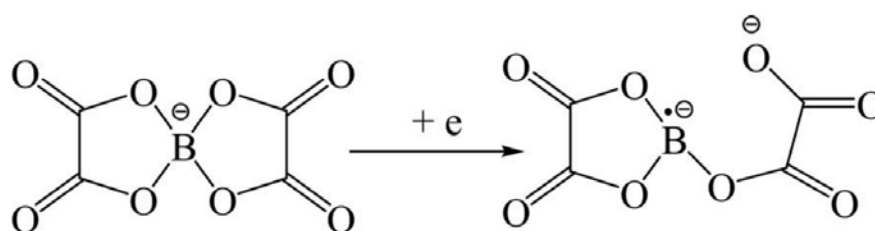
Fig. 1.25 Single electron transfer reaction of BOB⁻ anion resulting in opening of an oxalate ring

3. Interfacial layers i.e. the Solid Electrolyte interface (SEI) plays an important role in the performance of the battery. However, irreversible capacity loss due to electrolyte decomposition which wastes active lithium ion and reduces the coulombic efficiency. Further, formation of a less conductive unstable SEI layer increases the interfacial resistance and is a major drawback. One of the practical approaches to decrease the irreversible capacity loss is surface modification of the anode. Various boron compounds have been developed in the past that reduce the electrode-electrolyte interfacial resistance[103]. Hence, we aim to incorporate boron in an electronically conducting polymer and carrying out the surface modification of the anodes thereby helping in reduction of the interfacial resistance.

Hence, the present work aims to synthesize materials at a three-fold utilization to

1. Enhance the overall capacity of graphite electrodes.

2. Improve the cycle life and performance of a battery.

3. Study the interfacial characteristics on graphite electrodes using.

4. Modify the active surface of the carbon electrodes and improve their electrode characteristics.

References

1.   J. M. Tarascon and M. Armand, *Nature*, 2001, **414**, 359-367.

2.   D. Aurbach, E. Zinigrad, Y. Cohen and H. Teller, *Solid State Ionics*, 2002, **148**, 405-416.

3.   L. G. Lu, X. B. Han, J. Q. Li, J. F. Hua and M. G. Ouyang, *J Power Sources*, 2013, **226**, 272-288.

4.   J. W. Wen, Y. Yu and C. H. Chen, *Mater Express*, 2012, **2**, 197-212.

5.   D. H. Doughty, *Sampe J*, 1996, **32**, 75-81.

6.   D. Aurbach, B. Markovsky, I. Weissman, E. Levi and Y. Ein-Eli, *Electrochim Acta*, 1999, **45**, 67-86.

7.   S. H. Lee, I. S. Jo and J. Kim, *Surf Interface Anal*, 2014, **46**, 570-576.

8.   H. Shi, J. Barker, M. Y. Saidi and R. Koksbang, *J Electrochem Soc*, 1996, **143**, 3466-3472.

9.   J. J. Chen, *Materials*, 2013, **6**, 156-183.

10.   M. Wakihara, *Mat Sci Eng R*, 2001, **33**, 109-134.

11.   M. Endo, C. Kim, K. Nishimura, T. Fujino and K. Miyashita, *Carbon*, 2000, **38**, 183-197.

12.   T. Piao, S. M. Park, C. H. Doh and S. I. Moon, *J Electrochem Soc*, 1999, **146**, 2794-2798.

13.   M. Winter, J. O. Besenhard, M. E. Spahr and P. Novak, *Adv Mater*, 1998, **10**, 725-763.

14.   D. Billaud, F. X. Henry and P. Willmann, *J Power Sources*, 1995, **54**, 383-388.

15.   P. Novak, F. Joho, M. Lanz, B. Rykart, J. C. Panitz, D. Alliata, R. Kotz and O. Haas, *J Power Sources*, 2001, **97-8**, 39-46.

16.   X. H. Hou, S. J. Hu, W. S. Li, L. Z. Zhao, H. W. Yu and C. L. Tan, *Acta Phys Sin-Ch Ed*, 2008, **57**, 2374-2379.

17.   M. D. Fleischauer, M. N. Obrovac and J. R. Dahn, *J Electrochem Soc*, 2008, **155**, A851-A854.

18.   H. S. Kim, M. G. So and S. M. Lee, *B Korean Chem Soc*, 2008, **29**, 2441-2444.

19.   S. D. Beattie, D. Larcher, M. Morcrette, B. Simon and J. M. Tarascon, *J Electrochem Soc*, 2008, **155**, A158-A163.

20.   J. Hassoun, F. Bonaccorso, M. Agostini, M. Angelucci, M. G. Betti, R. Cingolani, M. Gemmi, C. Mariani, S. Panero, V. Pellegrini and B. Scrosati, *Nano Lett*, 2014, **14**, 4901-4906.

21.   Y. X. Yu, *Phys Chem Chem Phys*, 2013, **15**, 16819-16827.

22.   J. Hassoun and B. Scrosati, *J Electrochem Soc*, 2015, **162**, A2582-A2588.

23.   E. Levi, M. D. Levi, G. Salitra, D. Aurbach, R. Oesten, U. Heider and L. Heider, *Solid State Ionics*, 1999, **126**, 97-108.

24.   D. Aurbach, M. D. Levi, E. Levi, H. Teller, B. Markovsky, G. Salitra, U. Heider and L. Heider, *J Electrochem Soc*, 1998, **145**, 3024-3034.

25.   Z. Wei, H. X. Han, A. S. Filatov and E. V. Dikarev, *Chem Sci*, 2014, **5**, 813-818.

26.   A. Manthiram, *J Phys Chem Lett*, 2011, **2**, 373-373.

27.   P. G. Bruce, B. Scrosati and J. M. Tarascon, *Angew Chem Int Edit*, 2008, **47**, 2930-2946.

28.   G. E. Blomgren, *J Power Sources*, 2003, **119**, 326-329.

29.   V. Aravindan, J. Gnanaraj, S. Madhavi and H. K. Liu, *Chem-Eur J*, 2011, **17**, 14326-14346.

30.   Z. G. Xue, D. He and X. L. Xie, *J Mater Chem A*, 2015, **3**, 19218-19253.

31.   M. Ishikawa, T. Sugimoto, M. Kikuta, E. Ishiko and M. Kono, *J Power Sources*, 2006, **162**, 658-662.

32.   J. Reiter and M. Nadherna, *Electrochim Acta*, 2012, **71**, 22-26.

33.   M. A. Taige, D. Hilbert and T. J. S. Schubert, *Z Phys Chem*, 2012, **226**, 129-139.

34.   I. Osada, H. de Vries, B. Scrosati and S. Passerini, *Angew Chem Int Edit*, 2016, **55**, 500-513.

35.   Y. S. Ye, J. Rick and B. J. Hwang, *J Mater Chem A*, 2013, **1**, 2719-2743.

36.   K. Angenendt and P. Johansson, *J Phys Chem B*, 2011, **115**, 7808-7813.

37.   P. X. Yang, L. Liu, L. B. Li, J. Hou, Y. P. Xu, X. F. Ren, M. Z. An and N. Li, *Electrochim Acta*, 2014, **115**, 454-460.

38.   A. M. Stephan, *Eur Polym J*, 2006, **42**, 21-42.

39.   M. A. Mehta and T. Fujinami, *Solid State Ionics*, 1998, **113**, 187-192.

40.   M. Marcinek, J. Syzdek, M. Marczewski, M. Piszcz, L. Niedzicki, M. Kalita, A. Plewa-Marczewska, A. Bitner, P. Wieczorek, T. Trzeciak, M. Kasprzyk, P. Lezak, Z. Zukowska,

A. Zalewska and W. Wieczorek, *Solid State Ionics*, 2015, **276**, 107-126.

41.   B. M. Wiers, M. L. Foo, N. P. Balsara and J. R. Long, *J Am Chem Soc*, 2011, **133**, 14522-14525.

42.   M. Wakihara, Y. Kadoma, N. Kumagai, H. Mita, R. Araki, K. Ozawa and Y. Ozawa, *J Solid State Electr*, 2012, **16**, 847-855.

43.   M. Park, X. C. Zhang, M. D. Chung, G. B. Less and A. M. Sastry, *J Power Sources*, 2010, **195**, 7904-7929.

44.   K. Xu, *Chem Rev*, 2014, **114**, 11503-11618.

45.   M. Petrowsky and R. Frech, *J Phys Chem B*, 2009, **113**, 5996-6000.

46.   R. V. Chamberlin, *Phys Rev B*, 1993, **48**, 15638-15645.

47.   C. T. Imrie, M. D. Ingram and G. S. McHattie, *Adv Mater*, 1999, **11**, 832-+.

48.   Z. Gadjourova, Y. G. Andreev, D. P. Tunstall and P. G. Bruce, *Nature*, 2001, **412**, 520-523.

49.   J. Sakuda, E. Hosono, M. Yoshio, T. Ichikawa, T. Matsumoto, H. Ohno, H. S. Zhou and T. Kato, *Adv Funct Mater*, 2015, **25**, 1206-1212.

50.   A. Yoshino, *Angew Chem Int Edit*, 2012, **51**, 5798-5800.

51.   N. S. Choi, Z. H. Chen, S. A. Freunberger, X. L. Ji, Y. K. Sun, K. Amine, G. Yushin, L. F. Nazar, J. Cho and P. G. Bruce, *Angew Chem Int Edit*, 2012, **51**, 9994-10024.

52.   N. Loeffler, D. Bresser, S. Passerini and M. Copley, *Johnson Matthey Tech*, 2015, **59**, 34-44.

53.   R. L. Patel, H. Xie, J. Park, H. Y. Asl, A. Choudhury and X. H. Liang, *Adv Mater Interfaces*, 2015, **2**.

54.   K. Xu, *Energies*, 2010, **3**, 135-154.

55.   R. R. Unocic, X. G. Sun, R. L. Sacci, L. A. Adamczyk, D. H. Alsem, S. Dai, N. J. Dudney and K. L. More, *Microsc Microanal*, 2014, **20**, 1029-1037.

56.   A. M. Andersson, D. P. Abraham, R. Haasch, S. MacLaren, J. Liu and K. Amine, *J Electrochem Soc*, 2002, **149**, A1358-A1369.

57.   P. Lu, C. Li, E. W. Schneider and S. J. Harris, *J Phys Chem C*, 2014, **118**, 896-903.

58.   A. M. Andersson and K. Edstrom, *J Electrochem Soc*, 2001, **148**, A1100-A1109.

59.   S. S. Zhang, M. S. Ding, K. Xu, J. Allen and T. R. Jow, *Electrochem Solid St*, 2001, **4**,

A206-A208.

60.   D. Aurbach, K. Gamolsky, B. Markovsky, G. Salitra, Y. Gofer, U. Heider, R. Oesten and M. Schmidt, *J Electrochem Soc*, 2000, **147**, 1322-1331.

61.   D. Aurbach, B. Markovsky, G. Salitra, E. Markevich, Y. Talyossef, M. Koltypin, L. Nazar, B. Ellis and D. Kovacheva, *J Power Sources*, 2007, **165**, 491-499.

62.   M. Nie and B. L. Lucht, *J Electrochem Soc*, 2014, **161**, A1001-A1006.

63.   M. Ue, *J Electrochem Soc*, 1994, **141**, 3336-3342.

64.   D. Aurbach, Y. Einely and A. Zaban, *J Electrochem Soc*, 1994, **141**, L1-L3.

65.   A. Schechter, D. Aurbach and H. Cohen *Langmuir*, 1999, **15**, 3334-3342.

66.   E. Levi, M. D. Levi, G. Salitra, D. Aurbach, R. Oesten, U. Heider and L. Heider, *Solid State Ionics*, 1999, **126**, 109-119.

67.   D. Aurbach and Y. Cohen, *Electrochem Solid St*, 1999, **2**, 16-18.

68.   Y. Cohen and D. Aurbach, *Rev Sci Instrum*, 1999, **70**, 4668-4675.

69.   J. O. Besenhard, M. Winter, J. Yang and W. Biberacher, *J Power Sources*, 1995, **54**, 228-231.

70.   J. Barthel, M. Wuhr, R. Buestrich and H. J. Gores, *J Electrochem Soc*, 1995, **142**, 2527-2531.

71.   S. S. Zhang and C. A. Angell, *J Electrochem Soc*, 1996, **143**, 4047-4053.

72.   H. S. Lee, X. Q. Yang, C. L. Xiang, J. McBreen and L. S. Choi, *J Electrochem Soc*, 1998, **145**, 2813-2818.

73.   X. Sun, H. S. Lee, X. Q. Yang and J. McBreen, *Electrochem Solid St*, 2002, **5**, A248-A251.

74.   M. A. Mehta and T. Fujinami, *Chem Lett*, 1997, DOI: DOI 10.1246/cl.1997.915, 915-916.

75.   M. A. Mehta, T. Fujinami and T. Inoue, *J Power Sources*, 1999, **81**, 724-728.

76.   M. A. Mehta, T. Fujinami, S. Inoue, K. Matsushita, T. Miwa and T. Inoue, *Electrochim Acta*, 2000, **45**, 1175-1180.

77.   X. G. Sun and C. A. Angell, *Electrochim Acta*, 2001, **46**, 1467-1473.

78.   N. Matsumi, K. Sugai and H. Ohno, *Macromolecules*, 2002, **35**, 5731-5733.

79.   N. Matsumi, K. Sugai and H. Ohno, *Macromolecules*, 2003, **36**, 2321-2326.

80.   N. Matsumi, M. Nakashiba and H. Ohno, *Polym Bull*, 2003, **50**, 259-264.

81.   N. Matsumi, T. Mizumo and H. Ohno, *Polym Bull*, 2004, **51**, 389-394.

82.   N. Matsumi, M. Miyake and H. Ohno, *Chem Commun*, 2004, DOI: 10.1039/b408839e, 2852-2853.

83.   Y. Chujo, I. Tomita and T. Saegusa, *Polym J*, 1991, **23**, 743-746.

84.   T. Mizumo, K. Sakamoto, N. Matsumi and H. Ohno, *Electrochim Acta*, 2005, **50**, 3928-3933.

85.   T. Mizumo, T. Watanabe, N. Matsumi and H. Ohno, *Polym Advan Technol*, 2008, **19**, 1445-1450.

86.   N. Matsumi, Y. Nakamura, K. Aoi, T. Watanabe, T. Mizumo and H. Ohno, *Polym J*, 2009, **41**, 437-441.

87.   T. Mizumo, K. Sakamoto, N. Matsumi and H. Ohno, *Chem Lett*, 2004, **33**, 396-397.

88.   N. Matsumi, K. Sugai, K. Sakamoto, T. Mizumo and H. Ohno, *Macromolecules*, 2005, **38**, 4951-4954.

89.   R. Kanno and M. Maruyama, *J Electrochem Soc*, 2001, **148**, A742-A746.

90.   T. Kato, N. Mizoshita and K. Kishimoto, *Angew Chem Int Edit*, 2006, **45**, 38-68.

91.   R. L. Kerr, S. A. Miller, R. K. Shoemaker, B. J. Elliott and D. L. Gin, *J Am Chem Soc*, 2009, **131**, 15972-+.

92.   J. Sakuda, M. Yoshio, T. Ichikawa, H. Ohno and T. Kato, *New J Chem*, 2015, **39**, 4471-4477.

93.   T. Kato, *Angew Chem Int Edit*, 2010, **49**, 7847-7848.

94.   A. Narita, W. Shibayama, K. Sakamoto, T. Mizumo, N. Matsumi and H. Ohno, *Chem Commun*, 2006, DOI: 10.1039/b517019b, 1926-1928.

95.   N. Matsumi, K. Sugai, M. Miyake and H. Ohno, *Macromolecules*, 2006, **39**, 6924-6927.

96.   K. S. Smaran, R. Vedarajan and N. Matsumi, *Int J Hydrogen Energ*, 2014, **39**, 2936-2942.

97.   P. L. Gai, O. Stephan, K. McGuire, A. M. Rao, M. S. Dresselhaus, G. Dresselhaus and C. Colliex, *J Mater Chem*, 2004, **14**, 669-675.

98.   I. Mukhopadhyay, N. Hoshino, S. Kawasaki, F. Okino, W. K. Hsu and H. Touhara, *J Electrochem Soc*, 2002, **149**, A39-A44.

99.   Z. Zhou, J. J. Zhao, X. P. Gao, Z. F. Chen, J. Yan, P. V. Schleyer and M. Morinaga, *Chem Mater*, 2005, **17**, 992-1000.

100.   R. H. Miwa, T. B. Martins and A. Fazzio, *Nanotechnology*, 2008, **19**.

101.   A. S. Claye, J. E. Fischer, C. B. Huffman, A. G. Rinzler and R. E. Smalley, *J Electrochem Soc*, 2000, **147**, 2845-2852.

102.   B. M. Way and J. R. Dahn, *J Electrochem Soc*, 1994, **141**, 907-912.

103.   G. M. Swain and R. Ramesham, *Anal Chem*, 1993, **65**, 345-351.

104.   D. W. Wang, F. Li, Z. G. Chen, G. Q. Lu and H. M. Cheng, *Chem Mater*, 2008, **20**, 7195-7200.

105.   R. P. Hardikar, D. Das, S. S. Han, K. R. Lee and A. K. Singh, *Phys Chem Chem Phys*, 2014, **16**, 16502-16508.

106.   M. Endo, C. Kim, T. Karaki, T. Tamaki, Y. Nishimura, M. J. Matthews, S. D. M. Brown and M. S. Dresselhaus, *Phys Rev B*, 1998, **58**, 8991-8996.

107.   C. Kim, T. Fujino, T. Hayashi, M. Endo and M. S. Dresselhaus, *J Electrochem Soc*, 2000, **147**, 1265-1270.

108.   Y. J. Chae, S. O. Kim and J. K. Lee, *J Alloy Compd*, 2014, **582**, 420-427.

109.   E. Rodriguez, I. Camean, R. Garcia and A. B. Garcia, *Electrochim Acta*, 2011, **56**, 5090-5094.

110.   Z. S. Wu, W. C. Ren, L. Xu, F. Li and H. M. Cheng, *Acs Nano*, 2011, **5**, 5463-5471.

111.   T. Doi, K. Takeda, T. Fukutsuka, Y. Iriyama, T. Abe and Z. Ogumi, *Carbon*, 2005, **43**, 2352-2357.

112.   Z. H. Chen, W. Q. Lu, J. Liu and K. Amine, *Electrochim Acta*, 2006, **51**, 3322-3326.

113.   W. H. Pu, X. M. He, L. Wang, C. R. Wan and C. Y. Jiang, *Prog Chem*, 2006, **18**, 1703-1709.

114.   K. Xu, S. S. Zhang, U. Lee, J. L. Allen and T. R. Jow, *J Power Sources*, 2005, **146**, 79-85.

115.   K. Xu, S. S. Zhang, T. R. Jow, W. Xu and C. A. Angell, *Electrochem Solid St*, 2002, **5**, A26-A29.

116.   C. Taubert, M. Fleischhammer, M. Wohlfahrt-Mehrens, U. Wietelmann and T. Buhrmester, *J Electrochem Soc*, 2010, **157**, A721-A728.

117.   E. Zygadlo-Monikowska, Z. Florjanczyk, P. Kubisa, T. Biedron, A. Tomaszewska, J. Ostrowska and N. Langwald, *J Power Sources*, 2010, **195**, 6202-6206.

118.   Z. H. Chen, J. Liu and K. Amine, *Electrochem Solid St*, 2007, **10**, A45-A47.

119.   V. Aravindan, P. Vickraman and K. Krishnaraj, *Polym Int*, 2008, **57**, 932-938.

120.   J. L. Allen, S. D. Han, P. D. Boyle and W. A. Henderson, *J Power Sources*, 2011, **196**, 9737-9742.

121.   Y. Qin, Z. H. Chen, J. Liu and K. Amine, *Electrochem Solid St*, 2010, **13**, A11-A14.

Chapter 2

Cyclic Boric Ester Type Crystalline Electrolyte Derived from Ethylene Glycol

Abstract

Conduction mechanisms in SPEs of Li ion batteries have always been a concern due to their theoretical limitation in conductivity value. In an attempt to increase the ionic conductivity of solid state electrolytes, used in lithium ion secondary batteries (LiBs), we studied the synthesis and conductive properties of a low molecular weight cyclic organoboron crystalline electrolyte. This electrolyte was expected to show better electrochemical properties than other solid polymer electrolytes. The electrolyte was prepared by a dehydrocoupling reaction under inert atmosphere at room temperature. Since the final product was crystalline in nature, to study its ion conducting properties was interesting and important. For doping with LiTFSI salt, two different methods were employed, i.e. facile grinding of the crystalline sample with lithium salt under nitrogen atmosphere and conventional method of solvent dissolution and evaporation under vacuum. The electrochemical properties were studied under specific composition of Li salt. The presence of crystallinity in the electrolyte can be considered as an important factor behind the high ionic conductivity and high lithium ion transference number in an all solid electrolyte of this type. The conduction mechanism can be associated with the formation of regulated ion conductive path (ionic channel) templated by crystalline boron compound along with the effective trapping of the TFSI$^-$ anions by the vacant p-orbitals of boron. Charge-discharge properties of electrolyte were carried out in anodic half-cell configuration.

2.1 Introduction

Organic carbonate solvents used as the conventional liquid electrolytes[1] have been employed in commercial lithium ion batteries (LiBs) due to their high ionic conductivities (1.7-11.1 Scm^{-1}) and practical usage at ambient temperature[2]. Their low viscosities and impressive ability to form a stable and conductive SEI adds to their advantage as the commercial battery electrolytes. However, there were demerits such as flammability of solvents (flash point < than 39 ^{o}C), reaction of Li-salts with the other materials in the electrolyte and impurities such as water, instability at high temperatures and failure of the solvent mixtures in working at both low and high temperatures. Hence, an alternative with a simple insertion procedure of the electrolyte during the manufacture of LiBs were the two main reasons which triggered the use of Solid Polymer Electrolyte (SPE) in LiBs[3, 4]. SPEs, though provide advantages such as simple design, resistance to shock and vibration, easy film formation, better processability, resistance to pressure and temperature variations, cost-effectiveness and lighter weight, they suffer from limitations ranging from poor ionic conductivity to low lithium ion transference number etc[5, 6].

In this context, various types of SPEs broadly classified as gel-type polymers[7, 8], solvent free polymers[7], inorganic crystalline compounds[9] and inorganic glasses were discovered and investigated for their use in lithium ion batteries. These polymer electrolytes in general showed higher ionic conductivity and the ease of processability when compared to the crystalline electrolytes and hence, are being studied extensively for the use in LiBs. In these organic polymer electrolytes, segmental motion of polymer chains is considered responsible for the transport of ions[10]. Formation or breaking of co-ordination sphere of solvated ions lead to free

space for ions to diffuse under the influence of electric field[11]. But, ion conduction require local relaxation and segmental motion that occurs above the glass transition temperature[12, 13]. And hence, temperature restriction in cation mobility leads to a theoretical limitation in ionic conductivity based on the segmental motion that has been predicted to be 10^{-3} to 10^{-5} Scm^{-1}. As already discussed, this value of ionic conductivity is couple of orders lower as compared to its liquid counterpart.

In order to override the limitation caused due to segmental motion in SPE and to exceed the theoretical limit, several reports were produced informing about electrolytes. The need to seek for an altogether new ion conductive mechanism[14-16] that is different from ordinary polymer electrolytes led to the development of several novel and interesting materials. Ohno *et al.* for the first time, in 2003[17], demonstrated the agility in ion conduction mechanism by designing liquid crystals[17-19] based on long alkyl chain ionic liquids. The authors observed unusually high ionic conductivity due to the presence of liquid crystalline smectic phase which facilitated the passage of ions through self-assembled channels. On the other hand, coordination polymers[20] are reported to conduct through long nano channels formed by the self-assembly of metal centers incorporated in a molecular backbone[21]. Another material of interest is the inorganic amorphous glassy electrolyte. A single cation conduction in inorganic glassy material has been reported as early as 1986 by Angell. The report claimed the conduction in amorphous conducting glassy materials to be high because the mode of ion conduction relaxation was decoupled from the mode of structural relaxation and these systems were termed as the decoupled systems. However, the main problem associated with crystalline or amorphous glassy electrolytes are the cumbersome processing experienced during their manufacture[22].

Hence, a material having the combined property of the ease of handling as in polymer electrolyte and the segmental motion independent ionic conductivity as in amorphous glass would prove to be a beneficial electrolyte for LiBs.

With the development in synthetic organic chemistry, alternative designs of ion conduction were explored. For instance, in 2011, inorganic crystalline electrolytes[9] such as lithium ion super conductors were projected as major competitors to the organic electrolytes with an ionic conductivity of 10^{-3} S cm^{-1} at 50–80 °C. As another[23, 24] unique approach, Leclerc *et al.*[25] reported that anion doped π-conjugated systems without any radical carrier species exhibited high conductivity. However, electronic conduction was not prohibited in their systems and it was believed that lithium ions were attached to the main chains, and their high mobility could be due to an interaction with the delocalized anion on π-conjugated polymers. Recently metal organic frameworks[26-28] have also gathered significant attention, though mostly as electrode materials[29, 30]. However, the use of metal organic frameworks as electrolyte materials has been reported by Wiers *et al.*,[31] who said that lithium alkoxide based MOFs can lead to high ionic conductivity at ambient temperatures as open metal centres can bind to the anions leaving the Li$^+$ ions free to move along the channels. In order to override the limitation caused due to segmental motion in ordinary SPEs and to exceed the theoretical limit, there is a need to seek an altogether new ion conductive mechanism that is different from ordinary polymer electrolytes. The electrolyte can be a single ionic conductor in order to enhance the ionic conductivity and Li ion transference number. In this context, recent approach of incorporating organoboron electrolytes with an idea of immobilizing the anion serves excellently. There are various boron based salts and electrolytes (as discussed in Chapter 1, Section 1.7) that are used

effectively in the Li ion battery. However most of these organoboron electrolytes are polymeric in nature. These organoboron SPEs show low ionic conductivity as the ion conduction in them occur via polymer segmental motion. Hence, the aforementioned demand for alternate electrolyte along with the recent trend in utilization of organoboron compounds in electrolyte, led us to design a new crystalline cyclic organoboron compound for lithium ion conduction.

2.2 Objective of Research

This research work deals with the designing of novel low molecular weight solid organoboron electrolyte with an aim to study its ion conduction properties and conduction mechanism in detail. This chapter details an anomalous ion conductive behavior observed in the ionic conductivity of the crystalline low molecular weight organoboron electrolyte.

2.3 Experimental

Materials and Instruments

Dehydrated ethylene glycol was purchased from WAKO Co. Ltd. and used as received. Hexane, for washing the product, was purchased from WAKO Co. Ltd. and was used as received. Lithium bis(triflouromethanesulfonyl)imide, used for doping with the crystalline compound, was procured from Kanto Chemicals. NMR spectroscopic analysis was done by using Bruker model Avance III 400. IR spectroscopic analysis was done using JASCO FT/IR-4100. Thermogravimetric analysis was done by Evans Analytical Group (EAG). Raman spectroscopic analysis was done using Raman scattering equipment of Horiba, Jobin-Yvon make; model T64000. TEM micrographs were obtained using Transmission Electron Microscope, Hitachi H-7650. Single Crystal XRD (X-Ray Diffraction) was measured in IIT-M (Indian Institute of Technology-Madras), Chennai, India.

Ionic conductivity was measured with a complex-impedance gain-phase analyzer Solartron model 1260, under the frequency range from 0.1 Hz to 1 MHz using an AC amplitude of 100 mV over a temperature range of 30-60 $^{\circ}$C. The sample was sandwiched between two gold-coated blocking electrodes. Prior to the experiment all the samples were thoroughly dried under reduced pressure at room temperature. The temperature dependence of ionic conductivity was studied over a range of 30-60 $^{\circ}$C at an interval of 3 $^{\circ}$C between two consecutive temperatures. However, all the ionic conductivities mentioned further, are reported at 51 $^{\circ}$C. Li^{+} ion measurements were done by Evans method explained in section 1.4.3.1. DC current measurements were done on a Potentiostat/ Galvanostat of Princeton Applied Research; model

Versastat-3 with an applied constant potential of 30 mV and AC impedance analysis for measuring the charge transfer resistance before and after DC polarization was carried out with the same instrument with an AC amplitude of 10 mV. Potential Window measurement was done using Potentiostat/ Galvanostat made by Princeton Applied Research model Versastat-3 by LSV technique in a beaker type cell (section 2.4.2.3).

Preparation of cyclic crystalline product:

To mesitylborane[32, 33] (1.42g, 0.0107moles), equimolar amount of dehydrated ethylene glycol (0.598 mL, 0.0107 moles) was added at 0 °C and the reaction mixture was kept for stirring at room temperature for 5 hours under N_2 atmosphere (Scheme 1). The resulting mixture was washed with hexane several times and was dried under vacuum for 3 hours to obtain crystalline white powder as the product. The final product was recrystallized using hexane to obtain needle shaped crystals. Fig. 2.1 shows the image of needle crystals and further, formed single crystal of **1**.
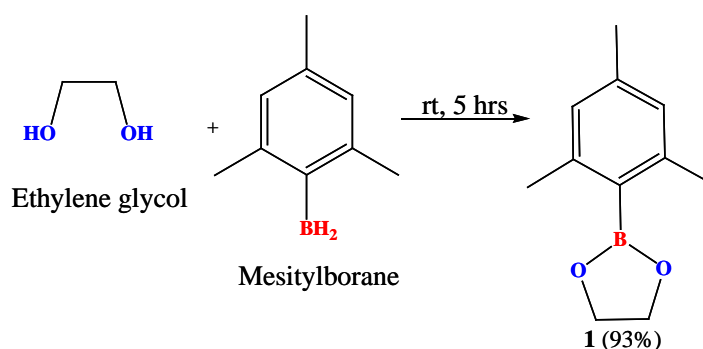
Scheme 1
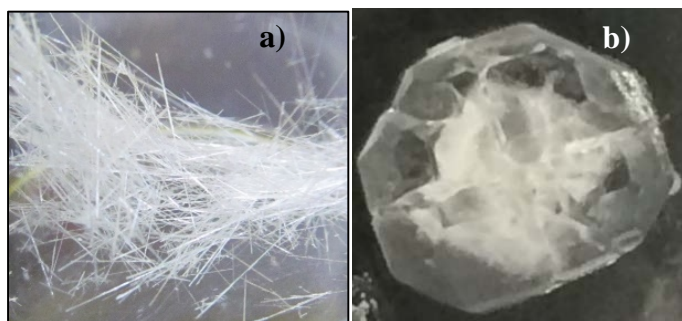
Fig. 2.1 a) needle crystal image of **1** and b) Single crystal image of **1**

2.4 Results and Discussion

2.4.1   Characterization of Cyclic Crystalline Product

2.4.1.1 NMR Spectroscopy

The synthesized low molecular weight cyclic organoboron electrolyte, **1** (EGMB) was characterized by ^{11}B-NMR in DMSO-d_6 at 400 MHz showing a peak at 31.3 ppm referring to incorporation of boron as a boric ester (Fig. 2.2 a). A single peak in ^{11}B-NMR confirmed the presence of a single pure environment of boron. Further, ^{1}H-NMR confirmed the complete structure of **1**(EGMB). The absence of broad peaks and presence of sharp peaks along with appropriate proton integrals were also in accord with the formation of cyclic structure of **1** (EGMB) (Fig. 2.2 b)**.** [^{11}BNMR (DMSO-d_6)]: 31.3 ppm; [^{1}HNMR (400MHz, DMSO-d_6): 6.79-6.72(phenyl ring protons), 4.30(-CH$_2$- groups of ethylene glycol), 3.33 (H$_2$O), 2.50 (DMSO-d_6), 2.27-2.08 (-CH$_3$ protons of mesityl group)].
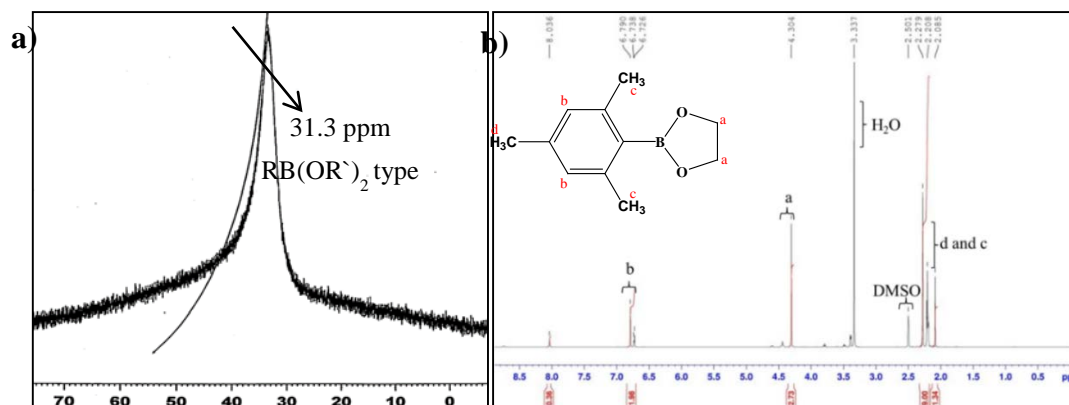
Fig. 2.2 a) ^{11}B-NMR of **1** in DMSO-d_6 b) ^{1}H-NMR of **1** in DMSO-d_6

2.4.1.2 Thermogravimetric Analysis

TGA was done under argon atmosphere between 30 ºC to 300 ºC at the rate of

10 ºC/min. TGA analysis of the cyclic organoboron electrolyte showed that the compound is

thermally stable up to 100 ºC (Fig. 2.3).
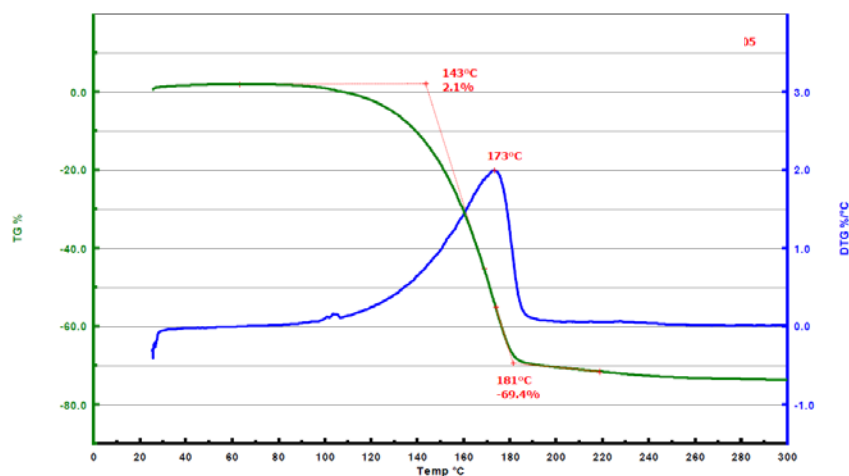
Fig. 2.3 TGA profile of **1**

2.4.1.3 Raman Spectroscopy (Theoretical and Experimental)

Raman spectrum was also studied under 531 nm laser beam. The Raman spectrum obtained experimentally (Fig. 2.4) was confirmed through a simulated spectrum for an optimized structure of **1** (EGMB) using Gaussian 09 software with a density functional theory (DFT) calculations using a basis set of B3LYP-6-311G.
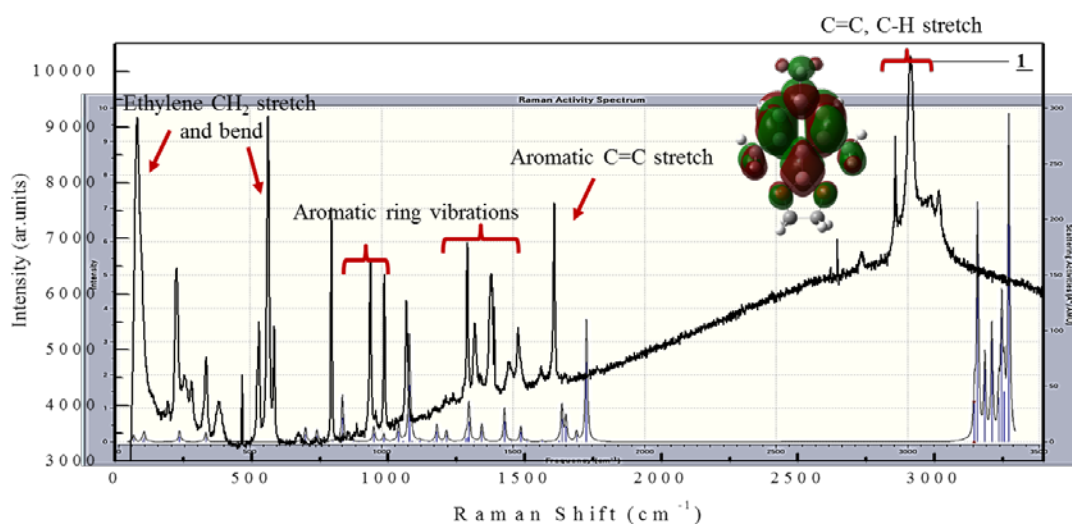
Fig. 2.4 Raman Spectrum of **1** under 531 nm merged with Gaussian09 simulated Raman Spectrum for an optimized structure of **1** (inset: optimized structure of **1**)

The observed Raman frequencies are listed below:

2950 – 3000 cm^{-1}, C=C, C-H (alkyl free) vibrations; 1580- 1620 cm^{-1}, aromatic $CH_2=CH_2$ stretch; 1350 -1450 cm^{-1}, aromatic ring vibrations; 950 – 1000 cm^{-1}, aromatic ring vibrations; 50 cm^{-1} and 550 cm^{-1}, ethylene CH_2 stretch and bend.

2.4.1.4 IR Spectrum
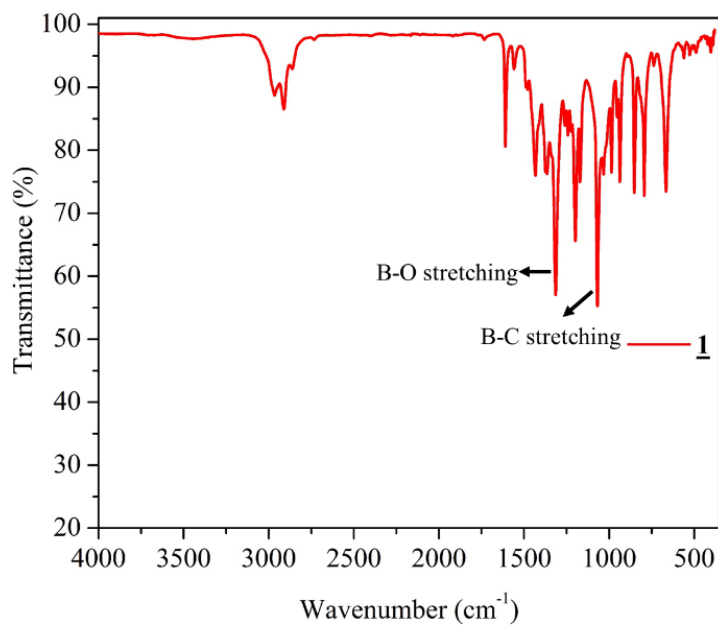
Fig. 2.5 IR Spectrum of **1**

The observed IR frequencies are listed below:

3000 - 2950 cm^{-1}, aromatic CH stretching conjugated with C=C; 1620-1580 cm^{-1}, aromatic CH$_2$=CH$_2$ stretch; 1450-1300 cm^{-1}, B-O bond stretching; 1050-950 cm^{-1}, B-C stretching.

2.4.1.5 High-Resolution Transmission Electron Microscopy (HRTEM/HREM)

Fig. 2.6 shows the transmission electron micrographs of the crystalline material EGMB (**1**). A definite geometry and an unresolved lattice fringes like pattern apparently evinces the formation of organic crystals.
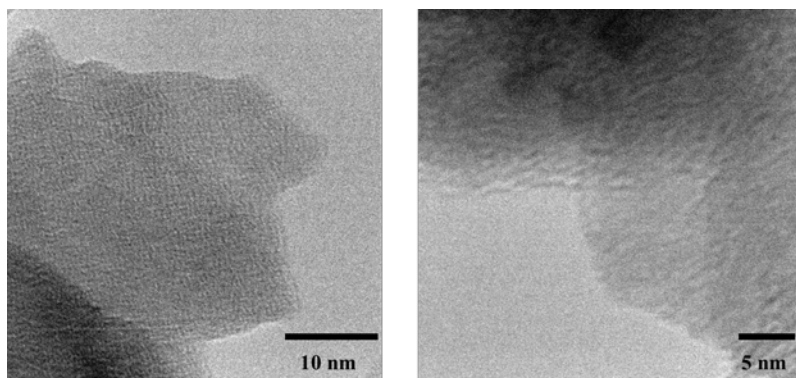
Fig. 2.6 Transmission Electron Micrographs of **1**

2.4.2 Electrochemical Analysis

For electrochemical analysis, **1**(EGMB) was doped with Li salt, LiTFSI[34], which changed the physical aspect of **1**(EGMB) from transparent crystal to an opaque powder. Addition of Li salt was carried out by two different methods. In the first case, the conventional method of inserting the salt using a solvent (THF)[3] was employed. In the second case, a rather simple grinding of **1**(EGMB) with LiTFSI was adapted.

2.4.2.1 *Ionic conductivity studies*

Ionic conductivities were measured by EIS technique between 30-60 ºC. Fig. 2.7 (a) and (b) shows the Arrhenius plots of samples prepared by conventional method and by grinding method, respectively. Most samples prepared by conventional methods showed a monotonous increase in ionic conductivity with increase in temperature under relatively low concentrations of lithium salt (Arrhenius behaviour). On the other hand, the samples prepared by grinding method obeyed different behaviour exhibiting lower activation energy of ion transport. This implied that different ion conduction mechanisms prevailed in the two samples prepared by the two different methods. Another feature observed in these samples was that the ionic

conductivity initially increased with increase in the Li salt concentration and decreased drastically after an optimum concentration of lithium salt. In the first case, the maximum ionic conductivity was observed to be 2.7×10^{-4} Scm^{-1} at 51 °C while the maximum ionic conductivity observed by the facile grinding method reached 7.1×10^{-4} Scm^{-1} (51 °C).
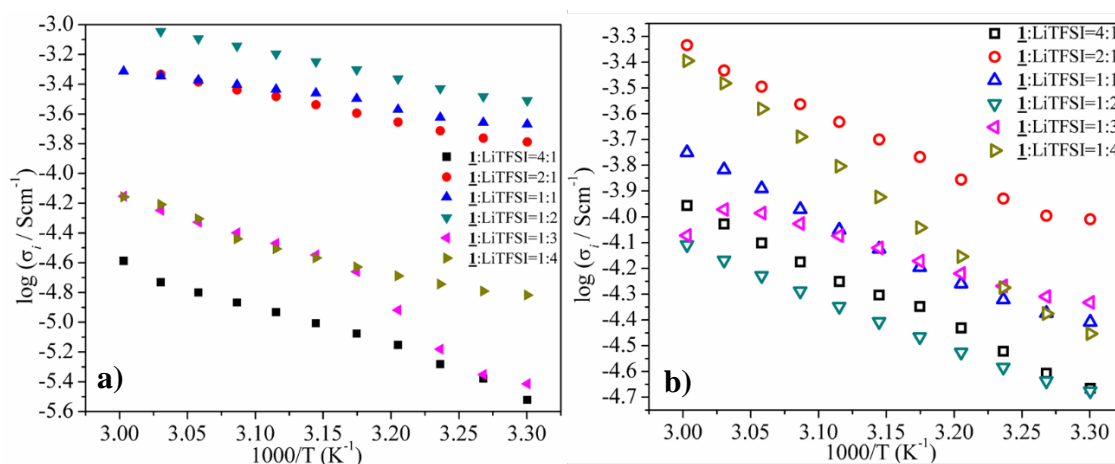
Fig. 2.7 Arrhenius plots for samples doped with LiTFSI by a) grinding method and b) conventional method of dissolving in THF

The conductivities shown by the samples prepared by grinding method were significantly higher at the optimal concentration of lithium salt. This can be due to the retainment of crystallinity of a Lewis acidic ordered structure by grinding which otherwise might be lost in the case of conventional samples due to solvation. The temperature dependence of ionic conductivity was studied by VFT analysis. Fig. 2.8 (a) and (b) shows the VFT plots for the samples prepared by both the methods. The lower values of ionic conductivity at lower concentration of lithium salt can be attributed to the minimal availability of ions for conduction. The lowering of ionic conductivity at higher concentration of salt can be due to an increased

activation energy required for ion transportation. The high conductivity seen at an optimal concentration of lithium salt in the sample prepared by grinding can be hypothesized to the formation of nanochannels[12, 35-37] by an arrangement of anions scaffolded by the undisturbed crystalline nature of the sample through boron anion interaction[38-43], allowing easier and faster transportation of ions by ion hopping mechanism[7]. This becomes evident from the fact that ionic conductivity for a concentration of **1**: LiTFSI=1:2 prepared by conventional method shows a very low value as compared to the sample prepared by grinding of same composition. This can be due to the absence of any such nanochannel formation in the conventional method.
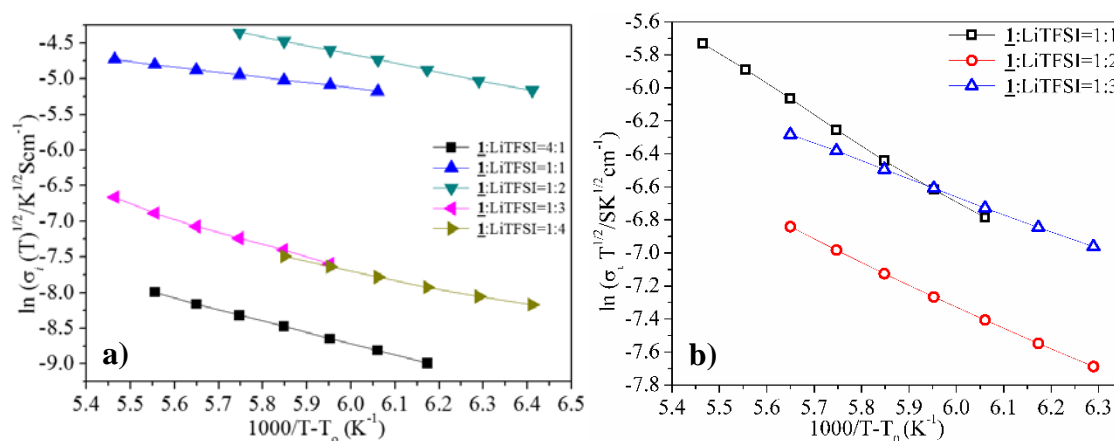
Fig. 2.8 VFT plots for the samples doped with LiTFSI (a) by grinding method and (b) by conventional method of dissolving in THF

A closer look at the VFT parameters (Table 2.1) of 3 samples prepared by grinding method (sample 2, 3 and 4) showed very low activation energy of ion transport (B). This led to markedly higher ionic conductivity. On the other hand, the samples prepared by conventional method showed relatively high activation energy and low ionic conductivity under the same composition. As a specific instance, comparison between grinding and conventional method

for a composition of **1**: LiTFSI=1:1 shows that although the carrier ion number in the sample prepared by grinding is only 1.72, its ionic conductivity is 3.5 times higher than that of the sample prepared by conventional method of same composition in which carrier ion number was 59.2.

Table 2.1 Comparison of VFT parameters for the samples prepared by conventional method and grinding

Sample (*1:LiTFSI*)	*S. No.*	*Grinding Method*				*S. No.*	*Conventional Method*			
		A (Scm^{-1} K$^{1/2}$)	**B** (K)	**R^2**	σ$_i$ at 51ºC (Scm^{-1})		**A** (Scm^{-1} K$^{1/2}$)	**B** (K)	**R^2**	σ$_i$ at 51ºC (Scm^{-1})
4:1	**1**	2.52	1607	0.9997	1.4×10^{-5}	**7**	4.74	1555	0.9964	6.6×10^{-5}
2:1	**2**	6.90	1209	0.9992	3.6×10^{-4}	**8**	4.81	1583	0.9992	2.7×10^{-4}
1:1	**3**	1.72	765.3	0.9995	3.9×10^{-4}	**9**	59.2	1796	0.9988	1.1×10^{-4}
1:2	**4**	15.7	1236	0.9994	7.1×10^{-4}	**10**	2.17	1350	0.9992	5.2×10^{-5}
1:3	**5**	33.7	1707	0.9998	3.9×10^{-5}	**11**	1.25	1071	0.9997	9.4×10^{-5}
1:4	**6**	0.66	1331	0.9992	3.6×10^{-5}	**12**	1.32	1232	0.9990	6.1×10^{-5}

Hence, in the case of grinded samples, low activation energy of ion transport resulted into high ionic conductivity. This evinces our hypothesis of formation of special channelized pathways resulting into low activation energy allowing facile transportation of Li$^+$ ions. Some samples prepared by conventional method (sample 10, 11 and 12) also show low activation energy of ion transport (B), under high concentration of LiTFSI. However, enhancement of ionic conductivity was not observed for these systems due to small carrier ion number (A).

2.4.2.2 X-ray Diffraction Analysis

XRD analysis was done for the sample with highest ionic conductivity (1: LiTFSI=1:2, prepared by grinding method). The data obtained is shown in Fig. 2.9. This data was compared with the pure crystalline sample, **1** and with the sample prepared by conventional method in same molar ratio.
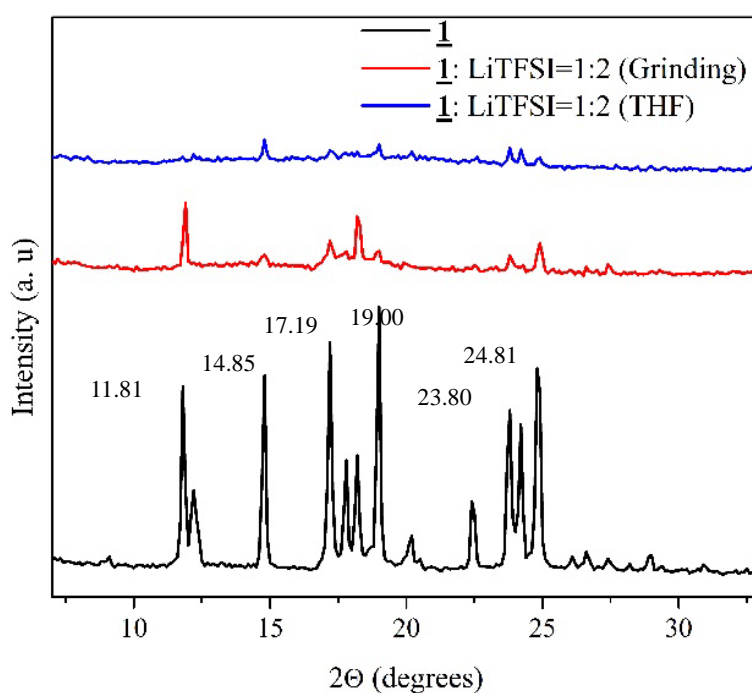
Fig. 2.9 a) XRD pattern of **1** and sample of 1 doped with Li salt by two methods in 1:2 molar ratio
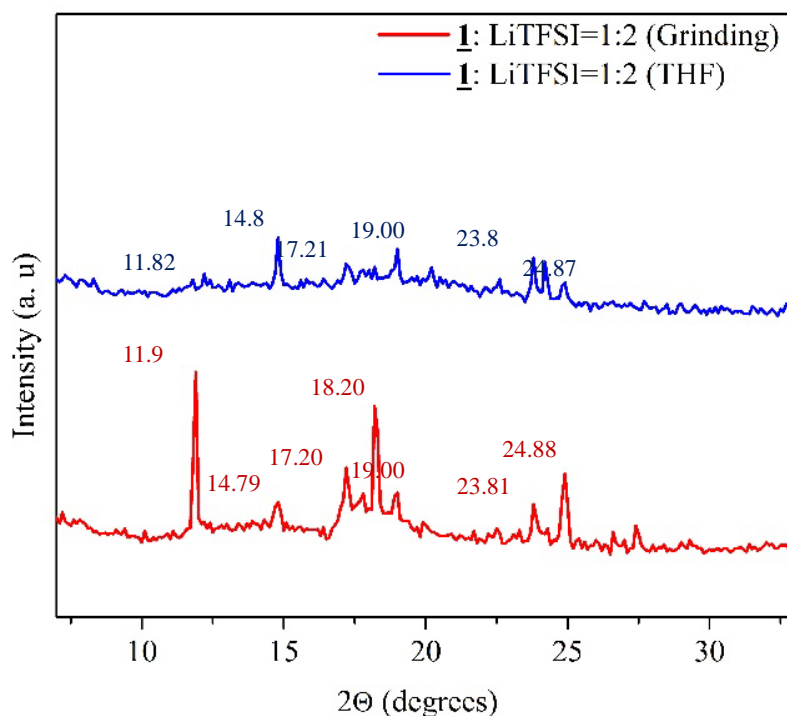
Fig. 2.9 b) zoom in spectra of 1 doped with Li salt

XRD patterns obtained for the three samples gave a clear idea that in the case of conventional sample that involves the use of THF, the crystallinity of the sample is getting lost. Pure sample **1** and the sample prepared by grinding method shows similar peaks with the 100% peak at the same 2Θ value (11.9). The high ionic conductivity of the ground sample **1**:LiTFSI=1:2 (grinding) can be associated with this intactness of the 100% peak and similarity in other peaks like pure **1** and can be attributed to the retainment of crystallinity leading to formation of channels for ion conduction. However, in the case of conventional sample, the 100% peak shifted to $2\Theta = 14.8$ indicating the change in structure.

2.4.2.3 *Li Ion Transference Number*

The cell employed for measuring the lithium ion transference number was a symmetrical cell consisting of a Li/electrolyte/Li configuration. The measurement was carried out via

Bruce-Vincent-Evans method as described in Chapter 1, section 1.4.3. The transference number was measured for the sample for the molar ratio **1**: LiTFSI = 2:1 under argon atmosphere. For an all solid state electrolyte of this type, the Li ion transference number was found out to be 0.28 (Fig. 2.10).
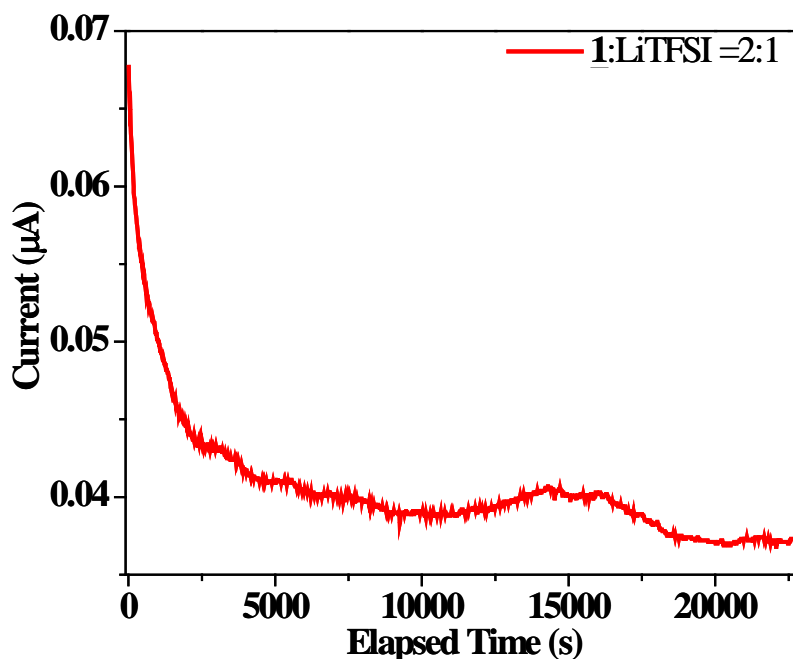
Fig. 2.10 DC Polarization data for the sample 1: LiTFSI=2:1

The transference number was also measured using the crystalline sample as a co-electrolyte to study the anion-trapping effect of boron (Fig. 2.11). In this analysis, to 15 mL solution of 1.0 M LiTFSI in EC: DEC=1:1 (v/v), **1** was added in various molar ratio from 0.25 to 1.25 moles. Interestingly, as the amount of boron increased in the electrolytic solution, the transference number increased to a maximum value of 0.92. However, after reaching the saturation, the electrolyte behaved similar to a solid state electrolyte and the Li^+ ion transference number decreased to a similar value (0.22) like the solid state electrolyte mentioned earlier (0.28).
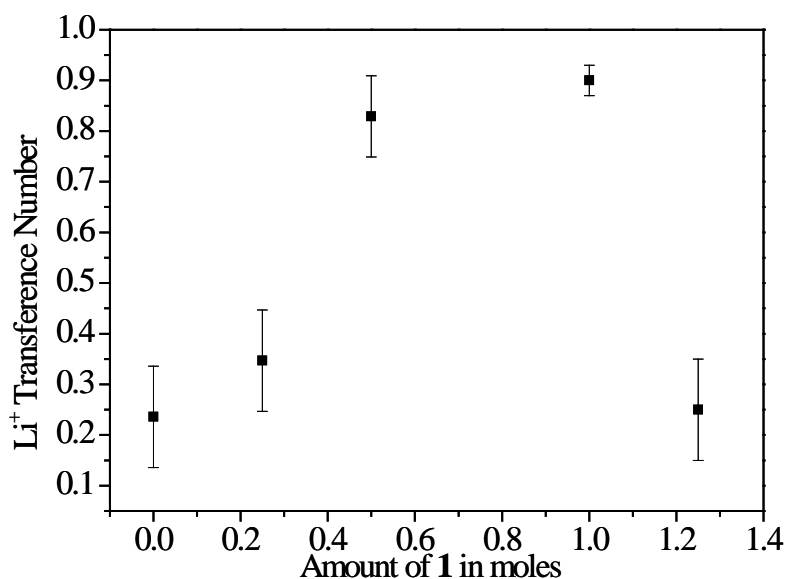
Fig. 2.11 Li transference number of **1** as co-electrolyte with 1.0 M LiTFSI in EC:DEC=1:1

As the amount of boron increased in the electrolyte solution, efficient trapping of the TFSI$^-$ anion by the p-orbital of boron resulted in availability of only Li$^+$ ions to contribute to the total transference number. Hence, owing to the selective cation conduction, the Li$^+$ ion transference number increased to a value of 0.92 in the **1**/LiTFSI range of 0 to 1.25 moles. However, the trapping of the anion at high concentration (1.25 moles of **1** as co-electrolyte) was not as effective as in lower concentrations thereby resulting in a t_{Li}^+ value of 0.22 as it behaved similar to the solid electrolyte after reaching saturation.

2.4.2.4 *Electrochemical Stability*

Electrochemical window was determined in a 3 electrode beaker type cell (using Pt-Pt electrode (wire) vs Ag/AgNO$_3$) under argon atmosphere using 0.01M **1** in 0.1M LiTFSI in 15mL EC: DEC =1:1 as the electrolyte via linear sweep voltammetry technique explained in

chapter 1, section 1.4.4. The potential window of the sample was found to be 5.3 V (Fig. 2.12).
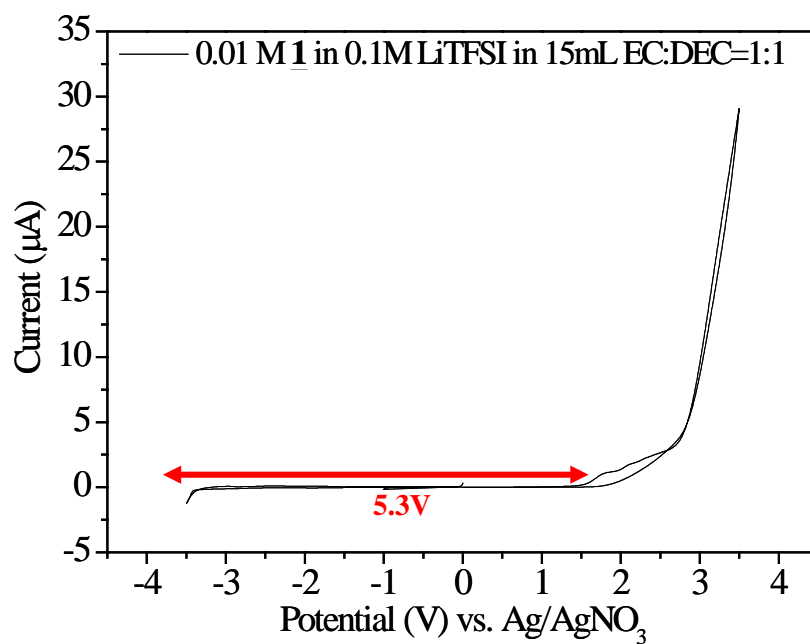
Fig. 2.12 Cyclic Voltammogram for the sample **1** in 0.1M LiTFSI in 15mL EC:DEC=1:1 vs

Ag/AgNO₃

2.5 Conclusions

In this chapter, the detailed synthesis and electrochemical properties of a low molecular weight cyclic organoboron crystalline electrolyte synthesized using ethylene glycol and mesityl borane was discussed. The electrolyte was obtained as needle shaped crystal in high yields. The crystallinity exhibit by the electrolyte was an important characteristic feature and showed interesting effect on the ionic conductivity after externally doping with the lithium salt via two different methods namely conventional method and grinding method. The electrochemical analysis of the sample obtained by grinding method exhibited high ionic conductivity of 7.1 x 10^{-4} Scm^{-1} at an optimized concentration of lithium salt. Facile grinding technique of the lithium salt addition with the prepared organoboron compound resulted in high ionic conductivity compared to the conventional method of mixing by dissolution and evaporation with solvents. The presence of crystallinity in Lewis acidic EGMB can be considered as an important factor behind the high ionic conductivity of the electrolyte prepared by grinding due to more regulated ion conduction path in the matrices.

References

1.   D. Aurbach, Y. Talyosef, B. Markovsky, E. Markevich, E. Zinigrad, L. Asraf, J. S. Gnanaraj and H. J. Kim, *Electrochim Acta*, 2004, **50**, 247-254.

2.   A. M. Andersson and K. Edstrom, *J Electrochem Soc*, 2001, **148**, A1100-A1109.

3.   A. M. Stephan, K. S. Nahm, M. A. Kulandainathan, G. Ravi and J. Wilson, *Eur Polym J*, 2006, **42**, 1728-1734.

4.   M. Wakihara, Y. Kadoma, N. Kumagai, H. Mita, R. Araki, K. Ozawa and Y. Ozawa, *J Solid State Electr*, 2012, **16**, 847-855.

5.   Y. S. Kim, Y. G. Cho, D. Odkhuu, N. Park and H. K. Song, *Sci Rep-Uk*, 2013, **3**.

6.   W. H. Meyer, *Adv Mater*, 1998, **10**, 439.

7.   M. Park, X. C. Zhang, M. D. Chung, G. B. Less and A. M. Sastry, *J Power Sources*, 2010, **195**, 7904-7929.

8.   A. M. Stephan, *Eur Polym J*, 2006, **42**, 21-42.

9.   N. Kamaya, K. Homma, Y. Yamakawa, M. Hirayama, R. Kanno, M. Yonemura, T. Kamiyama, Y. Kato, S. Hama, K. Kawamoto and A. Mitsui, *Nat Mater*, 2011, **10**, 682-686.

10.   Q. Li, E. Wood and H. Ardebili, *Appl Phys Lett*, 2013, **102**.

11.   G. M. Mao, R. F. Perea, W. S. Howells, D. L. Price and M. L. Saboungi, *Nature*, 2000, **405**, 163-165.

12.   Z. Gadjourova, Y. G. Andreev, D. P. Tunstall and P. G. Bruce, *Nature*, 2001, **412**, 520-523.

13.   A. M. Christie, S. J. Lilley, E. Staunton, Y. G. Andreev and P. G. Bruce, *Nature*, 2005, **433**, 50-53.

14.   W. A. Henderson, D. M. Seo, Q. Zhou, P. D. Boyle, J. H. Shin, H. C. De Long, P. C. Trulove and S. Passerini, *Adv Energy Mater*, 2012, **2**, 1343-1350.

15.   L. Ramon-Gimenez, R. Storz, J. Haberl, H. Finkelmann and A. Hoffmann, *Macromol Rapid Comm*, 2012, **33**, 386-391.

16.   A. Sato, T. Okumura, S. Nishimura, H. Yamamoto and N. Ueyama, *J Power Sources*, 2005, **146**, 423-426.

17.   K. Hoshino, M. Yoshio, T. Mukai, K. Kishimoto, H. Ohno and T. Kato, *J Polym Sci Pol Chem*, 2003, **41**, 3486-3492.

18.   C. T. Imrie, M. D. Ingram and G. S. McHattie, *Adv Mater*, 1999, **11**, 832-+.

19.   T. Kato, Y. Kubota and T. Uryu, *Polym Bull*, 1997, **38**, 551-554.

20.   Y. Kubota, M. Takata, T. C. Kobayashi and S. Kitagawa, *Coordin Chem Rev*, 2007, **251**, 2510-2521.

21.   S. Kitagawa and R. Matsuda, *Coordin Chem Rev*, 2007, **251**, 2490-2509.

22.   M. J. G. Jak, F. G. B. Ooms, E. M. Kelder, W. J. Legerstee, J. Schoonman and A. Weisenburger, *J Power Sources*, 1999, **80**, 83-89.

23.   N. Matsumi, M. Nakashiba and H. Ohno, *Polym Bull*, 2003, **50**, 259-264.

24.   T. Q. Yong, J. L. Wang, Y. J. Mai, X. Y. Zhao, H. Luo and L. Z. Zhang, *J Power Sources*, 2014, **254**, 29-32.

25.   M. Ranger and M. Leclerc, *Macromolecules*, 1999, **32**, 3306-3313.

26.   R. Ameloot, M. Aubrey, B. M. Wiers, A. P. Gomora-Figueroa, S. N. Patel, N. P. Balsara and J. R. Long, *Chem-Eur J*, 2013, **19**, 5533-5536.

27.   J. L. C. Rowsell and O. M. Yaghi, *Angew Chem Int Edit*, 2005, **44**, 4670-4679.

28.   H. C. Zhou, J. R. Long and O. M. Yaghi, *Chem Rev*, 2012, **112**, 673-674.

29.   C. Combelles, M. Ben Yahia, L. Pedesseau and M. L. Doublet, *J Phys Chem C*, 2010, **114**, 9518-9527.

30.   J. Shin, M. Kim, J. Cirera, S. Chen, G. J. Halder, T. A. Yersak, F. Paesani, S. M. Cohen and Y. S. Meng, *J Mater Chem A*, 2015, **3**, 4738-4744.

31.   B. M. Wiers, M. L. Foo, N. P. Balsara and J. R. Long, *J Am Chem Soc*, 2011, **133**, 14522-14525.

32.   N. Matsumi, K. Sugai and H. Ohno, *Macromolecules*, 2003, **36**, 2321-2326.

33.   N. Matsumi and Y. Chujo, *Polym Bull*, 1997, **38**, 531-536.

34.   V. Aravindan, J. Gnanaraj, S. Madhavi and H. K. Liu, *Chem-Eur J*, 2011, **17**, 14326-14346.

35.   S. Vorrey and D. Teeters, *Electrochim Acta*, 2003, **48**, 2137-2141.

36.   T. Nakamura, T. Akutagawa, K. Honda, A. E. Underhill, A. T. Coomber and R. H. Friend, *Nature*, 1998, **394**, 159-162.

37.   S. B. R. S. Adnan and N. S. Mohamed, *Int J Electrochem Sc*, 2012, **7**, 9844-9858.

38.   N. Matsumi, K. Sugai, K. Sakamoto, T. Mizumo and H. Ohno, *Macromolecules*, 2005, **38**, 4951-4954.

39.   N. Matsumi, M. Nakashiba, T. Mizumo and H. Ohno, *Macromolecules*, 2005, **38**, 2040-2042.

40.   N. Matsumi, K. Sugai and H. Ohno, *Macromolecules*, 2002, **35**, 5731-5733.

41.   N. Matsumi, K. Sugai, M. Miyake and H. Ohno, *Macromolecules*, 2006, **39**, 6924-6927.

42.   T. Mizumo, K. Sakamoto, N. Matsumi and H. Ohno, *Electrochim Acta*, 2005, **50**, 3928-3933.

43.   D. Shanmukaraj, S. Grugeon, G. Gachot, S. Laruelle, D. Mathiron, J. M. Tarascon and M. Armand, *J Am Chem Soc*, 2010, **132**, 3055-3062.

Chapter 3

Lithium Borate Type Low Molecular Weight Electrolytes Derived from Oxalic Acid/Glycerol

Abstract

Single ion conductors are known to be effective electrolytes with high ionic conductivities and high transference numbers for Li ion secondary batteries. In an attempt to further study the ion conduction mechanisms of novel organoboron low molecular weight electrolytes, we studied the synthesis and electrochemical properties of lithium borate type electrolyte derived from glycerol/oxalic acid. Incorporation of Li^+ ions was done *in-situ* using lithium mesitylhydroborate as the intermediate. These electrolytes were expected to show higher ionic conductivities than other solid state electrolytes. These electrolytes exhibited ionic conductivities in the range of 10^{-2} to 10^{-3} Scm^{-1} when measured in presence of an ionic liquid viz., AMImTFSI. Highest transference number of 0.81 was obtained for electrolyte derived from oxalic acid in ionic liquid. The electrochemical properties of these lithium borate type electrolytes were also compared to organoboron crystalline electrolyte studied in Chapter 2.

3.1 Introduction

Like other batteries, the functioning and performance of Li ion battery is also dependent on the stable electrodes and electrolytes used in the battery. Considerable progress can be seen in the area of novel or performance enhancing electrode materials[1-4] to increase the energy capacity of the batteries. Electrolytes[5,6] have gathered much less attention in terms of improving the battery performance.[7,8] However, an effective electrolyte is an important factor behind the safe and stable working of these batteries. A large number of electrolytes are now existing to be used in lithium batteries such as conventional organic carbonate solvents with the combination of various Li salts[9] and organic carbonate solvents[5]. These Li salts play a vital role in functioning of the battery as well as the designing of the interfacial layer onto electrodes.

The need for a highly ion conductive Li salt that can facilitate the process of diffusion inside a Li ion battery effectively, requires no introduction. Providing the electrolyte with advantages like improved conductivity, increased Li ion mobility, higher potential window, lower interfacial resistance, thermal stability, and finally, they should provide a highly conductive and stable SEI onto the anodes. Various research groups have focused on these properties of electrolytes and have shown improvement in performance of battery. Starting from the initial discoveries of salts like $LiPF_6$, $LiBF_4$ to the more recent ones, LiBOB in 2002, a large number of Li salts have been brought upon and some of them are commercialized too. Some of the salts such as $LiPF_6$, $LiAsF_6$, $LiCF_3SO_3$, $LiN(SO_2CF_3)_2$, $LiClO_4$, $LiBF_4$ and recently reported lithium bis-(oxalato)borate (LiBOB),[10-12] lithium oxalyldifluoroborate (LiODFB)[13] and lithium fluoroalkylphosphate (LiFAP),[14] are being presently used in the battery technology effectively.

Li salts have an important role in the designing of the SEI layer[15] and hence, the cycling characteristics and the performance of the battery containing that salt.[16,17] The salt being used as an effective electrolyte should meet some of the prerequisites,[18] a few of which are a) high thermal, chemical and electrochemical stabilities, b) high solubility in a wide range of solvents including alkyl carbonate solvents, c) high ionic conductivity and hence, high ionic mobility, and d) should passivate the electrode surfaces finely that can reduce capacity fading i.e. formation of a thin, highly conductive and stable solid electrolyte interface. To increase the ion mobility in a particular salt, it is preferable to have an anion of greater size. Greater size of anion results in weaker coordination and hence, high dissociating nature increasing the ion mobility. Larger anionic size also results in higher stability of the passivation film[18].

Generally, two approaches were widely followed to obtain Li salts with high Li^+ ion transference number based on either designing a single ion conductor or on introducing a Lewis acidic site to trap the anion in order to keep cations as sole conducting medium.[7,19-21] This promotes both ionic conductivity by enhancing salt dissociation and Li^+ ion transference number by immobilizing the corresponding anion.[22] Single ion conducting organoboron lithium salts like LiBOB attracts great attention today because of embracing both of these approaches. Various other organic Li salts also have been reported based on borates, imidazolates, triazolates, sulfonamides,[23] perflourinated polyimide anions[19] and carbonyl based molecules.[24] Incorporation of these organic groups help in enhancing the cationic transference number with sufficient ionic conductivity. Tagging a perfluorosulfonic moiety to the polymer chain of lower glass transition temperature, T_g, results in a decreased segmental motion due to an interaction between the polymer and the salt.[25] Further, salts having chelate

boron viz., lithium bis[1,2-benzenediolato(2-)o,o]borate (LBBB),[26] LiBOB,[11,27] lithium [(3-fluoro-1,2-benzenediolato(2-)-o,o-oxalato)]borate (FLBDOB)[28,29] and lithium [malonato oxalato]borate (LMOB)[30] include strong electron withdrawing group that induces extensive charge delocalization thereby resulting in highly conductive electrolytic solutions due to weakly coordinated anions and wider electrochemical stability windows due to lowered highest occupied molecular orbitals (HOMO).[28]

3.2 Objective of Research

Our previous work threw light on a new design of cyclic low molecular weight organoboron compounds which proved to be an efficient electrolyte for the use in LiBs by the addition of Li salt externally by facile grinding technique. Such a crystalline electrolyte, exhibited a different ion conduction mechanism possibly due to the arrangement of ionic species forming nanochannels for easy movement of ions. This inspired us to design a novel lithium borate type electrolyte without the need for an external addition of Li salt. One important merit of this compound would be prevention of the hindrance in formation of ionic channels due to loss of crystallinity by insertion of Li salt externally. Internal presence of Li salt ionically bonded to the boron moiety will increase the selective Li^+ ion conduction. This insertion method will also be helpful in controlling the formation of ion conduction channels by direct incorporation of Li^+ itself in the molecule. Herein, we report the synthesis and electrochemical behavior of a novel lithium borate type salt derived from glycerol/oxalic acid and lithium mesitylhydroborate.

3.3 Experimental

3.3.1 *Materials and Instruments*

Oxalic Acid ($C_2H_2O_4.2H_2O$) was procured from Sigma Aldrich while glycerol was purchased from Wako Chemicals and were used after drying at 100 ^{o}C under reduced pressure for 2 hours. Dehydrated THF was used as received. AMImTFSI (1-allyl-3-methylimidazolium (bis-(trifluoromethanesulfonyl) imide)) was synthesized after the ion exchange reaction of AMImCl (1-allyl-3-methylimidazolium chloride) with lithium (bis-(trifluoromethanesulfonyl) imide) (LiTFSI), purchased from TCI chemicals. EC:DEC=1:1 (v/v) solution was bought from Chameleon reagent and was used after drying over activated molecular sieves 5A 1/16.

NMR spectroscopic analysis was done by using Bruker model Avance III 400. Ionic conductivity was measured with a complex-impedance gain phase analyzer Solartron model 1260 after overnight drying of the samples under reduced pressure, under similar conditions as explained in Chapter 2, section 2.3. Li$^+$ ion transference number measurements were carried out by Evans method as explained in section 1.4.3.1. DC current measurements were made on a Potentiostat/ Galvanostat of Princeton Applied Research; model Versastat-3 with an applied constant potential of 30 mV. AC impedance analysis for measuring the charge transfer resistance before and after DC polarization was carried out under the frequency range from 0.1 Hz to 1 MHz with an AC amplitude of 10 mV.

3.3.2 *Preparation of lithium borates derived from Glycerol/Oxalic Acid:*

Lithium mesitylhydroborate[31] was synthesized according to the literature. Equimolar amount of dried glycerol (0.41 mL, 0.0056 moles) (Scheme 2)/ oxalic acid (0.51 g, 0.0056

moles) (Scheme 3) was added slowly to the THF solution of synthesized lithium mesitylhydroborate[1] (0.78 g, 0.0056 moles) at 0 $^\circ$C with vigorous stirring under nitrogen atmosphere. Appearance of bubbles confirmed the release of hydrogen during the reaction. Dehydrated THF was used in the process. Reaction mixture was kept for stirring at room temperature for 5 hours under N_2 atmosphere. THF was removed from the resulting mixture under reduced pressure and it was then washed with hexane several times. The product was dried under vacuum for 3 hours prior to any structural or electrochemical analysis. The products were obtained in high yields of 90% (**2**) and 85% (**3**).

Glycerol   **Lithium mesitylhydroborate**   **2 (90%)**

Scheme 2

Oxalic Acid   **Lithium mesitylhydroborate**   **3 (85%)**
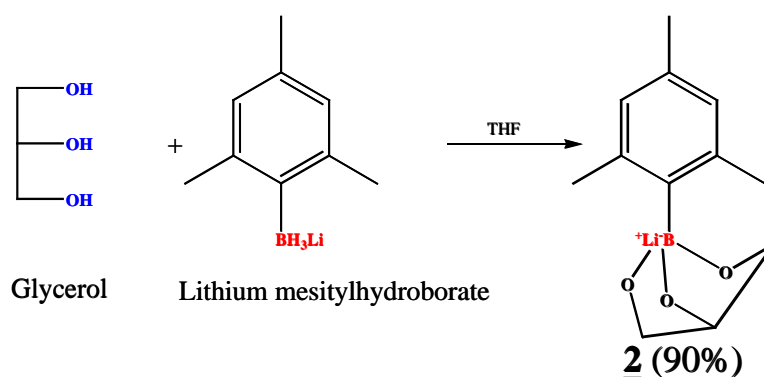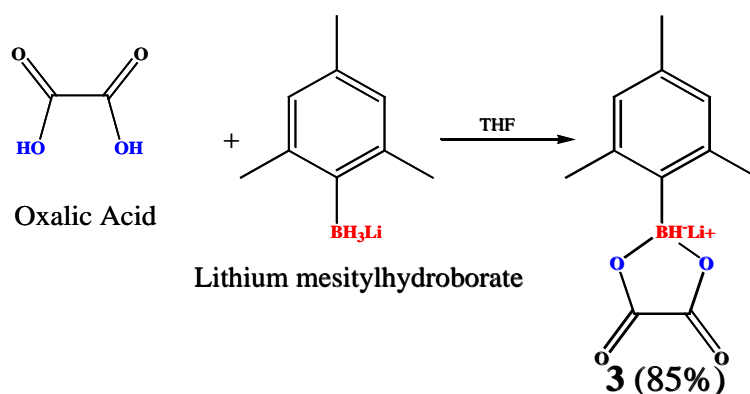
Scheme 3

3.3.3 *Characterization of lithium borates:*

3.3.3.1 *NMR Spectroscopy*

The synthesized low molecular weight lithium borate type electrolyte, **2** (GlyLiMB) and **3** (OxLiMB) were characterized by ^{11}B-NMR in DMSO-d_6 at 400 MHz showing a peak at 8.0 ppm (Fig. 3.1 a) and 7.3 ppm (Fig. 3.2 a), respectively referring to incorporation of boron as a borate moiety. Further, ^{1}H-NMR was also in accordance with the expected structure.

2: [^{11}BNMR (DMSO-d_6)]: 8.0 ppm; [^{1}HNMR (400MHz, DMSO-d_6): 6.5(phenyl ring protons, 2H), 3.61-3.10(-CH- protons of glycerol), 3.28 (H$_2$O), 2.50 (DMSO-d_6), 2.27-2.08 (-CH$_3$ protons of mesityl group)].

3: [^{11}BNMR (DMSO-d_6)]: 7.3 ppm; [^{1}HNMR (400MHz, DMSO-d_6): 6.79-6.72(phenyl ring protons), 3.33 (H$_2$O), 2.50 (DMSO-d_6), 2.27-2.08 (-CH$_3$ protons of mesityl group)].
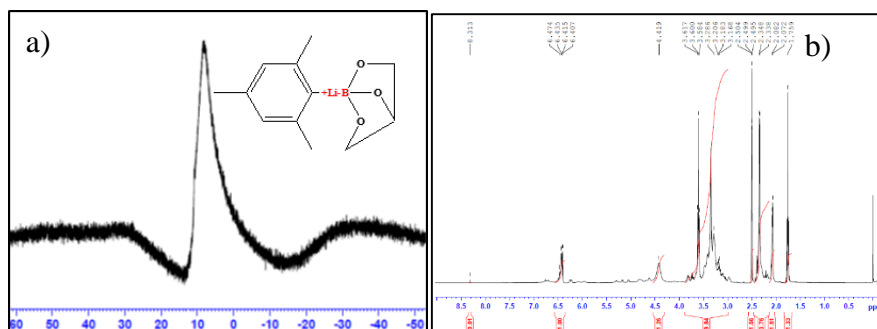
Fig. 3.1 a) ^{11}B-NMR of **2** in DMSO-d_6 b) ^{1}H-NMR of **2** in DMSO-d_6
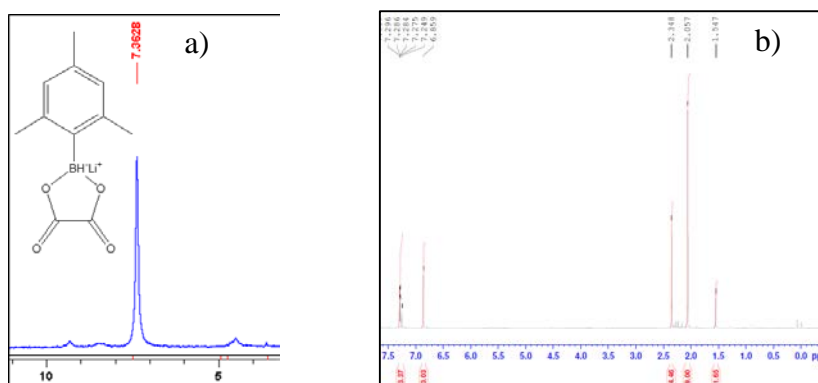
Fig. 3.2 a) ^{11}B-NMR of **3** in DMSO-d_6 b) ^{1}H-NMR of **2** in DMSO-d_6
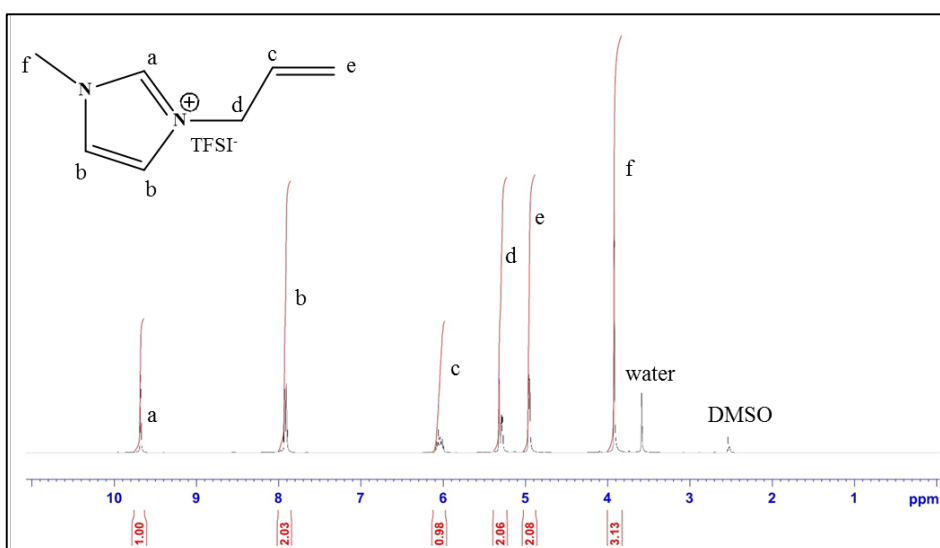
Fig. 3.3 ^{1}H-NMR of the ionic liquid used (AMImTFSI) in DMSO-d_6

3.3.3.2 *IR Spectrum of 3*
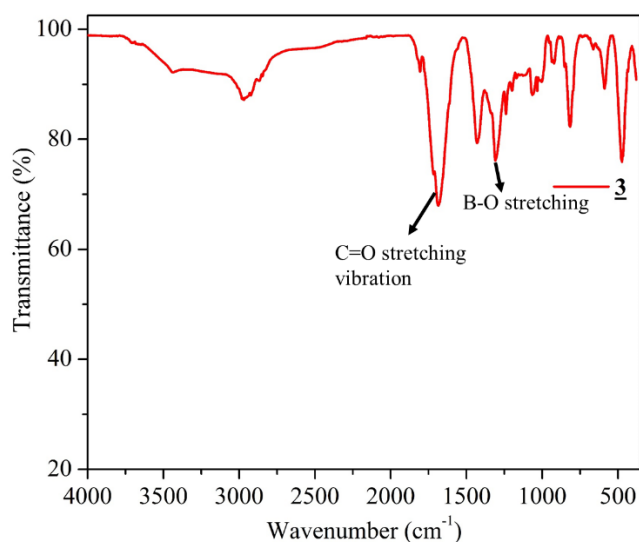
Fig. 3.4 IR spectrum of **3**

The observed IR frequencies are listed below:

3000 - 2950 cm^{-1}, aromatic CH stretching conjugated with C=C; 1620-1580 cm^{-1}, aromatic CH$_2$=CH$_2$ stretch and C=O stretching vibrations; 1450-1300 cm^{-1}, B-O bond stretching; 600-500 cm^{-1}, Mesityl ring out of plane deformation vibrations.

3.3.3.3 *XRD Analysis of 3*
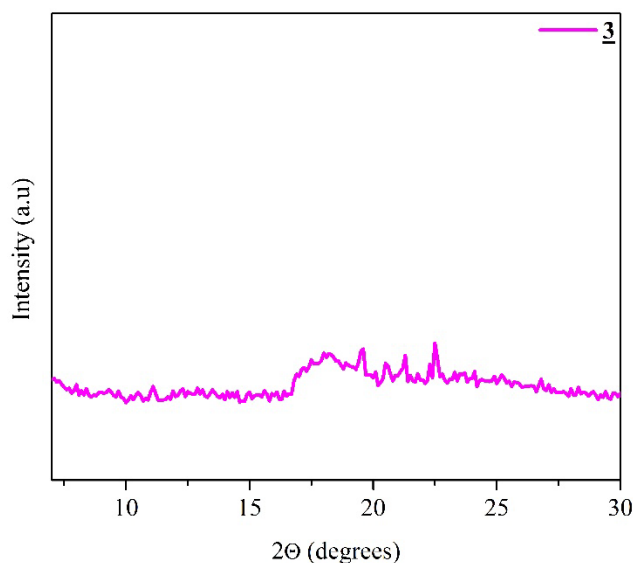
Fig. 3.5 XRD analysis of **3**

XRD patterns obtained for the sample **3** did not provide any significant information regarding the structure or the crystalline phases present in the sample. This might be because of the instability of the sample to air and moisture as it turned to gel phase after the XRD measurement was over.

3.4 Results and Discussion

3.4.1 Electrochemical Analysis:

3.4.1.1 Ionic conductivity studies

Ionic conductivity was studied by AC impedance spectroscopy between 30-60 ^{o}C. Lithium borate type electrolyte, **2**, derived from glycerol showed moderate ionic conductivity in the range of 10^{-6} Scm^{-1}. Fig. 3.6 shows the Arrhenius and VFT plots of the electrolyte **2** without any addition of the external salt or solvent. Non-linear profiles in Arrhenius plots showed that

the ion conduction mechanism was different from polymer segmental motion. The ionic conductivity was also measured in the presence of an ionic liquid viz., AMImTFSI.[32,33] In general, AMImTFSI is inherently low viscous and highly conductive, hence, AMImTFSI was employed to assess the mobility of **2**. Table 3.1 lists the VFT parameters obtained for electrolyte **2**.
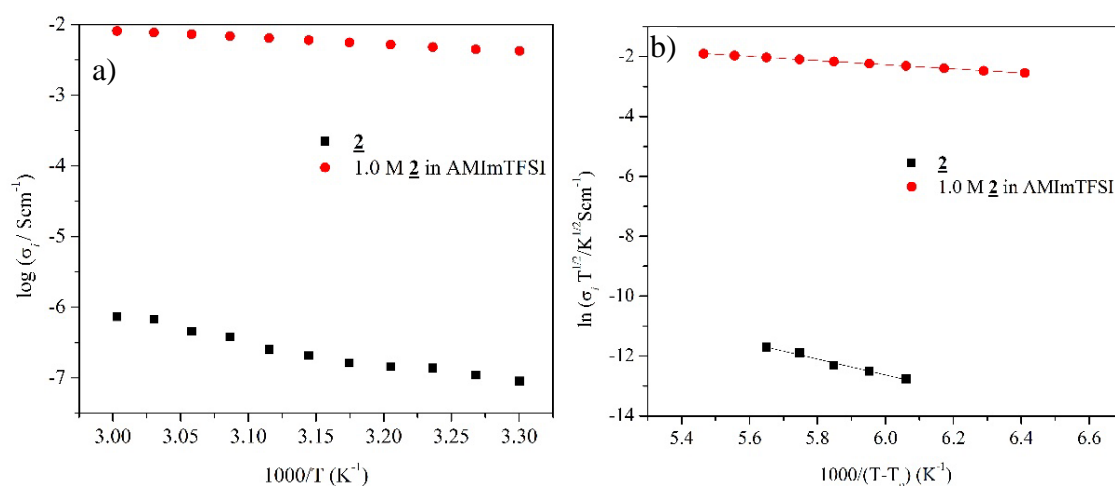
Fig. 3.6 a) Arrhenius plots and b) VFT plots for sample **2** and **2** dissolved in AMImTFSI

Table 3.1 VFT Parameters of sample **2**

S. No.	Sample	A($Scm^{-1}K^{1/2}$)	B(K)	R²	σ (Scm^{-1}) at 51 °C
13	**2**	3.008	2278	0.9551	3.8 x 10^{-7}
14	*1.0 M **2** in AMImTFSI*	6.453	688.6	0.9997	6.9 x 10^{-3}

Electrolyte sample, **3**, as such did not show very high ionic conductivity but in the presence of ionic liquid, AMImTFSI, the electrolytic salt showed a significantly high ionic conductivity of 1.42 x 10^{-2} Scm^{-1}. Fig. 3.7(a) shows the Arrhenius profiles for 1.0 M **3** in 1.0 mL of

AMImTFSI. The sample exhibited a very high conductivity in the range of 10^{-2} Scm^{-1} when dissolved in AMImTFSI. However, ionic liquids themselves are highly conductive and show ionic conductivities in the range of 10^{-3} Scm^{-1}. Therefore, comparison with the conductivity of pure AMImTFSI was required and it was observed that the lithium borate type salt enhances the ionic conductivity of pure ionic liquids to 10^{-2} Scm^{-1} when **<u>3</u>** was added.

Since the structure of the synthesized electrolyte, **<u>3</u>**, is similar to LiBOB (lithium bisoxalato borate) (Fig. 3.1, Section 3.1), the ionic conductivity experiments were also carried out for LiBOB in the ionic liquid, AMImTFSI in the temperature range of 30-60 °C. Surprisingly, the conductivity of 1.0 M **<u>3</u>** in AMImTFSI was higher than 1.0 M LiBOB in AMImTFSI. To understand more about the temperature dependence of ionic conductivity, Vogel-Fulcher-Tamman (VFT) equation was used to fit the ionic conductivity. Fig. 3.7 (b) shows the VFT plots for 1.0 M **<u>3</u>** in AMImTFSI (*sample no. <u>15</u>*), AMImTFSI itself (*<u>16</u>*) and LiBOB in AMImTFSI (*<u>17</u>*), respectively. The VFT parameters for all the samples as well as the ionic liquid are listed in Table 3.2. The activation energy parameter, **B**, was lowest for 1.0 M **<u>3</u>** in AMImTFSI among all the samples which would attribute to its higher ionic conductivity.
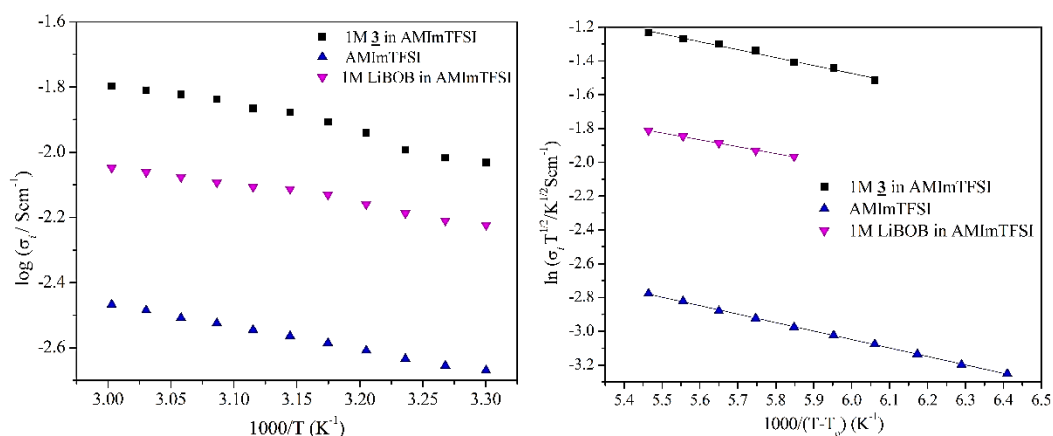
Fig. 3.7 a) Arrhenius plots and b) VFT plots for sample **3** dissolved in AMImTFSI and its comparison with ionic liquid and commercial salt LiBOB in AMImTFSI

Table 3.2 VFT Parameters of sample **3** in AMImTFSI, AMImTFSI and LiBOB in AMImTFSI

S. No.	*Sample*	*A(Scm^{-1}K$^{1/2}$)*	*B(K)*	*R^2*	*σ (Scm^{-1}) at 51 ºC*
15	*AMImTFSI*	1.043	501.00	0.9994	2.9 x 10^{-3}
16	*1.0 M **3** in AMImTFSI*	3.811	468.67	0.9883	1.4 x 10^{-2}
17	*1.0 M LiBOB in AMImTFSI*	1.513	407.36	0.9988	8.1 x 10^{-3}

3.4.1.2 *Li Ion Transference Number*

Li ion transference number for the electrolytic salt was calculated by the Evans *et. al.*, method using AC impedance spectroscopy coupled with DC polarization. Since both the electrolytes were solid in nature and completely dry, small amount of mixture of organic carbonate solvents, EC:DC=1:1 (v/v), was added to wet the sample in order to determine the Li$^+$ ion transference number. Fig. 3.8 shows the DC polarization profiles for both the samples in presence of EC:DC=1:1. For electrolyte **2**, the transference number was observed to be 0.34 in presence of EC:DC=1:1 and 0.48 in absence of EC:DC=1:1. Li$^+$ ion transference number for

electrolyte **3** was determined in presence of EC:DC=1:1 as well as ionic liquid AMImTFSI (Table 3.3). In the presence of those additional electrolytes, higher ionic conductivity was observed.
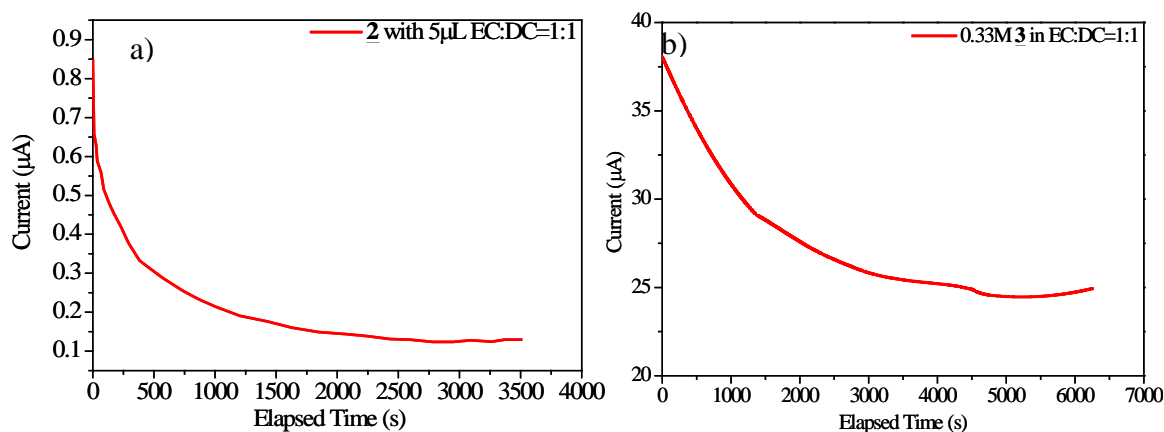
Fig. 3.8 DC polarization profiles for samples a) **2** and b) **3** in EC:DC=1:1 (v/v)

(Li/electrolyte/Li cell)

Table 3.3 The parameters used to obtain values of Li$^+$ transference numbers for both the lithium borate type electrolytes **2** and **3**.

Sample	Initial Current (I_o)/A	Steady State Current (I_s)/A	Initial Resistance (R_i)/Ω	Steady State Resistance (R_s)/Ω	Potential (V)	t_{Li^+}
2 *without EC:DC=1:1*	2.07×10^{-9}	7.6×10^{-10}	1000	9.7×10^{6}	0.03	**0.48**
2 *with EC:DC=1:1*	2.81×10^{-6}	8.70×10^{-7}	426.8	4624	0.03	**0.34**
1.0 M **2** *in AMImTFSI*	-2.8×10^{-4}	-5.43×10^{-5}	126.4	265	0.03	**0.28**
1.0 M LIBOB in AMImTFSI	9.27×10^{-4}	3.00×10^{-4}	508.9	621	0.03	**0.91**

*1.0 M **3** in AMImTFSI*	-8.11 x 10^{-5}	-0.49 x 10^{-5}	1428	1757	0.03	**0.81**
***3** with EC:DC=1:1*	4.38 x 10^{-5}	3.95 x 10^{-5}	91.70	86.81	0.03	**0.57**

Electrolyte **2** derived from glycerol showed a Li$^+$ ion transference number of 0.48 in the absence of EC:DC=1:1, whereas the electrolytic sample, **3** showed a Li$^+$ ion transference number of 0.81 in the presence of ionic liquid instead of EC:DEC=1:1 showing effective conduction of Li$^+$ ions. The transference number of both the electrolytes **2** (0.28) and **3** (0.81) was also studied in the presence of the ionic liquid AMImTFSI. This was compared with commercially available LiBOB in the ionic liquid, AMImTFSI which showed a transference number of 0.91. Though the transference number for electrolyte **3** was slightly lower than that of LiBOB in AMImTFSI, **3** exhibited higher ionic conductivity than LiBOB in the ionic liquid.

The higher Li ion transference number of the electrolytes **3** as compared to **2** can be attributed to relatively higher crystallinity of electrolyte **3** as compared to the glycerol based Li borate type electrolyte. Looking closer, the structure of **3** is remarkably similar to the commercially available Li salt LiBOB. In case of LiBOB, its high crystallinity can be associated to its symmetric structure.

3.5 Comparison of (**1**) / LiTFSI mixtures with electrolytes **2** and **3**

In the previous Chapter 2, we detailed the synthesis and electrochemical properties of tricoordinate boron (**1**) derived from ethylene glycol after addition of Li salt externally by two methods. As an attempt to further understand the behavior of cyclic organoboron electrolytes,

we studied the electrochemical properties of lithium borate type electrolytes **2** and **3** with inherent insertion of Li salt so as to avoid any hindrance from external factors such as moisture, air etc.

In tricoordinated boron/ LiTFSI mixtures, highest ionic conductivity was observed for the sample with molar ratio of **1**:LiTFSI=1:2. Lithium transference number of 0.28 was obtained without EC:DC=1:1 for the sample with molar ratio 2:1 prepared by grinding method. The reason for high ionic conductivity of **1**/LiTFSI mixture is attributed to the crystallinity of **1** which is useful to give some structural order of ion conductive path for regulated and easy conduction of Li ions.

In the case of lithium borate type electrolytes, **2** (GlyLiMB) showed moderate ionic conductivity at 51 ^{o}C i.e., 3.8×10^{-6} Scm^{-1} but the lithium ion transference number of 0.48 (in the absence of EC:DEC=1:1) was observed, which was much higher than previously reported tricoordinated boronic ester/LiTFSI mixture. **3** (OxLiMB) showed a very high ionic conductivity and lithium ion transference number in the presence of AMImTFSI. Fig. 3.9 shows the comparison between the three electrolytes in terms of ionic conductivities and Li$^+$ ion transference number along with their structures. Table 3.4 lists the conductivity values and transference numbers obtained in various solvents.
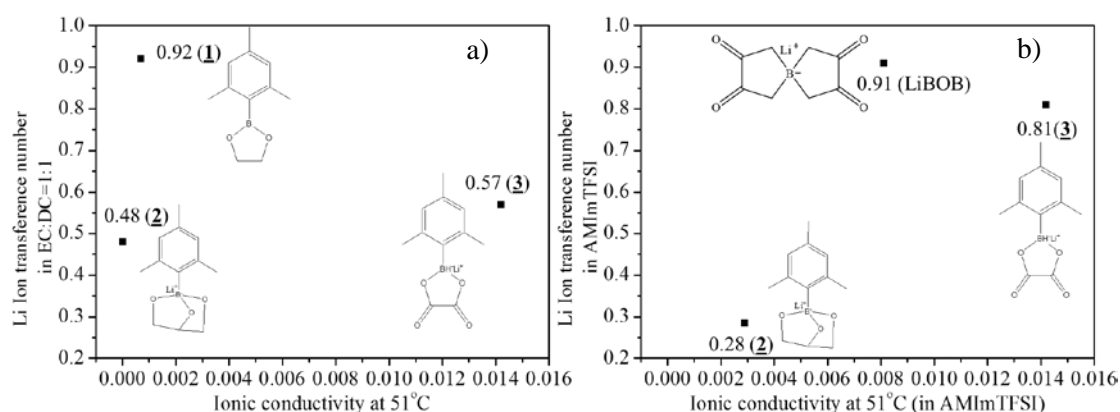
Fig. 3.9 Comparison of Ionic conductivity and Li ion transference number of a) **1**, **2** and **3** in EC:DEC=1:1 and of b) **2**, **3** and LiBOB in AMImTFSI

In the case of lithium borates, the electrolytes lack sufficient conductivity without ionic liquid. The mobility provided by the ionic liquid also makes the Li^+ ions labile for easier conduction. Further, since in such single ion conductors, the anions are comparably of larger size, Li^+ ions serve as the only conducting medium and hence, the transference number is higher for lithium borate type electrolytes **2** and **3** as compared to **1**/LiTFSI.

Table 3.4 Ionic conductivity and Li ion transference number for three samples **1**, **2**, **3** and LiBOB

Sample	σ (Scm^{-1}) at 51°C	t_{Li^+}	t_{Li^+} in EC:DEC=1:1	Solvent
1	7.1 x 10^{-4}	0.28	0.92	EC/DEC=1:1
2	3.8 x 10^{-6}	0.48	0.34	EC/DEC=1:1
3	1.4 x 10^{-2}*	0.81*	0.57	AMImTFSI
LiBOB	8.1 x 10^{-3}	0.91*	-	AMImTFSI

* In AMImTFSI

3.6 Conclusions

Lithium borate type electrolytes derived from glycerol (2) and oxalic acid (3) were synthesized successfully by treating with lithium mesitylhydroborate and were characterized by NMR spectroscopy. The electrolytes obtained were soft solid and appeared to be non-crystalline. The ionic conductivity of both the electrolytes was measured in the presence of AMImTFSI without any external addition of Li salt. Such single ion conductors with in-situ insertion of Li salt exhibited high ionic conductivity in the range of 10^{-3} (**2**) and 10^{-2} (**3**) Scm^{-1} when mixed with ionic liquid. Li$^+$ ion transference number obtained for electrolyte **3** in AMImTFSI was 0.81 which is high for a solid state electrolyte of this type. The electrochemical properties of these electrolytes were compared with the boric ester type electrolyte, **1**.

With all the studies discussed in this chapter and in chapter 2, it can be concluded that the low molecular weight organoboron compounds can be effectively used as electrolytes for Li ion batteries. Such electrolytes with a non-polymeric structure involving boron can help in effective anion trapping and increased ion transport. Electrolyte **1** with a crystalline nature might have helped in formation of ion channels for regulated ion movement and hence, increased the ionic conductivity. Further, using a method with no incorporation of solvent in the system for crystalline electrolytes like **1** can help retainment of crystallinity for studying the effect in the enhanced properties of the electrolytic system and in removal extensive procedures involving solvents. Further, single ion conductors with low molecular weight and Lewis acidic boron like **2** and **3** can be used to enhance the Li$^+$ ion mobility efficiently between the electrodes enhancing the overall performance.

References

1. J. Hassoun, F. Bonaccorso, M. Agostini, M. Angelucci, M. G. Betti, R. Cingolani, M. Gemmi, C. Mariani, S. Panero, V. Pellegrini and B. Scrosati, *Nano Lett*, 2014, **14**, 4901-4906.

2. S. Chaudhari, S. Y. Kwon and J. S. Yu, *Rsc Adv*, 2014, **4**, 38931-38938.

3. C. Combelles, M. Ben Yahia, L. Pedesseau and M. L. Doublet, *J Phys Chem C*, 2010, **114**, 9518-9527.

4. S. Rothermel, P. Meister, G. Schmuelling, O. Fromm, H. W. Meyer, S. Nowak, M. Winter and T. Placke, *Energ Environ Sci*, 2014, **7**, 3412-3423.

5. D. Aurbach, Y. Talyosef, B. Markovsky, E. Markevich, E. Zinigrad, L. Asraf, J. S. Gnanaraj and H. J. Kim, *Electrochim Acta*, 2004, **50**, 247-254.

6. W. H. Meyer, *Adv Mater*, 1998, **10**, 439.

7. Y. F. Zhang, G. D. Xu, Y. B. Sun, B. Han, B. W. T. Teguh, Z. X. Chen, R. Rohan and H. S. Cheng, *Rsc Adv*, 2013, **3**, 14934-14937.

8. M. Wakihara, *Mat Sci Eng R*, 2001, **33**, 109-134.

9. K. Xu, *Chem Rev*, 2004, **104**, 4303-4417.

10. K. Xu, S. S. Zhang, B. A. Poese and T. R. Jow, *Electrochem Solid St*, 2002, **5**, A259-A262.

11. K. Xu, S. S. Zhang, T. R. Jow, W. Xu and C. A. Angell, *Electrochem Solid St*, 2002, **5**, A26-A29.

12. X. L. Chen, W. Xu, M. H. Engelhard, J. M. Zheng, Y. H. Zhang, F. Ding, J. F. Qian and J. G. Zhang, *J Mater Chem A*, 2014, **2**, 2346-2352.

13. J. L. Allen, S. D. Han, P. D. Boyle and W. A. Henderson, *J Power Sources*, 2011, **196**, 9737-9742.

14. M. Schmidt, U. Heider, A. Kuehner, R. Oesten, M. Jungnitz, N. Ignat'ev and P. Sartori, *J Power Sources*, 2001, **97-8**, 557-560.

15. A. M. Andersson and K. Edstrom, *J Electrochem Soc*, 2001, **148**, A1100-A1109.

16. K. Xu, *Chem Rev*, 2014, **114**, 11503-11618.

17. M. Nie and B. L. Lucht, *J Electrochem Soc*, 2014, **161**, A1001-A1006.

18. V. Aravindan, J. Gnanaraj, S. Madhavi and H. K. Liu, *Chem-Eur J*, 2011, **17**, 14326-14346.

19. H. Tokuda, S. Muto, N. Hoshi, T. Minakata, M. Ikeda, F. Yamamoto and I. Watanabe, *Macromolecules*, 2002, **35**, 1403-1411.

20. S. R. Shankar and N. Matsumi, *Polym Bull*, 2012, **68**, 721-727.

21. N. Matsumi, Y. Toyota, P. Joshi, P. Puneet, R. Vedarajan and T. Takekawa, *Int J Mol Sci*, 2014, **15**, 21080-21089.

22. N. Matsumi, K. Sugai and H. Ohno, *Macromolecules*, 2002, **35**, 5731-5733.

23. S. Ladouceur, S. Paillet, A. Vijh, A. Guerfi, M. Dontigny and K. Zaghib, *J Power Sources*, 2015, **293**, 78-88.

24. H. Y. Chen, M. Armand, M. Courty, M. Jiang, C. P. Grey, F. Dolhem, J. M. Tarascon and P. Poizot, *J Am Chem Soc*, 2009, **131**, 8984-8988.

25. X. Ollivrin, F. Alloin, J. F. Le Nest, D. Benrabah and J. Y. Sanchez, *Electrochim Acta*, 2003, **48**, 1961-1969.

26. J. Barthel, M. Wuhr, R. Buestrich and H. J. Gores, *J Electrochem Soc*, 1995, **142**, 2527-2531.

27. W. Xu and C. A. Angell, *Electrochem Solid St*, 2001, **4**, E1-E4.

28. Z. M. Xue, C. Q. Ji, W. Zhou and C. H. Chen, *J Power Sources*, 2010, **195**, 3689-3692.

29. Z. M. Xue, J. F. Zhao, J. Ding and C. H. Chen, *J Power Sources*, 2010, **195**, 853-856.

30. W. Xu and C. A. Angell, *Electrochem Solid St*, 2000, **3**, 366-368.

31. N. Matsumi, K. Sugai, K. Sakamoto, T. Mizumo and H. Ohno, *Macromolecules*, 2005, **38**, 4951-4954.

32. P. X. Yang, L. Liu, L. B. Li, J. Hou, Y. P. Xu, X. F. Ren, M. Z. An and N. Li, *Electrochim Acta*, 2014, **115**, 454-460.

33. K. Angenendt and P. Johansson, *J Phys Chem B*, 2011, **115**, 7808-7813.

Chapter 4

Charge-discharge Analysis of Low Molecular Weight Electrolytes

Abstract

Low molecular weight electrolytes have been evaluated as electrolytes for lithium ion batteries through charge-discharge studies in anodic-half cell configuration using graphite anodes. The average capacity for alkylborane type electrolyte EGMB, discussed in Chapter 2, ranged from 150-200 mAh/g. Electrolyte EGMB showed a stable and conductive SEI layer formation implicit from impedance analysis. Electrolyte GLiMB and OxLiMB, synthesized in Chapter 3, based on lihium borate type electrolyte exhibited charge-discharge capacity in the range of 150-200 mAh/g and 75-80 mAh/g respectively.

4.1 Introduction

Among electrolytes, liquid electrolytes[2] comprising of alkyl carbonate solvents and Li salts[3] have been studied widely with respect to their charge discharge characteristics, SEI formation, morphology of electrodes[4], effect of temperature[5] and additives[6,7]. However, their volatility and flammability mars their safety. Efforts have been made to develop new electrolytes with non-flammable solvents[8], with new Li salts such as LiBOB[9] and new polymeric/gel and solid state electrolytes[10]. There had been reports[6,11,12] on the charge-discharge studies explaining the process of intercalation and deintercalation of liquid, polymeric and gel type electrolytes[13], however much fewer number of reports have been produced concerning the charge-discharge behavior of solid state electrolytes.

As explained in Chapter 1, Section 1.3.4, charge-discharge mechanism involves intercalation and deintercalation of Li^+ ions to and from the host material[14]. This needs an electrolyte with high conductivity, low viscosity and efficient mobility of Li^+ ions, which is provided easily by the liquid electrolytes. However, poor electrolyte diffusion in case of solid electrolytes limits their use in Li ion batteries. It is necessary for an electrolyte to provide good wetting property with the electrode in order to access the interior of the electrodes effectively[15]. Solid state batteries based on polymeric electrolytes have gained interest and have been studied for their charge-discharge characteristics[16]. There have been fewer number of reports on the solid state electrolyte systems. Recently, charge-discharge behavior of a solid state battery consisting of a $LiCoO_2$ cathode, a $Li_{10}GeP_2S_{12}$ electrolyte and an In (Indium plate) metal anode[17] which exhibited a discharge capacity of 120 mAh/g and coulombic efficiency of 100% after 2nd cycle was reported to demonstrate the use of solid electrolytes in Li ion battery as an

impressive alternative to liquid electrolytes. Another report in 2015 detailed the charge-discharge behavior of a quasi-solid electrolyte system (Fig. 4.1) employed with lithiated ionic liquid and micro-flakes of clay[15]. Charge-discharge behavior of solid state organic-inorganic hybrid system based on boron moieties in ionic liquids[18] have also been studied and understood.
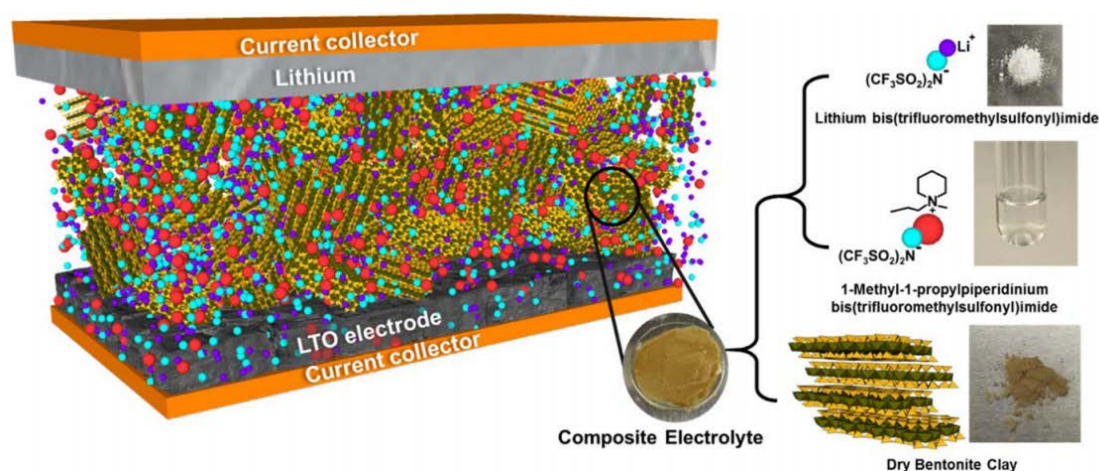
Fig. 4.1 Schematic representation of quasi-solid state electrolyte system (adapted from 6)

In this work, we have dealt with low molecular weight solid state organoboron electrolytes and have studied their charge-discharge behavior.

4.2 Objective of Research

This part of research deals with evaluating the electrolytes prepared in earlier chapters for real-time battery application. The chapter details the charge-discharge characteristics and interfacial behavior of the electrolytes with an aim to understand and interpret the capability of these organoboron electrolytes for solid state energy storage.

4.3 Experimental

Materials and Instruments

For charge-discharge studies, graphite based anodic half-cells were prepared using CR2025 type coin cells with graphite as the working electrode (diameter = 15Φ, PIOTREK), lithium metal as the counter electrode (15 mm, Honjo metals, Japan) and a ring shaped polypropylene based membrane (Celgard$^®$) as separator (outer diameter = 16 mm, inner diameter= 12 mm). The cell assembly is shown in Fig. 4.2.
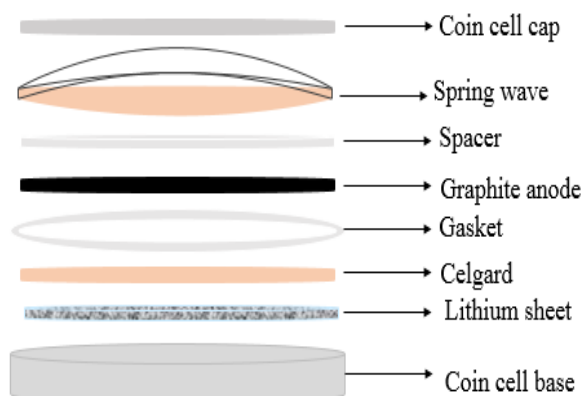
Fig. 4.2 Set-up of the assembled anodic-half cells

The prepared graphite based anodic half-cells were charged and discharged in a galvanostatic mode with restriction in potential using compact charge and discharge system of EC Frontier; ECAD-1000. For charge-discharge studies, anodic half-cells were fabricated

The structure of the three electrolytes synthesized are shown in Fig. 4.3.
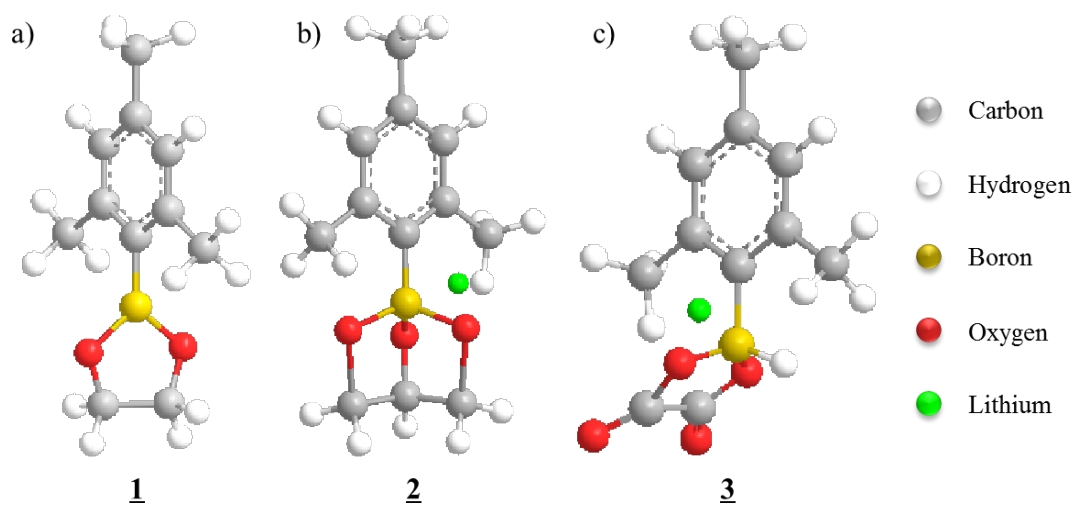
Fig. 4.3 Structure of the electrolytes, **1** (EGMB), **2** (GlyLiMB) and **3** (OxLiMB)

4.3.1   Selection of Electrolyte, Additives, Solvents and Cell Fabrication

The selection of electrolyte and optimization of amount of solvents and additives are necessary before charge-discharge analysis. Ionic conductivities and transference number calculations formed the basis for the choice of the electrolyte. For charge-discharge analysis of sample **1**, powdered electrolyte prepared by the grinding method in molar ratio **1**:LiTFSI=2:1 (sample with highest ionic conductivity) was chosen. The choice of electrolyte was done on the basis of the observed ionic conductivity at 51 $^{\circ}$C. Here, Fig. 4.4 enables a quick recapitulation of the ionic conductivity of all the samples prepared by the two different methods viz., grinding and conventional method.
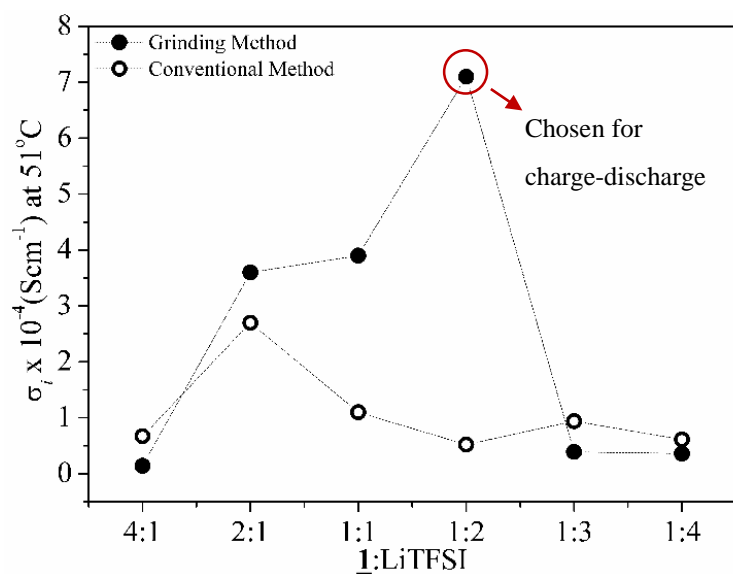
Fig. 4.4 Comparison between ionic conductivities of samples prepared by grinding and conventional method at various lithium salt concentrations at 51 °C

However, in the case of the other two electrolytes, **2** and **3**, they were used as-synthesized for charge discharge analysis without any further addition of Li salt. Three cells were fabricated using the electrolytes, **1**, **2** and **3** which are listed in Table 4.1. The cells were fabricated inside a glove box under argon atmosphere. Along with the electrolyte used, optimum amount of EC: DEC=1:1 (30µL) was added to wet the surface of the electrode while fabricating the cell in order to ensure easy mobility of ions and a steady SEI formation. After assembling, they were kept for stabilization. The prepared anodic coin half-cells were charged and discharged at a constant current rate.

Table 4.1 Cells fabricated for charge-discharge analysis

#	Cell	Electrolyte	Solvent	Anode
1	Cell 1E	**1**:LiTFSI=2:1	30μL of EC:DC=1:1	Graphite
2	Cell 2G	**2**	30μL of EC:DC=1:1	Graphite
3	Cell 3O	**3**	30μL of EC:DC=1:1	Graphite

C rate at constant current mode is the rate at which a battery can handle current[19]. The current rate was increased gradually in order to study the change in capacities with changing current rates. The prepared anodic coin half-cells were charged and discharged at a constant current rate ranging from 0.01C (0.0313 mA) to 0.2C (0.616 mA). The current rate was increased gradually in order to study the change in capacities with changing current rates. The interfacial characteristics were monitored by measuring the charge-transfer resistance before and after charge-discharge analysis via EIS technique. In general, the spectrum obtained while measuring the impedance is fit using an equivalent circuit which gives certain values for the different type of resistances. The extent of fitting is given by the χ^2 (chi-square) value, which gives the precision of fit between a set of experimental values and theoretical values. Lower the χ^2 value, better will be the fit. The χ^2 value for each impedance spectra, shown later in this chapter, has been provided in order to compare the extent of fitting.

4.4 Results and Discussion

4.4.1 Charge-discharge Studies of **1**

Cell 1E was fabricated using electrolyte **1** and its charge discharge was first carried out at a lower current rate *i.e.,* 0.01C (0.03 mA) and was increased to 0.05C (0.15 mA) after 10

cycles. The result of charge discharge at 0.05C for 10 cycles is shown in Fig. 4.5.
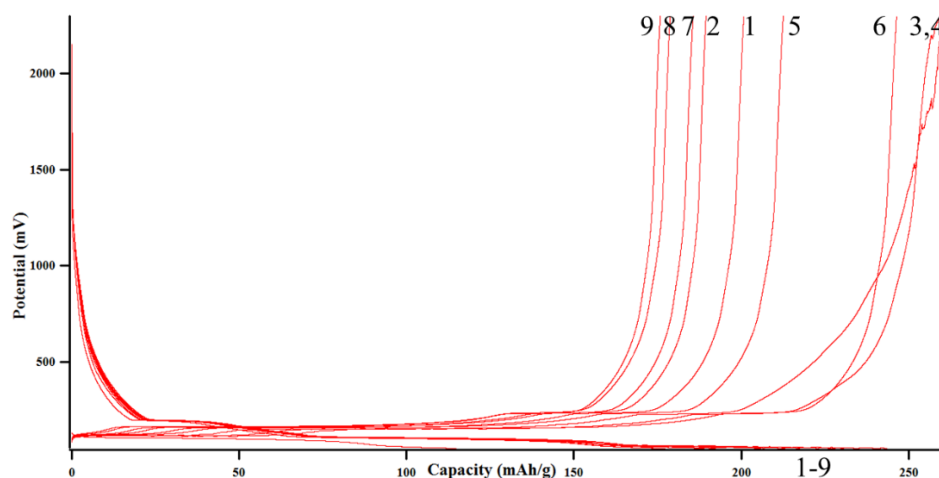
Fig. 4.5 Charge discharge profiles of **1**: LiTFSI = 1:2 with 30 µL of EC: DEC=1:1 at 0.05C

As it can be clearly observed, the cell was able to charge up to ~250 mAh/g and discharge completely. A plateau observed at 0.2 V while charging marked the intercalation of the Li$^+$ ions into graphite. The charge-discharge profiles showed first an increase in the capacity from 1st to 4th cycle and then, continued with decrease in the capacity from 5th to 10th cycle. This increase can be attributed to the formation of the stable electrode-electrolyte interface during 4th to 6th cycle, after which the capacity continues to decrease gradually. A similar kind of plateau was observed in the discharging profiles as well. Coulombic efficiency of the cell was observed to be ~100% for all the cycles. *Coulombic efficiency is defined as the ratio of the output charge of the cell to the input charge of the cell. High coulombic efficiency (~100 %) refers to high reversibility of the cell[20]*. Fig. 4.6 shows the coulombic efficiency of the **cell 1E** for the 10 cycles at 0.05 C.
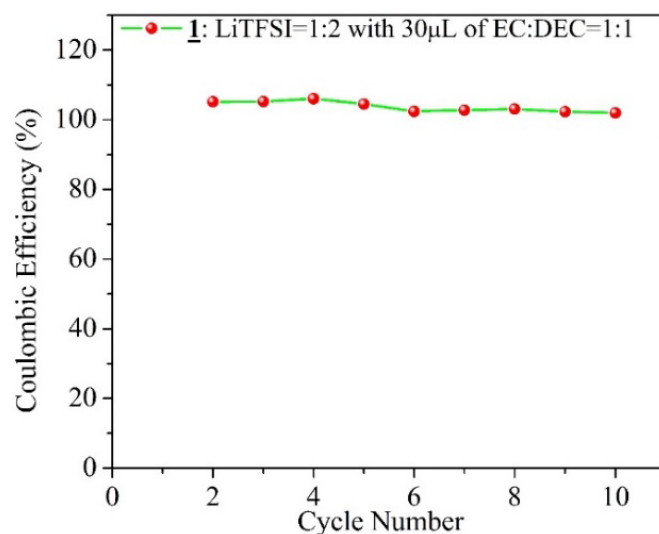
Fig. 4.6 Coulombic efficiency profile of cell **1E**, Li/ **1**: LiTFSI = 1:2 with 30 μL of EC:

DEC=1:1/ C, at 0.05 C

We further, checked the cell's charge-discharge characteristics at higher current rate in order to obtain a battery with a faster charging rate and high capacity. The cell was then charged at a current rate of 0.2 C (0.616) mA per hour. The cell was able to deliver a charge-discharge capacity of 100~150 mAh/g during 16 cycles at 0.2 C. The capacity first decreased to 80 mAh/g till the 10th cycle and then further increased to 120 mAh/g till 16th cycle indicating the formation of a stable interface after 10th cycle. Fig. 4.7a shows the charge discharge profiles of the cell at 0.2 C and 4.7b shows the coulombic efficiency for 16 cycles to be ~99%.
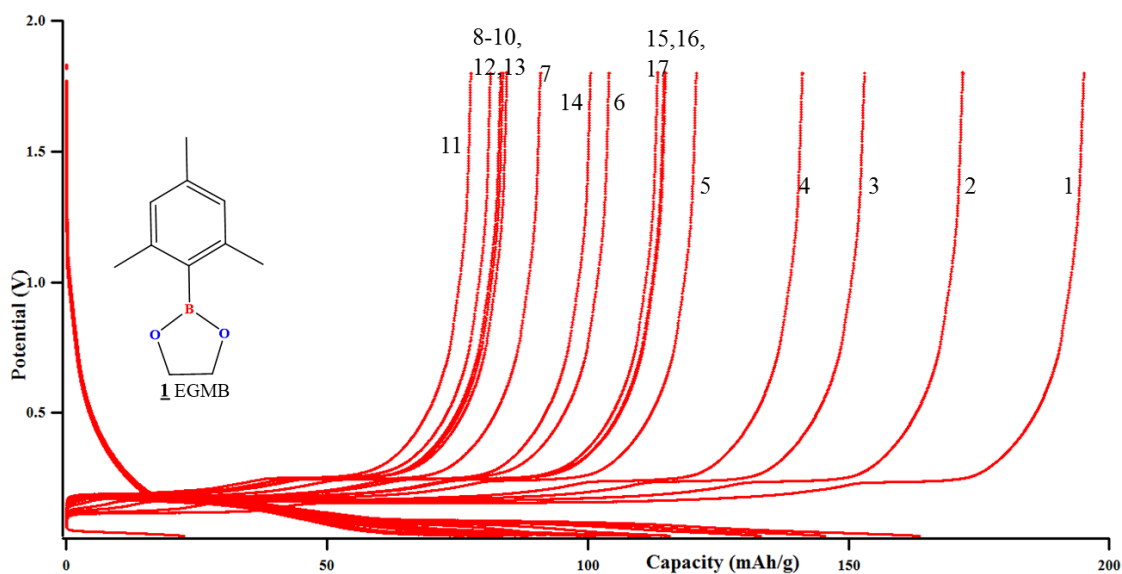
Fig. 4.7 a) Charge discharge profiles of **cell 1E** with **1**: LiTFSI=1:2 in 30 μL of EC:DEC=1:1

as electrolyte at 0.2 C
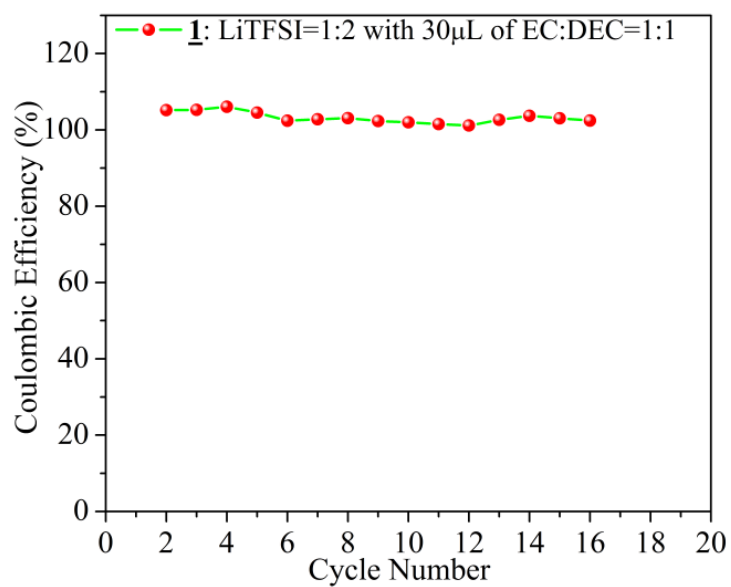
Fig. 4.7 b) Coulombic efficiency profile of anodic half-cell, cell **1E** at 0.2 C.

Interfacial Characteristics

Impedance analysis before charge discharge of **cell 1E** was done to determine the interfacial resistance (Fig. 4.8) and was evaluated by using an equivalent circuit, EqC1, provided in Fig. 4.9. Table 4.2 gives the values of all the resistances present in the system evaluated by the equivalent circuit, EqC1. The charge transfer resistance, R_{ct}, was obtained as 237.2 Ω before the charge-discharge was started. However, after 10 cycles, interfacial resistance for the cell reduced to 26.09 Ω indicating the formation of a conducting interface and occurrence of an effective charge-transfer process due to the formation of a stable and highly conductive SEI layer.
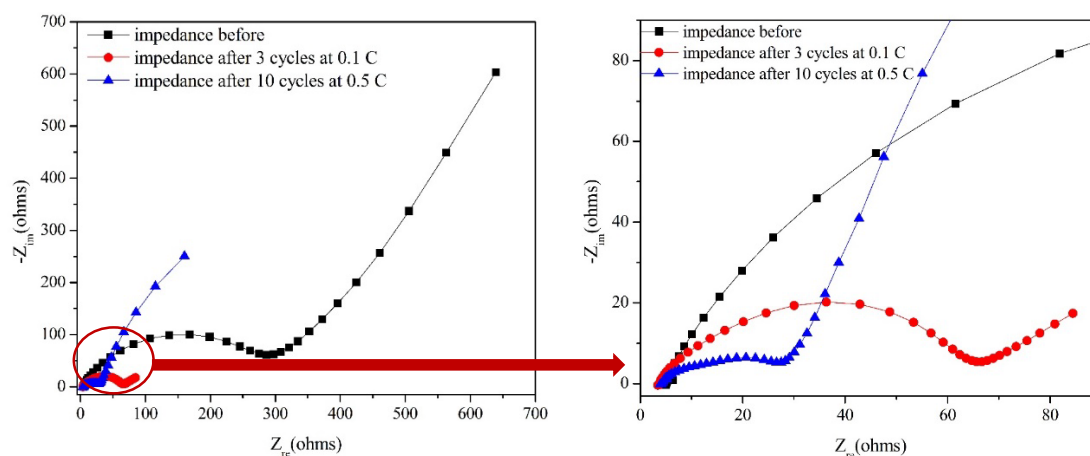
Fig. 4.8 a) Impedance analysis before and after charge-discharge, b) zoom in version of Fig. 4.8 (a).
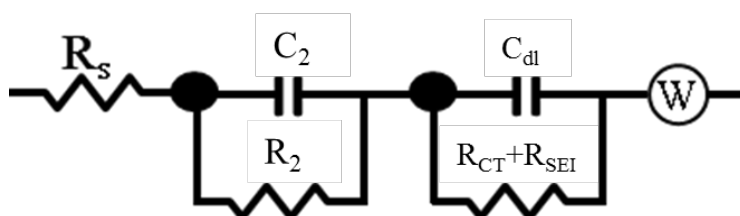
Fig. 4.9 Equivalent circuit, EqC 1, used for fitting the charge-discharge data for **Cell 1E**

Table 4.2 Values of solution and interfacial resistance obtained for **Cell 1E**

Imp. Data	Solution Resistance, R_s/R_1 (Ω)	Li Migration Through Surface, R_2 (Ω)	Interfacial Resistance, $R_{ct}+R_{SEI}$ (Ω)	χ^2
Impedance Before	5.193	18.34	237.2	2.9 X 10^{-3}
Impedance After 10 Cycles	3.567	630.5	26.09	1.4 x 10^{-3}

A reduction in R_{ct} with number of cycles along with no reduction in capacity evinces the formation of a stable SEI. Formation of such an SEI layer is advantageous in improving the performance of the cell.

4.4.2 Charge Discharge Analysis of 2, (GlyLiMB)

Fig. 4.10 shows the charge discharge profiles for 10 cycles for **cell 2G** fabricated using electrolyte **2**. The cell exhibited a high charge-discharge capacity of approximately 150-200 mAh/g for 8 cycles. Though the charge capacity for the first cycle was 398 mAh/g, higher than the theoretical capacity of graphite (372 mAh/g). One of the hypothesis behind the higher charge capacity is the generation of active voids onto the surface of the electrode because of the solid electrolyte. The generation of voids onto the surface of the electrode will allow more Li^+ ions to intercalate than 1 Li per 6 carbons (LiC_6; 372 mAh/g)[6] leading to the increment of capacity. Also, the first discharge capacity was found to be as low as 136 mAh/g. However, after an average capacity of 130 mAh/g for the first three cycles, the cell started showing higher charge and discharge capacities for the rest of the cycles and showed an ambiguous behavior.

Lower discharge capacity of 1st cycle and an average capacity of 130 mAh/g for all other cycles, shows that the generation of active voids is irreversible.
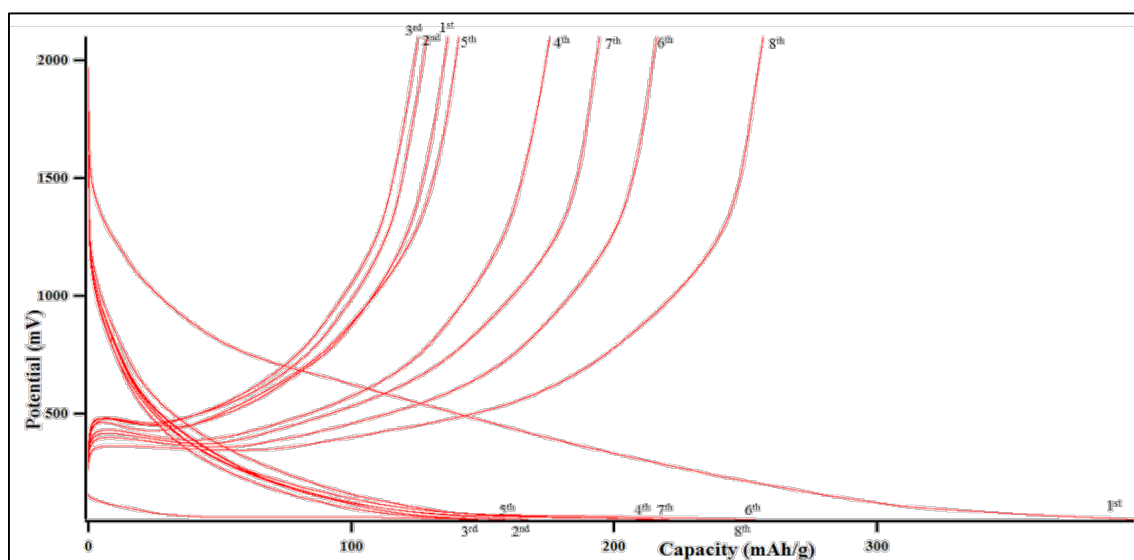
Fig. 4.10 Charge discharge profiles of **cell 2G** with 30µL of EC:DEC=1:1 for 8 cycles at 0.01C

Cell 2G broke down after 8 cycles, hence further charge-discharge could not be carried out. The increase in the capacity after the first three cycles can be attributed to the formation of interfacial layer or the SEI layer after the three cycles. Fig. 4.11 shows the coulombic efficiency plot for the 8 cycles.
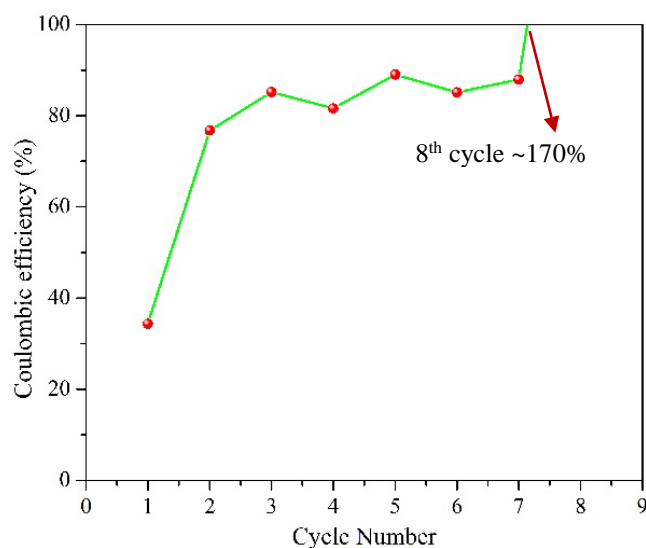
Fig. 4.11 Coulombic efficiency plots for 8 cycles of charge-discharge for **cell 2G**

The coulombic efficiency obtained for the first 7 cycles is ~85% which means that there is incomplete discharging during the 7 cycles and hence, accumulation of charge at the anode with increasing number of cycles. However the increase of coulombic efficiency at 8th cycle to 170% can be hypothesized to be due to the breaking of SEI layer resulting into the flow of all the accumulated charge towards the cathode increasing the overall discharge capacity and hence, the coulombic efficiency for the 8th cycle.

4.4.3 Charge Discharge Analysis of 3, (OxLiMB)

Fig. 4.12 shows the charge discharge profiles for 9 cycles. **Cell 3O** exhibited a charge-discharge capacity of 75-80mAh/g at a current rate of 0.01C (0.0313 mA). The first charge capacity is 129 mAh/g whereas the discharge capacity is quite low (53 mAh/g) resulting into a high capacity loss and low coulombic efficiency (41%). However, after the first cycle, all the cycles showed charge-discharge capacity in the range of 78-84 mAh/g for a commercial

graphite with a capacity of 162 mAh/g. Fig. 4.13 shows the coulombic efficiency plot for total

9 cycles for **Cell 3O**.
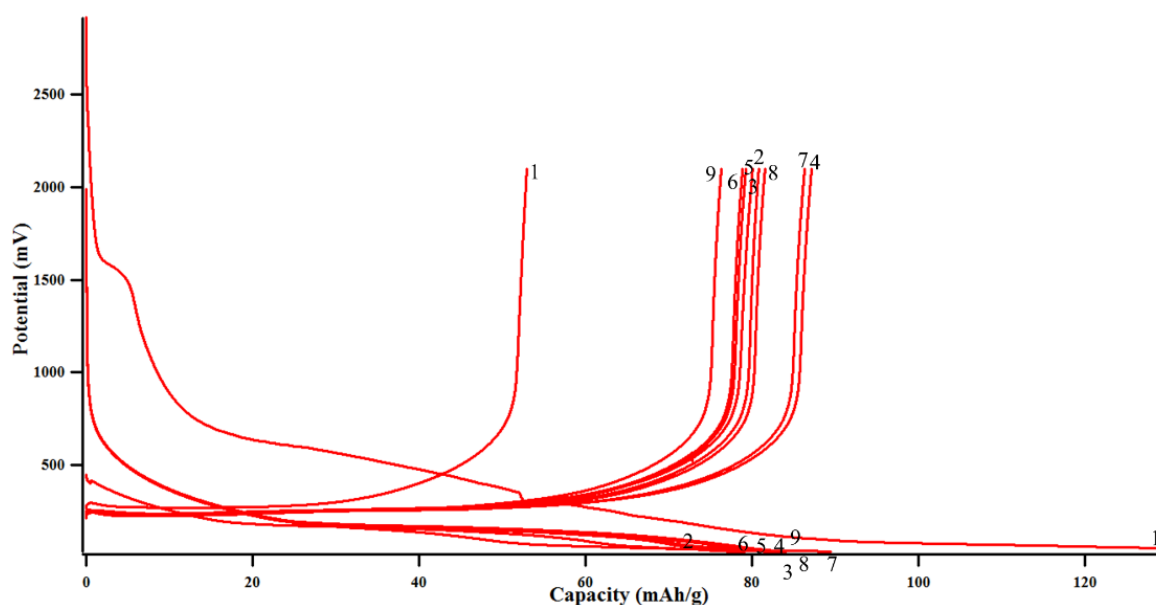
Fig. 4.12 Charge discharge profiles of **cell 3O** with 30µL of EC:DEC=1:1 for 9 cycles
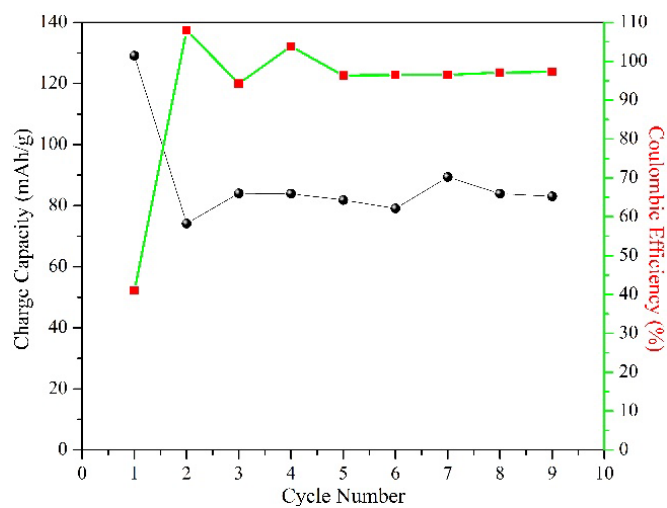
Fig. 4.13 Coulombic efficiency plots for 9 cycles of charge-discharge for **cell 3O** (Black:

Charge Capacity (mAh/g); Red: Coulombic Efficiency (%))

Interfacial Characteristics

Impedance analysis was done before and after charge discharge analysis for **cell 3O** (Fig. 4.14 a). The cell showed an interfacial resistance of 3221 Ω before the initiation of charge-discharge analysis. However, after completion of 10 cycles, the interfacial resistance for the cell reduced to the 51.07 Ω. A drastic fall in the interfacial resistance was attributed to the formation of a conducting SEI layer on the anodes. Fig. 4.15 shows the equivalent circuit, EqC2, used for fitting the impedance data and Table 4.3 gives the values of the types of resistance present in the system evaluated by the equivalent circuit, EqC2.
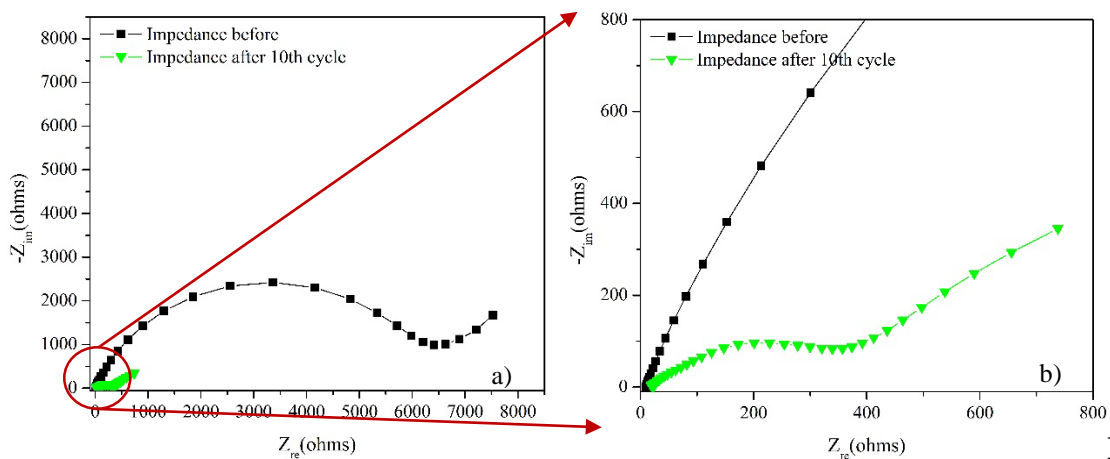
Fig. 4.14 a) Impedance analysis before and after charge-discharge, b) zoom in version of Fig. 4.13 (a).
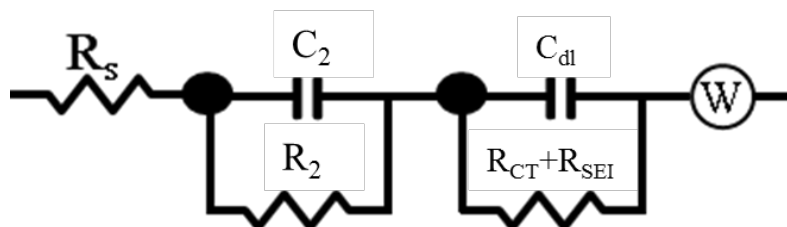
Fig. 4.15 Equivalent circuit, EqC 2, used for fitting the charge-discharge data for **Cell 3O**

Table 4.3 Values of solution and interfacial resistance obtained for **Cell 3O**

Imp. Data	Solution Resistance, R_s (Ω)	Li Migration Through Surface, R_2 (Ω)	Interfacial Resistance, $R_{ct}+R_{SEI}$ (Ω)	χ^2
Impedance Before	9.676	6478	3221	5.9 X 10^{-4}
Impedance After 20 Cycles	16.47	284.5	51.07	2.8 x 10^{-4}

Though the physical significance is given by the integer value, in order to obtain a perfect fit, one has to highlight the decimal values without which the χ^2 value or the error bar increases. Even a small change in the decimal place of the resistance values can bring the χ^2 value from 10^{-4} to 10^{-3}.

4.5 Conclusions

Low molecular weight cyclic organoboron electrolytes were tested for their charge-discharge characteristics and interfacial behavior for Li ion secondary batteries. The crystalline sample, **1** (EGMB) when mixed with LiTFSI in a molar ratio of 1:2 by grinding method showed an impressive charge discharge behavior with a charging capacity in the range of 150-200 mAh/g and was studied with different current rates and different number of cycles. The sample was also studied for its interfacial characteristics by studying impedance before and after charge discharge using EIS when the cell was completely discharged. A stable and a conductive interface can be considered to be formed and as a result the interfacial resistance decreased to a lower value of 26.09 Ω from 237.2 Ω after 10 cycles of charge discharge.

In the case of lithium borate type electrolytes, electrolyte **2** was used as synthesized for studying the charge-discharge analysis with the addition of 30 µL of EC:DC=1:1. The cell was studied at a very low current rate of 0.01 C for 10 cycles. It was capable of exhibiting a charging capacity in the range of 150-200 mAh/g, however the observed coulombic efficiency was 34% for the 1st cycle and increased to ~85% for 7 cycles. The cell broke down after 8 cycles and hence, could not be studied further. Unlike electrolyte **2**, electrolyte **3** showed a low capacity of 78-84 mAh/g for 9 cycles of charge-discharge.

However, one important conclusion was that the Li ion cells showed reversible charge-discharge without the addition of any commercial Li salts. All the above results confirm a real-time application of these electrolytes in lithium ion batteries.

References

1.   K. Smith, A. Pelter and Z. Jin, *Angew. Chem. Int. Ed. Engl.*, 1994, **33**, 851–853.

2.   G. E. Blomgren, *J. Power Sources*, 2003, **119**, 326–329.

3.   V. Aravindan, J. Gnanaraj, S. Madhavi and H.-K. Liu, *Chem. - Eur. J.*, 2011, **17**, 14326–14346.

4.   P. Lu, C. Li, E. W. Schneider and S. J. Harris, *J. Phys. Chem. C*, 2014, **118**, 896–903.

5.   A. M. Andersson and K. Edström, *J. Electrochem. Soc.*, 2001, **148**, A1100–A1109.

6.   D. Aurbach, B. Markovsky, I. Weissman, E. Levi and Y. Ein-Eli, *Electrochimica Acta*, 1999, **45**, 67–86.

7.   S. S. Zhang, *J. Power Sources*, 2006, **162**, 1379–1394.

8.   S. S. Zhang, K. Xu and T. R. Jow, *J. Power Sources*, 2003, **113**, 166–172.

9.   K. Xu, S. Zhang, T. R. Jow, W. Xu and C. A. Angell, *Electrochem. Solid-state Lett.*, 2002, **5**.

10.   M. Park, X. Zhang, M. Chung, G. B. Less and A. M. Sastry, *J. Power Sources*, 2010, **195**, 7904–7929.

11.   D. Aurbach, B. Markovsky, A. Shechter, Y. Ein-Eli and H. Cohen, *J. Electrochem. Soc.*, 1996, **143**, 3809–3820.

12.   M. Yamagata, N. Nishigaki, S. Nishishita, Y. Matsui, T. Sugimoto, M. Kikuta, T. Higashizaki, M. Kono and M. Ishikawa, *Electrochimica Acta*, 2013, **110**, 181–190.

13.   A. M. Stephan, *Eur. Polym. J.*, 2006, **42**, 21–42.

14.   D. Linden and T. B. Reddy, *3rd Ed. McGraw-Hall Companies, Inc*, 2001.

15.   K. Kalaga, M.-T. F. Rodrigues, H. Gullapalli, G. Babu, L. M. R. Arava and P. M. Ajayan, *ACS Appl. Mater. & interfaces*, 2015, **7**, 25777–25783.

16.   Y. Liu, Y. Ono, T. Matsumura, A. Hirano, T. Ichikawa, N. Imanishi and Y. Takeda, *Res. Rep. Fac. Eng. Mie. Univ*, 2005, **30**, 1–12.

17.   N. Kamaya, K. Homma, Y. Yamakawa, M. Hirayama, R. Kanno, M. Yonemura, T. Kamiyama, Y. Kato, S. Hama and K. Kawamoto, *Nat. Mater.*, 2011, **10**, 682–686.

18.   K. S. Smaran, R. Vedarajan and N. Matsumi, *Int. J. Hydrog. Energy*, 2014, **39**, 2936–2942.

19.   A guide to understanding battery specifications, MIT Electric Vehicle Team, 2008.

20.   J. K. Park, *Principles and applications of lithium secondary batteries*, John Wiley & Sons, 2012.

Chapter 5

Control of Charge-transfer Resistance via Electropolymerization of Borylated Thiophene Monomer on Anodes

Abstract

Modification of electrode surface resulting into the formation of a pre-formed SEI allows ready-to use anodes, curbing the need for any loss in capacity during the first few cycles of charging and discharging. Herein, we report the utilization of organoboron containing conducting polymers to reduce the interfacial resistance at SEI. The effect of SEI formation was evaluated by charge discharge analysis and impedance spectroscopy. Electropolymerization via repeated cyclic voltammetric cycling of the monomer led to formation of a π-conjugated polymer which was expected to provide high power, high chemical stability, high capacity, and long-term cyclability. The electrolyte for electropolymerization via cyclic voltammetric analysis was prepared by mixing borylated thiophene monomer and LiTFSI salt in acetonitrile-AMImTFSI (ionic liquid: 1-Allyl-3-methyl imidazolium bis (trifluromethanesulfonyl) imide) / BMImTFSI (ionic liquid: 1-butyl-3-methyl imidazolium bis (trifluromethanesulfonyl) imide) solution.

Charge-discharge characteristics of half-cell with borylated thiophene polymer over graphite was studied and compared with graphite without any modification and polythiophene coated graphite. All the half-cells showed capacitive loss with increasing number of cycles. However, the capacity loss in the case of borylated thiophene polymer electrode was minimal. Also, the interfacial resistance studies using electrochemical impedance spectroscopy indicated only a

marginal increase in the resistance for the borylated thiophene polymer coated graphite electrode compared to the drastic increase in the case of other two electrodes.

5.1 Introduction

In lithium ion batteries, highly graphitized carbonaceous materials have been used till now[1–4]. These graphitized carbon materials result in a high irreversible capacity loss after the first cycle. This is one of the reason that many researchers have focused on this aspect of the lithium ion batteries i.e., reduction of irreversible capacity loss and improvement of the overall performance of the battery[5]. As already explained, during the first charge of the batteries, reduction of electrolyte leads to the formation of solid electrolyte interface (SEI) which should be thin, conductive and stable in nature[6]. However, this also leads to a drawback. Since, generally used, Li and Li-C electrodes are passivated by the surface films in optimized electrolyte solutions, unceasing reactions between electrodes and electrolytes are inescapable[7]. Hence, this irreversible decomposition of electrolyte solvent leads to reduction of electrochemically active lithium and Li-C anodes[7,8]. These irreversible reactions are generally parasitic in nature[9,10] and has to be inhibited in order to obtain a high performance battery.

Several approaches are examined to improve the battery performance such as designing new electrolyte materials[11,12], change of electrodes from graphitic electrode material to high capacity electrode materials such as silicon[13,14] or carbon-silicon composites[15–17]. Among all this, surface modification of anodes is one of the practical approach to reduce the irreversible capacities arising because of an unstable SEI formation[18]. Methods such as oxidation, fluorination, ceramic coating and electropolymerization have already been applied and studied. An earlier report says electropolymerization of a conducting polymer with heterocyclic aromatic monomer units show high thermal and chemical stability. Also, the process of electropolymerization can be easily controlled and result into surface films with strong

adhesion[19].

Thiophenes have gained significant attention and are studied well in this field. Its structural versatility and environmental stability of its doped and undoped states leads to their application in the field of electrodes, conductors and semiconductors[20]. Modification of the electrodes using pyrrole[18], thiophene[18], derivatives of thiophene such as α-terthiophene[21], α-tetrathiophene[22] etc., have been reported. The mechanism of electropolymerization involves several chemical and electrochemical steps. The first step involves oxidation of the monomer to generate its radical cation. The electron transfer process in this step is faster than the diffusion of monomer from the electrolyte solution to the electrode and hence, a high concentration of radicals remain near the electrode surface. 2 moles of the generated radical cations combine together forming a dihydrocationdimer first and finally, an oligomer after two electrons and rearomatization. Since, electropolymerization occurs at an applied potential, the dimer gets easily oxidized than the monomer, generates a dimeric radical cation and couples with a monomeric radical cation. These successive electrochemical steps leads to the deposition of the polymer onto the electrode surface[20].

However, boron incorporation into thiophene or making boron-thiopene compounds that can electropolymerize to form a surface film over electrodes has not been studied till now. Boron doped carbon[23] results into oxidation resistant materials[24]. Incorporation of boron into conducting monomers like thiophene can help in reduction of the electrode-electrolyte interfacial resistance. Boron being Lewis acidic in nature, leads to generation of hole-carriers when doped with graphite, thereby increasing its electrical conductivity and hence, discharge

capacity[25]. In a similar manner, formation of a conducting polymer surface film doped with boron is expected to increase the overall electrical conductivity of graphite-polymer film electrode and hence, result into a highly conductive SEI layer that will further enhance the lithiation and delithiation mechanism improving the performance of the battery.

5.2 Objective of Research

To address the problem of poor cyclability and reversibility arising due to anodes, this chapter's aim is to modify the electrode surface with an electronically conductive polymer which will help in reducing the charge-transfer resistance at the electrode-electrolyte interface and lead to higher capacities. In this chapter, the detailed synthesis of a low molecular weight boron monomer and its electropolymerization onto the graphite electrodes is studied. Electropolymerization has been carried via two different methods,

i) **pre-modifying electrodes** and then testing for battery applications and,

ii) directly carrying out *in-situ* **electropolymerization** via charge-discharge analysis. *In-situ* electropolymerization requires addition of the conducting monomer as an additive with the electrolyte in the fabricated cell for charge-discharge.

This method is advantageous as compared to pre-modified anodes as in this method, electropolymerization of monomer and reduction of electrolyte take place simultaneously to form a boron rich SEI layer with electropolymerization being the dominant reaction. Since, electropolymerization is supposed to be the major reaction, this would result in boron-rich interfacial layer that is expected to be highly stable and conductive in nature. Further, such an SEI layer will not allow any species other than Li^+ ions to pass through the electrode surface.

5.3 Experimental

5.3.1 *Materials and Instruments*

Table 5.1 Details of the materials procured for the synthesis and other experiments

S. No.	Materials used	Companies
1.	Mesitylbromide	TCI Chemicals
2.	Mg turnings (Mg)	Wako Chemicals
3.	Trimethoxyborane (B(OCH$_3$)$_3$)	Wako Chemicals
4.	Dehydrated tetrahydrofuran (THF)	Wako Chemicals
5.	Dehydrated diethylether (Et$_2$O)	Wako Chemicals
6.	2-bromothiophene	TCI Chemicals
7.	n-hexane	Wako Chemicals
8.	Dehydrated Methanol (MeOH)	Wako Chemicals
9.	Thiophene (Thp)	TCI Chemicals
10.	Acetonitrile (AcCN)	Wako Chemicals
11.	Lithium (bis-(trifluoromethanesulfonyl) imide (LiTFSI)	Kanto Kagaku
12.	EC:DEC=1:1	Chameleon Reagent

Mg turnings were activated by heating in vacuum prior to the reaction. Dehydrated THF and dehydrated ether were used as received for all the syntheses. Acetonitrile was dried over activated molecular sieves (Wako chemicals) 5A 1/16 prior to use. AMImTFSI/ BMImTFSI were synthesized after the ion exchange reaction of AMImCl (1-allyl-3-methylimidazolium chloride)/ BMImCl (1-butyl-3-methylimidazolium chloride) with lithium (bis-(trifluoromethanesulfonyl) imide) (LiTFSI). EC:DEC=1:1 (v/v) solution was used after drying over activated molecular sieves 5A 1/16.

NMR spectroscopic analysis was done by using Bruker model Avance III 400. The

morphology of the electropolymerized electrodes were analysed by using Scanning Electron Microscope (Hitachi 400). The prepared graphite based anodic half-cells were charged and discharged in a galvanostatic mode using compact charge and discharge system of EC Frontier; ECAD-1000. For charge-discharge studies, anodic half-cells were fabricated using CR2025 type coin cells. The cells were assembled in a similar manner as explained in Chapter 1, Section 2.3 using surface modified graphite as the working electrode (diameter = 15Φ), lithium metal as the counter electrode (15 mm, Honjo metals, Japan). The two electrodes were separated by a Celgard® based separator cut in to a disk (diameter = 16 mm).

5.3.2 *Preparation of Boron-thiophene monomer:*

Dimethoxymesitylborane (**4b**) was synthesized by reacting trimethoxyborane in dehydrated diethylether with mesitylmagnesium bromide (**4a**) (Scheme 4). Thiophen-2-yl magnesium bromide (**4d**) was prepared in a similar manner like **4a** (Scheme 5). The final product, mesityldi(thiophen-2-yl)borane/boron-thiophene monomer (**4**) was synthesized by treating dimethoxymesitylborane (**4b**) (0.41 mL, 0.0056 moles) with thien-2-yl magnesium bromide (**4d**) in dehydrated diethyl ether (Scheme 6). All the reactions were carried out under nitrogen atmosphere. Final product was first filtered, washed with hexane and recrystallized in methanol. The product was obtained in 95% yield as off-white color crystals.

Scheme 4

Scheme 5

Scheme 6
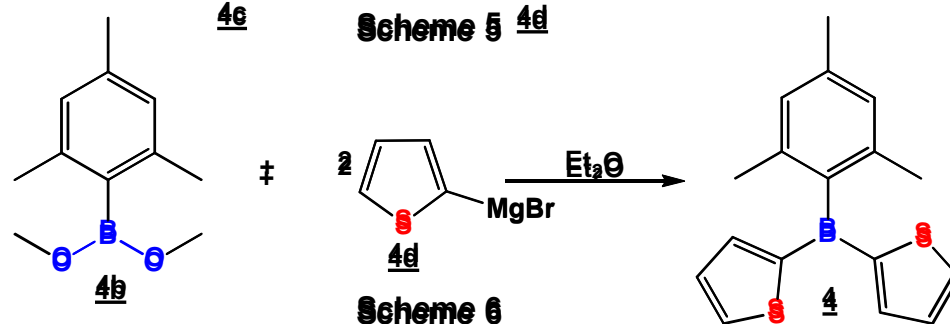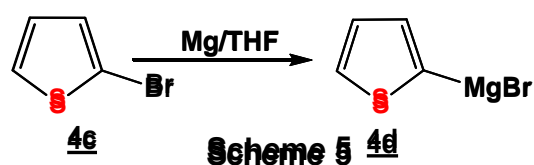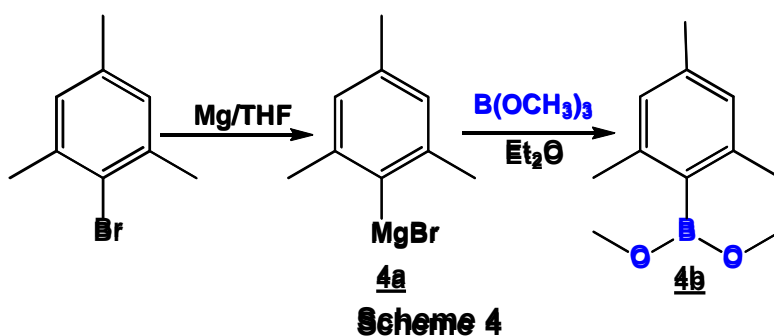
5.3.3 _Electropolymerization Methods:_

The synthesized monomer was electropolymerized in two different ways:

1. _Pre-modified Anodes_: The monomer was electropolymerized by carrying out cyclic sweeps between -2.0 to 2.0 V at a scan rate of 0.05 V/s using Ag/Ag^+ as the reference electrode in 0.02 M **4** in ionic liquid (AMImTFSI/BMImTFSI)/ acetonoitrile system as electrolyte. The working and the counter electrodes were graphite and Pt chip respectively. A box cell (flat-cell) was used in this method of electropolymerization with N_2 purging. The electropolymerized samples were studied visually and by using SEM. The SEI characteristics were studied by using these pre-modified electrodes for charge-discharge analysis.

2. *In-situ modified Anodes*: The second method was electropolymerization while the electrode was subjected to charge-discharge. Graphitic anode half-cells were fabricated using Li foil as the reference and counter electrode with 0.1 M **4** in 1 M LiTFSI in EC:DEC=1:1 as the electrolyte. The separator was dipped into the electrolyte and was used in the cell with additional 30 µL of the electrolyte. Repeated charge-discharge cycles while monitoring the overall impedance changes before and after the charge discharge led to the understanding that the electropolymerization of the monomer **4** has been accomplished. This data was compared with an anodic half-cell with 0.1M thiophene in 1.0 M LiTFSI in EC:DEC=1:1 as the electrolyte.

In both the cases, a very dilute monomer concentration of the conducting monomer was taken (0.01 M thiophene/**4**). A lower concentration of monomer will not compete with the electrochemical intercalation of Li^+ ions. Since, the concentration of monomer is very low as compared to the concentration of Li^+ ions in the system, maximum amount of the monomer would get consumed in electropolymerization reaction facilitating the diffusion of Li^+ ions. It would also result in a thin but conducting electropolymerized layer.

5.3.4 *Characterization of B-Thp monomer, 4*

5.3.4.1 *NMR spectroscopy*

The synthesized low molecular weight boron monomer, **4** (B-Thp) was characterized by ^{11}B-NMR in $CDCl_3$ at 400 MHz showing a peak at 55.0 ppm (Fig. 5.1 a) referring to the incorporation of boron as an alkylborane. Further, ^{1}H-NMR in $CDCl_3$ also supported the

expected structure. ^{11}B-NMR (δ ppm, 400MHz, CDCl$_3$): 55.7 ppm; ^{1}H-NMR (δ ppm, 400MHz, CDCl$_3$): 7.95 (s, Ar-CH (Thiophene), 1 proton), 7.82 (s, Ar-CH (Thiophene), 1 proton), 7.28 (s, Ar-CH (Thiophene), 1 proton), 6.88 (s, Ar-CH (mesityl), 2 protons), 2.38 (s, Ar-CH$_3$ (mesityl), 3 protons), 2.05 (s, Ar-CH$_3$ (mesityl), 6 protons).
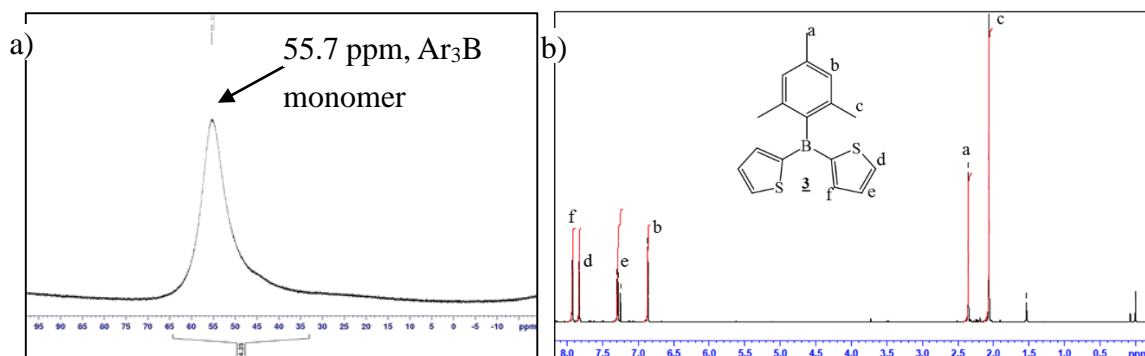

Fig. 5.1 a) ^{11}B-NMR and b) ^{1}H-NMR spectra of **4** (structure given in **Fig. 5.1 b**) in CDCl$_3$
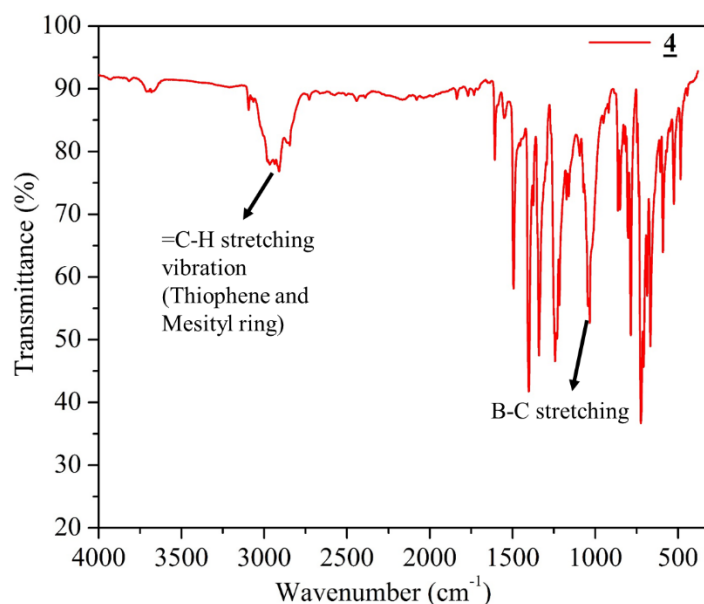
5.3.4.2 *IR spectroscopy*

Fig. 5.2 IR spectrum of **4**

The observed IR frequencies are listed below:

3000 - 2950 cm^{-1}, aromatic CH stretching conjugated with C=C (Thiophene and mesityl ring); 1550-1195 cm^{-1}, C=C in-plane vibrations (thiophene); 1020 cm^{-1}, B-C bond stretching; 600-500 cm^{-1}, Mesityl ring out of plane deformation vibrations.

5.3.4.3 *Scanning Electron Microscopy*

The electropolymerized pre-modified electrodes were morphologically characterized by SEM which showed the formation of the smooth and compact layer on the graphite electrodes. A thick polymerized coating was formed which was indicated by the formation of a blue-green layer onto the carbon. Fig. 5.3 shows the image of the carbon anode electropolymerization and the SEM image exhibiting the layer-by-layer polymerization of monomer **4** on carbon anode.
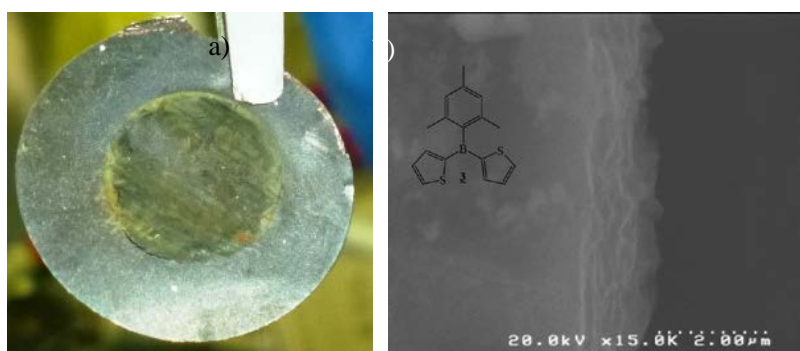

Fig. 5.3 a) Image of carbon electrode after electropolymerization and b) SEM image showing layer-by-layer formation of polymer during the repeated cycles

5.4 Results and Discussion

5.4.1 Pre-modified Anodes

The formation of electropolymerized layer onto the graphite anodes can be clearly seen in

SEM images and further, is supported by electrochemical impedance spectroscopic analysis. Impedance spectroscopy measurement was carried out after every 5 cycles. Till 15 cycles there was only one semicircle observed. Appearance of a second distinct semi-circle or a time constant after 15 cycles referred to the second phase which can be associated with the formation of a polymerized layer. The impedance spectra for all the sets of 5 cycles are shown in Fig. 5.4.
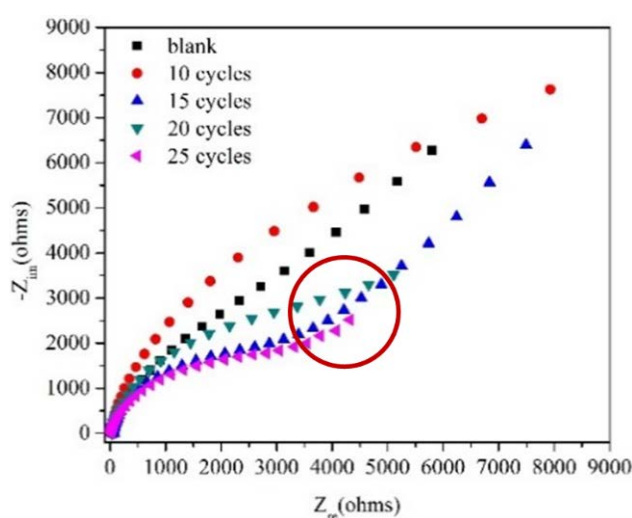
Fig. 5.4 Impedance spectra of electropolymerization with each set of 5 cyclic voltammetric cycles. The circle portion (marked with red) shows the formation of a second semicircle.

The pre-modified anodes were tested for charge-discharge behavior in an anodic half-cell. The charge-discharge behavior of pre-modified anode was compared with bare graphite for 10 continuous charge-discharge cycles at a rate of 0.5 C. Both the electrodes showed typical charge-discharge profiles showing intercalation at lower potentials. The uncoated or the bare graphite electrode showed a drastic decrease in the capacity with each cycle (Fig. 5.5a).
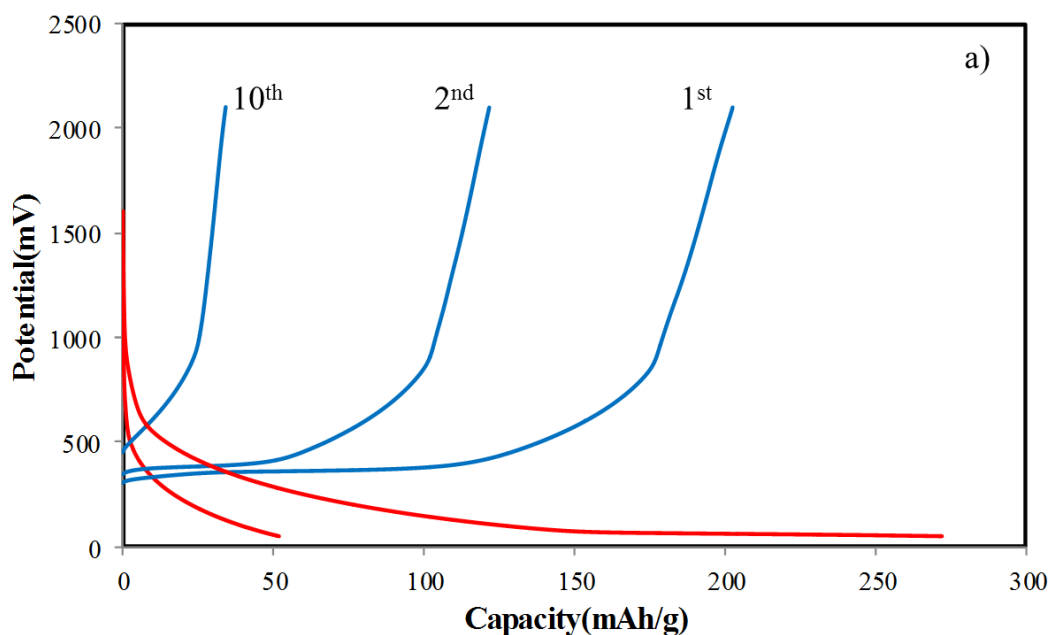
Fig. 5.5 a) Charge discharge profiles of anodic half-cell using ***bare graphite*** with 0.1 M

LiTFSI in EC:DC=1:1 as electrolyte at 0.1 C

This decrease in capacity from 200 mAh/g (1st cycle) to approx. 30 mAh/g (10th cycle) can

be due to the formation of a non-compatible SEI layer which is insulating in nature. This was

also asserted by the impedance spectra as shown Fig. 5.5 (b) depicting an increase in the

interfacial resistance from 1500 Ω to 3500 Ω after 10 cycles.
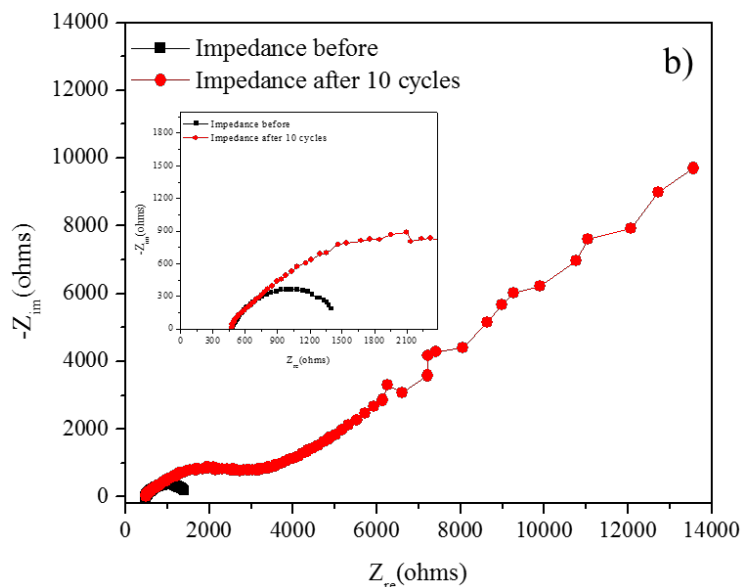
Fig. 5.5 b) Impedance analysis of anodic half-cell using graphite with 0.1 M LiTFSI in

EC:DC=1:1 as electrolyte at 0.1 C

In contrast, the charge-discharge cycles of graphite electrodes on which electropolymerization of boron-thiophene monomer was carried out did not show this capacity fading effect. In the case of boron-thiophene coated electrodes, the capacity for the 10 cycle was maintained at 125 mAh/g (Fig. 5.6 a) and the results from impedance analysis also correlated well by showing marginal increase from 1500 Ω to 2500 Ω (Fig. 5.6 b) unlike the one with bare graphite showing 3500 Ω. This can be attributed to the polymerized boron-thiophene film which might be acting as a conducting SEI layer and avoiding decomposition of any electrolyte over the graphite.

Fig. 5.6 a) Charge discharge profiles of anodic half-cell using electropolymerized graphite

with monomer **4** and 0.1 M LiTFSI in EC:DC=1:1 as electrolyte at 0.1 C
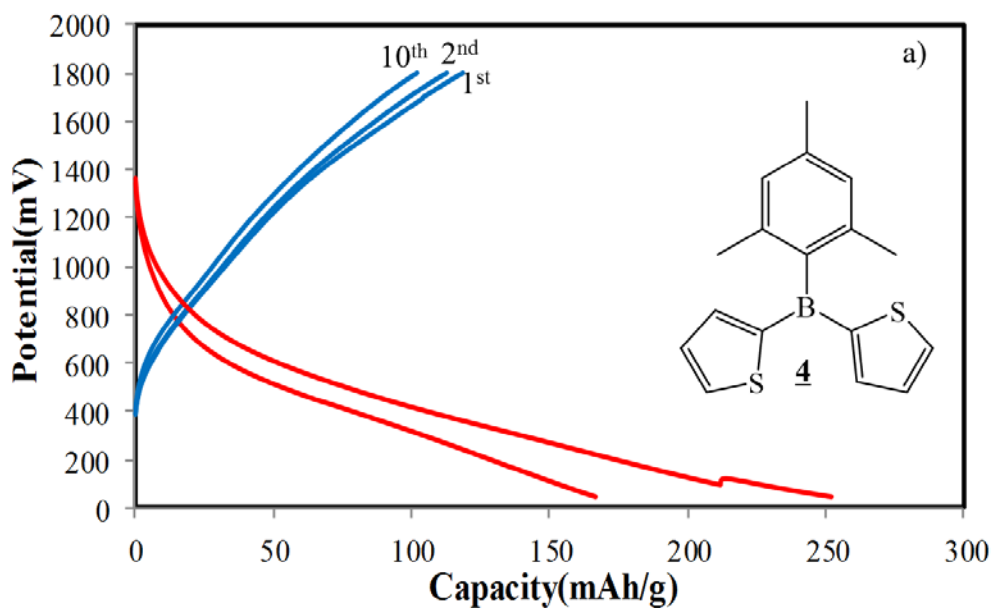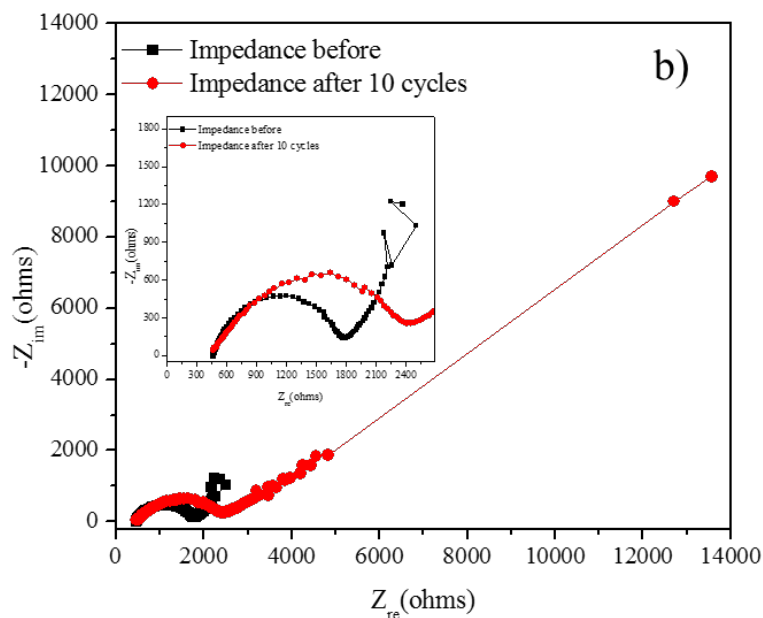

Fig. 5.6 b) Impedance analysis of anodic half-cell using electropolymerized graphite

with monomer **4** and 0.1 M LiTFSI in EC:DC=1:1 as electrolyte at 0.1 C

5.4.2 <u>In-situ modified Anodes</u>

In Fig. 5.6 (b), we observed an increase in the charge transfer resistance. This increase is attributed to the formation of SEI after charging-discharging over the electropolymerized film. In order to circumvent this problem of SEI layer forming onto the polymerized layer over the electrolyte, we thought of devising a method to incorporate the electropolymerization of thiophene as the major dominant reaction during the SEI formation with simultaneous reduction of electrolyte. Hence, *in-situ* modification of graphite electrode in galvanostatic mode was carried out.

In general, oxidation of thiophene when done via recurring cyclic potential sweeps occurs at 1.4 V - 2.3 V vs SCE (Saturated calomel electrode). Further, in acetonitrile-TBAP (tetrabutylammoniumperchlorate) systems, electropolymerization occurs at 1.6 V vs SCE. However, it is known that in galvanostatic mode, electropolymerization occurs at 0.5 V more positive than the oxidation potential of the monomer and results in more conducting and homogeneous polymerized films[20]. Based on the relationship between the standard electrode potentials of SCE electrode and Li^+/Li, the current peak potential of electropolymerization of thiophene at 1.6 V vs. SCE corresponds to 0.6 V vs. Li/Li^+ when done via cyclic sweep method and 1.1 V in galvanostatic mode.

Anodic half-cell with bare graphite were repeatedly cycled at 0.1 C with 0.1 M LiTFSI in EC:DC=1:1 as the electrolyte. Fig. 5.7 shows the charge discharge profiles and impedance spectra using thiophene as the additive. In this case, we observed an increase in the discharge capacity from 1st (21 mAh/g) to 7th cycle (58 mAh/g) and then, the capacity decreased from 7th

to 10th cycle (50 mAh/g). The impedance analysis showed a drastic decrease in the interfacial resistance before and after charge-discharge cycles. The charge transfer resistance decrease to 78 Ω after 10 cycles of charge discharge from 500 Ω (before charge-discharge). This was due to the use of thiophene as additive for modifying the electrode surface and making it electronically conducting. A potential plateau was observed at 1.6 V in the charge-discharge curve corresponding to the electropolymerization of thiophene. In the next step, surface modification was done using boron-thiophene as the additive with 0.1 M LiTFSI in EC:DC=1:1 as the electrolyte. As compared to thiophene, an improvement was seen in the charge-discharge cycles as well as in the reduction of interfacial resistance which can be seen in Fig. 5.7.
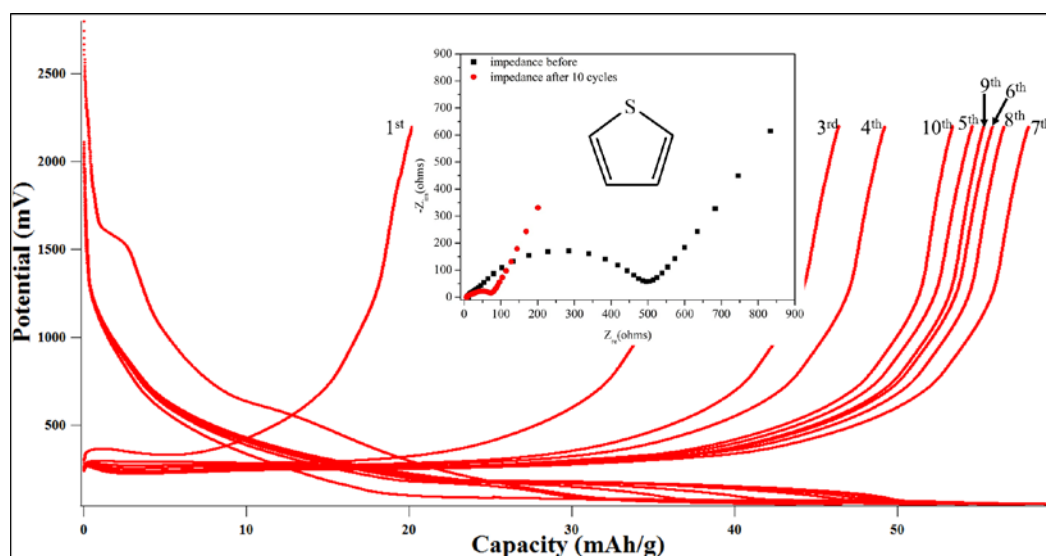

Fig. 5.7 *In-situ* electropolymerization via repeated charge discharge cycles and impedance analysis of anodic half-cell using 0.01 M thiophene in 0.1 M LiTFSI in EC:DC=1:1 as electrolyte under CC mode at 0.1 C
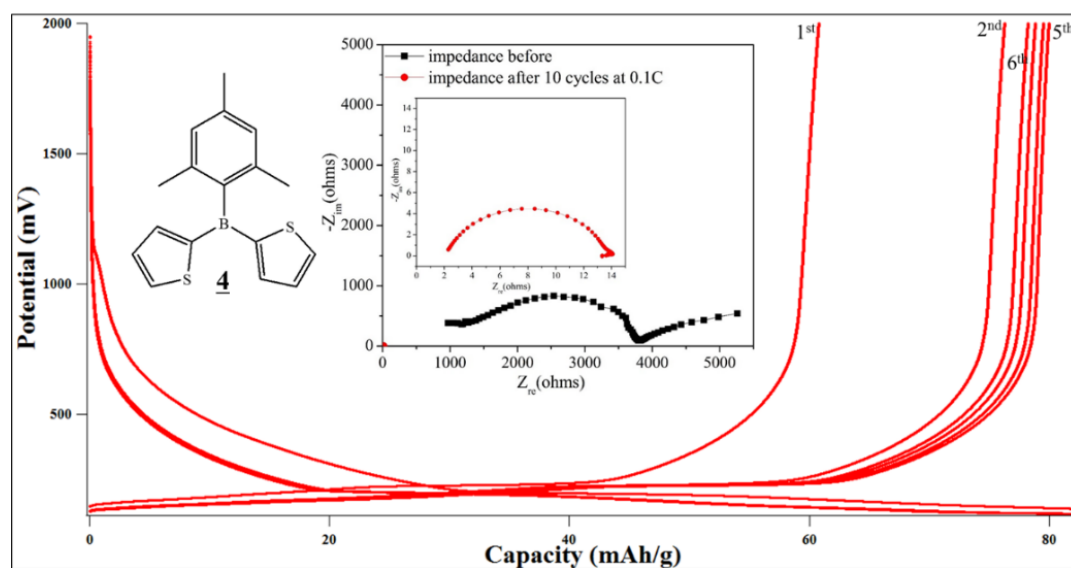
Fig. 5.8 *In-situ* electropolymerization via repeated charge discharge cycles and impedance analysis of anodic half-cell using 0.01 M **4** in 0.1 M LiTFSI in EC:DC=1:1 as electrolyte under CC mode at 0.1 C

The discharge capacity for the first cycle was observed to be 60 mAh/g and the rest of the cycles showed an average discharge capacity of 80 mAh/g which was higher as compared to the one with thiophene as the additive showing the formation of a polymerized layer. A plateau like slight dip at 1.1 V in the charging cycle referred to the electropolymerization of the boron-thiophene monomer. The charge transfer resistance before charge-discharge was 3849 Ω. However, a drastic fall was seen in the charge-transfer resistance (14 Ω) after *in-situ* electropolymerization of boron-thiophene. This decrease was due to the result of incorporation of boron in the monomer as boron is electron deficient, so its presence at the interface will result in increased interaction with the electrolyte and reduction of the electrode-electrolyte interfacial resistance. This polymerized layer of **4** which was formed onto the graphite electrode can be hypothesized to form simultaneously with the formation of SEI layer leading

to a large decrease in the interfacial resistance. Table 5.2 gives a comparison of charge-discharge capacities and interfacial resistances of pre-modified anodes and *in-situ* modified anodes.

Table 5.2 Summary of results

Graphite with additive	Surface modification of anode			In-situ electropolymerization		
	Capacity from 1st -10th cycle (mAh/g)	Cyclability	Interfacial Resistance after cycling (Ω)	Capacity of 1st cycle (mAh/g)	Cyclability	Interfacial Resistance after cycling (Ω)
No additive	200 to 30	Poor	3500	-	-	-
Thiophene	-	-	-	21	Poor	78
_4_	125-100	Good	2500	60	Good	14

5.5 Conclusions

A low molecular weight conjugated monomer, termed as boron-thiophene monomer, **4**, was synthesized in this chapter and was electropolymerized over carbon anodes to study the change in interfacial resistance . **4** was used for surface modification of anodes (Graphite) via cyclic voltammetry and repeated charge-discharge cycles in the presence of ionic liquids. Surface modification was done in two ways: 1. by pre-modifying the anodes and then using them for battery testing after characterization via SEM; and 2. by *in-situ* modification of bare graphite anodes for charge discharge cycles in the presence of boron-thiophene monomer as additive in the conventional electrolyte. The results obtained with the monomer were compared with the bare graphite electrodes. It was observed that in the case of pre-modified anodes, in the presence of boron-monomer, the cyclability had improved, however the charge-transfer resistance increased with a smaller value. Increment of charge transfer resistance can be due to the competing reactions leading to polymerization and to the reduction of electrolyte. In case of *in-situ* modified anodes, the capacity obtained using boron-thiophene monomer as additive was higher as compared to thiophene. A drastic fall in charge-transfer resistance in the lithium cell containing the boron-thiophene monomer asserted the charge-discharge data without any fading and can be attributed to the formation of a highly stable and conductive interface.

References

1. S. Flandrois and B. Simon, *Carbon*, 1999, **37**, 165–180.

2. Y. P. Wu, E. Rahm and R. Holze, *J. Power Sources*, 2003, **114**, 228–236.

3. M. Yoshio, H. Wang, K. Fukuda, T. Umeno, T. Abe and Z. Ogumi, *J. Mater. Chem.*, 2004, **14**, 1754–1758.

4. G. Wang, X. Shen, J. Yao and J. Park, *Carbon*, 2009, **47**, 2049–2053.

5. D. Aurbach, B. Markovsky, I. Weissman, E. Levi and Y. Ein Eli, *Electrochimica Acta*, 1999, **45**, 67–86.

6. A. Andersson, Surface phenomena in Li ion batteries, Acta Universitatis Upsaliensis. *Comprehensive Summaries of Uppsala Dissertations from the Faculty of Science and Technology,* Uppsala, 2001, 60.

7. D. Aurbach, B. Markovsky, M. D. Levi, E. Levi, A. Schechter, M. Moshkovich and Y. Cohen, *J. Power sources*, 1999, **81**, 95–111.

8. T. Doi, K. Takeda, T. Fukutsuka, Y. Iriyama, T. Abe and Z. Ogumi, *Carbon*, 2005, **43**, 2352–2357.

9. X. Zeng, G. L. Xu, Y. Li, X. Luo, F. Maglia, C. Bauer, S. F. Lux, O. Paschos, S. J. Kim, P. Lamp, J. Lu, K. Amine and Z. Chen, *ACS Appl. Mater. & Interfaces*, 2016, **8**, 3446–3451.

10. V. Agubra and J. Fergus, *Materials*, 2013, **6**, 1310–1325.

11. Y. S. Zhu, X. J. Wang, Y. Y. Hou, X. W. Gao, L. L. Liu, Y. P. Wu and M. Shimizu, *Electrochimica Acta*, 2013, **87**, 113–118.

12. M. Wakihara, Y. Kadoma, N. Kumagai, H. Mita, R. Araki, K. Ozawa and Y. Ozawa, *J. Solid State Electrochem.*, 2012, **16**, 847–855.

13. H. Kim, E. J. Lee and Y.-K. Sun, *Mater. Today*, 2014, **17**, 285–297.

14. S. D. Beattie, D. Larcher, M. Morcrette, B. Simon and J.-M. Tarascon, *J. Electrochem. Soc.*, 2008, **155**, A158–A163.

15. Y. Liu, K. Hanai, J. Yang, N. Imanishi, A. Hirano and Y. Takeda, *Electrochem. Solid-state Lett.*, 2004, **7**, A369–A372.

16. J. H. Lee, W. J. Kim, J. Y. Kim, S. H. Lim and S. M. Lee, *J. Power Sources*, 2008, **176**,

353–358.

17. Z. S. Wen, J. Yang, B. F. Wang, K. Wang and Y. Liu, *Electrochem. Commun.*, 2003, **5**, 165–168.

18. T. Doi, K. Takeda, T. Fukutsuka, Y. Iriyama, T. Abe and Z. Ogumi, 炭素, 2003, **210**, 217–220.

19. B. Pourabbas, N. Arsalani and A. A. Entezami, *Iran. J. Polym. Sci. Technol. Vol*, 1993, **2**.

20. J. Roncali, *Chem. Rev.*, 1992, **92**, 711–738.

21. S. Tepavcevic, Y. Choi and L. Hanley, *Langmuir*, 2004, **20**, 8754–8761.

22. M. A. Del Valle, L. I. Canales, A. Ramos, F. R. Díaz, L. A. Hernández, F. Armijo, J. C. Bernède, L. Cattin and G. Louarn, *Int. J. Electrochem. Sci*, 2013, **8**, 1422–1433.

23. M. Endo, C. Kim, T. Karaki, Y. Nishimura, M. J. Matthews, S. D. M. Brown and M. S. Dresselhaus, *Carbon*, 1999, **37**, 561–568.

24. G. M. Swain and R. Ramesham, *Anal. Chem.*, 1993, **65**, 345–351.

25. Y. Lee, D. Y. Han, D. Lee, A. J. Woo, S. H. Lee, D. Lee and Y. K. Kim, *Carbon*, 2002, **40**, 403–408.

Chapter 6

Conclusions

6.1 General Conclusions

It has become increasingly important in today's world to have ready access to energy in different forms. Rechargeable batteries are therefore becoming immensely important, by virtue of their ability to store electricity and make energy highly portable. The lithium ion (Li-ion) battery fulfills many of the demands made within the areas of portable electronics and EV/HEV's, and is superior in many ways to the more common nickel-cadmium (Ni-Cd) and nickel-metal hydride (Ni-MH) batteries (LIBs). Lithium-ion batteries have been widely used for popular power sources in portable electronic device in the past decades. However, considering the commercial aspect, a few setbacks in the ease of utilization of Li-ion battery lie in its highly flammable nature owing mainly to its electrolytes. Keeping this disadvantage in view, novel non-flammable low molecular weight electrolytes have been synthesized and the characteristic results of these compounds have been systematically drawn. This thesis has been drafted meticulously encompassing all of the results with the necessary interpretation.

In *Chapter 1*, the literature, the history, the evolution and the establishment of lithium ion batteries are detailed. With a brief introduction of the types of battery components, the first chapter emphasizes on the electrode-electrolyte interface. Interface or the Solid Electrolyte Interface (SEI) with respect to graphitic anodes plays a crucial role in the enhancement of the Li storage ability of

the anodes and hence, the overall performance of the battery. The chapter also focusses on the use of boron or organoboron moieties in designing the interface and the enhancing the capability of the battery. In case of electrolytes, boron incorporation helps in trapping the anion and its immobilization thereby making Li^+ ions as the only charge carrier in the electrolytic solution.

Chapter 2 focusses on designing a novel cyclic organoboron electrolyte in which the ion conduction mechanism is different than that of the polymer electrolytes. The electrolyte, synthesized from ethylene glycol and mesitylborane (**1**, EGMB), possesses a varying conduction mechanism depending on the mode of insertion of Li salt namely conventional method and grinding method. Grinding technique of the lithium salt allowed addition of the Li salt without any organic solvent and led to higher ionic conductivity compared to the systems prepared by the conventional method of mixing by dissolution and evaporation of solvents. This increased ionic conductivity was attributed to the undisturbed crystalline nature of the electrolyte which facilitated the formation of anion scaffolds arranged as crystalline structure. These ion channels ease the transportation of Li^+ ions via ion hopping mechanism. Fig. 6.1 summarizes the data of ionic conductivity obtained via grinding and conventional method of preparation of samples.
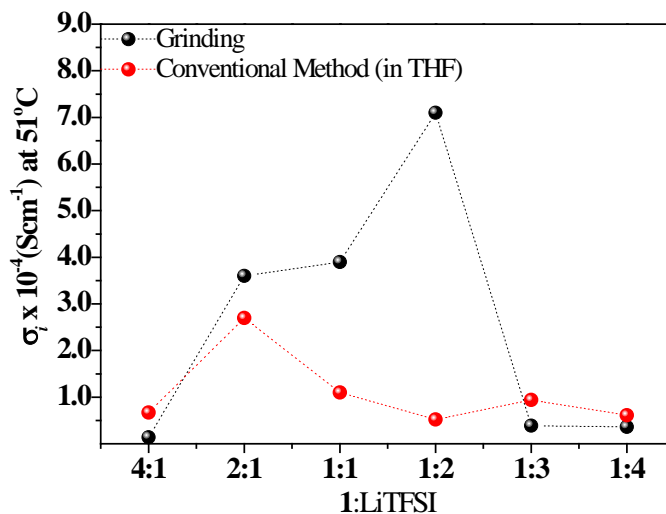
Fig. 6.1 Comparison of ionic conductivities of the samples prepared by the two methods

Since insertion of Li salt was carried out externally via any of the above mentioned methods, such Li insertion might prevent the effective formation of ionic channels. Hence, in ***Chapter 3***, the synthesis and electrochemical characteristics of other novelly designed electrolytes inherently containing an ionically bonded Li^+ ions were detailed. These electrolytes could be synthesized by the *in-situ* insertion of Li salt. With this in mind, two electrolytes based on glycerol (**2**, GLiMB) and oxalic acid (**3**, OxLiMB) were synthesized by dehydrocouplng reaction with lithium mesitylhydroborate. These electrolytes in the presence of ionic liquids exhibited high ionic conductivities in the order of 10^{-2} Scm^{-1}. Their electrochemical behavior was also compared with the electrolyte synthesized in Chapter 2 via external addition of Li salt. Fig. 6.2 summarizes the ionic conductivity and transference number of these three electrolytes.
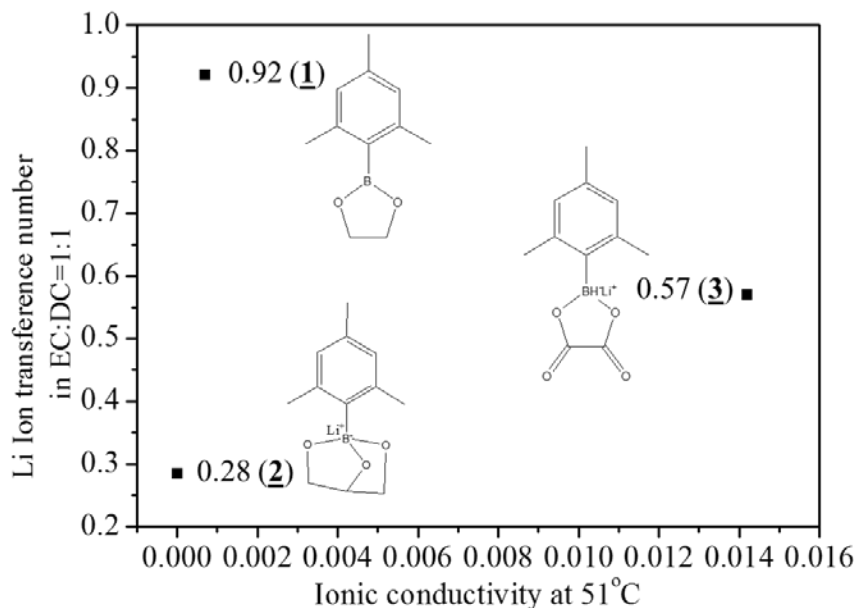
Fig. 6.2 Comparison of ionic conductivities and Li ion transference numbers in

EC:DEC=1:1 for the three electrolytes

Charge-discharge behavior of these three electrolytes was studied in detail in ***Chapter 4*** along

with their interfacial characteristics. The crystalline sample **1**, EGMB, when mixed with LiTFSI

in a molar ratio of 1:2 by grinding method showed a charge discharge capacity of 150-200 mAh/g

and an interfacial resistance of 26.09 Ω after 10 cycles of charge discharge. Sample **2**, GlyLiMB,

exhibited a charge-discharge capacity in the range of 150-200 mAh/g, however, the cell failed to

charge and discharge after 8 cycles. Electrolyte **3** (OxLiMB), displayed a charge-discharge

capacity of 78-84 mAh/g for 9 cycles and an interfacial resistance of 51.07 Ω after 20 cycles.

Though the electrolytes displayed moderate capacity, all the cells were able to function reversibly.

These charge-discharge behavior revealed a real-time application of these electrolytes in all solid-

state lithium ion batteries.

Lastly, ***chapter 5*** focuses directly on the electrode surface modification as one way of designing the interface and reducing the interfacial resistance. Surface modification of graphite was done via electropolymerization of a newly synthesized boron-thiophene monomer by two methods viz. pre-modification *via* cyclic voltammetry and *in-situ* modification *via* repeated charge discharge cycles in the presence of ionic liquids and organic carbonate solvents respectively. The cell prepared with an electrode containing electropolymerized layer of boron-thiophene monomer showed promising characteristics. Pre-modified anodes showed higher charge-discharge capacity as compared to bare graphite electrodes. However, the interfacial resistance increased after charge-discharge for both bare graphite electrodes and the electrode electropolymerized with boron-thiophene monomer. In contrast, *in-situ* anodes prepared via repeated charge-discharge cycles exhibited higher charge-discharge capacities and lower interfacial resistance.

List of Publications and Other Achievements

Prerna Joshi

A) Publications (Refereed)

1. Crystalline Low Molecular Weight Cyclic Organoboron Compound for Efficient Solid State Lithium Ion Transport,
Prerna Joshi, Raman Vedarajan and Noriyoshi Matsumi , *Chem. Commun.*, 51, **2015**, 15035-15038.

2. Optimization of potential boundaries with dynamic electrochemical impedance spectroscopy for an anodic half-cell based on organic–inorganic hybrid electrolytes
Kumar Sai Smaran, Prerna Joshi, Raman Vedarajan, and Noriyoshi Matsumi, *ChemElectroChem*, **2015,** 2, 1913.

3. Boric Ester Type Molten Salt via Dehydrocoupling Reaction
Noriyoshi Matsumi , Yoshiyuki Toyota, Prerna Joshi, Puhup Puneet, Raman Vedarajan, Toshihiro Takekawa, *Int. J. Mol. Sci.*, MDPI, 15, **2014,** 21080-21089.

B) Awards

2014: **Student Award for Oral presentation** on "Ion Conductive Behavior of Low Molecular Weight Solid Organoboron Electrolyte for Lithium Ion Secondary Batteries", *Energy and Fuels Division, 247th ACS National Meeting & Exposition*, Dallas, USA, March 16-20, 2014.

C) International presentations:

2015

1. **Oral:** Low molecular weight cyclic organoboron electrolytes for Li ion batteries; Prerna Joshi, Raman Vedarajan, Noriyoshi Matsumi in *Pacifichem 2015*, Honolulu, Hawaii, USA, December 15-20, 2015.

2. **Oral:** Cyclic low molecular weight organoboron electrolyte for lithium ion secondary batteries; Prerna Joshi, Raman Vedarajan, Noriyoshi Matsumi in *The 56th Battery Symposium in Japan*, Nagoya, Japan, November 11-13, 2015.

2014

3. **Oral:** Ion Conductive Behavior of Low Molecular Weight Solid Organoboron Electrolyte for Lithium Ion Secondary Batteries; Prerna Joshi, Raman Vedarajan and Noriyoshi Matsumi; in *247th ACS Chemical Meeting and Exposition*, Dallas, USA, on March 16-20, 2014.

4. **Oral:** Ion Conductive Behavior of Low Molecular Weight Solid Organoboron Electrolyte; Prerna Joshi, Raman Vedarajan and Noriyoshi Matsumi; in *1st JAIST Japan-India symposium on Automotive Technologies (Energy, Fuels and Plastics)*, JAIST, Japan, on August 4-5, 2014.

5. **Poster:** Ion Conductive Properties of Cyclic Organoboron Electrolytes; P. Joshi, R. Vedarajan and N. Matsumi in *Green Research Innovative Polymers-2014*, Kanazawa, Japan, March 6-7, 2014.

D) Domestic presentations:

2015

6. **Oral:** Lithium Ion Conducting Solid Organoboron Electrolyte; Prerna Joshi, Katsuhito Iwai, Raman Vedarajan, Noriyoshi Matsumi in *Regional Meeting of SPSJ*, JAIST, JAPAN, November 14, 2015.

7. **Oral:** 結晶性ホウ素化合物を足場としたイオン伝導パスの制御 （北陸先端大院マテリアル）；ジョーシ プレルナ, ヴェーダラージャン ラーマン, 松見紀佳 in 第 **34** 回無機高分子研究討論会, Tokyo, Japan, November 5-6, 2015.

8. **Poster:** Control of Charge-transfer Resistance via Electropolymerization of Boron Monomer on Electrodes; Prerna Joshi, Raman Vedarajan and Noriyoshi Matsumi in *SPSJ (Society of Polymer Science, Japan) Spring Meeting*, Sapporo, JAPAN between 27-29 May, 2015.

2014

9. **Poster:** Electrochemical Properties of Cyclic Organoboron Electrolytes; Prerna Joshi, Raman Vedarajan, 松見 紀佳 in *Regional meeting of Chemical Society of Japan (CSJ)*, Toyama, Japan, November 21, 2014.

10. **Oral:** Ion Conductive Behavior of Low Molecular Weight Solid Organoboron Electrolyte; <u>Prerna Joshi</u>, Raman Vedarajan and Noriyoshi Matsumi in *SPSJ Fall meeting*, Nagasaki, Japan, on September 24-26, 2014.

11. **Poster:** Ion Conductive Behavior of Cyclic Organoboron Electrolyte Derived from Glycerol; <u>Prerna Joshi,</u> Raman Vedarajan, Noriyoshi Matsumi in *63rd SPSJ Annual Meeting*, Nagoya Congress Center, Nagoya, Japan, May 28-30, 2014.

2013

12. **Poster:** 低分子環状ホウ素化合物のイオン伝導特性；<u>Joshi Prerna</u>, Vedarajan Raman, 松見 紀佳 in *Conference on Ionic Liquids* in Keio University Higashi Campus, Tokyo, Japan, November 20-21, 2013.

13. **Poster:** Novel Cyclic Low Molecular Weight Organoboron Electrolyte for Li-ion Transport; <u>Prerna Joshi</u>, Raman Vedarajan, Noriyoshi Matsumi in *International Symposium on Advanced Materials-JAIST*, Ishikawa, Japan, October 17-18, 2013.

2012

14. **Poster:** 環状ホウ素系電解質の合成とリチウムイオン輸送特性; <u>Prerna Joshi</u>、 Raman Vedarajan、松見紀佳 in *Conference on Ionic Liquids*, Okinawa, JAPAN, December 6-9, 2012.

15. **Poster:** Ion Conductive Characteristics of Cyclic Organoboron Electrolyte; <u>プレルナ ジョーシ</u>、ラーマン ヴェーダラージャン、 松見紀佳 in *Regional meeting of Chemical Society of Japan (CSJ)* in Fukui, Japan, November 17, 2012.

16. **Poster:** Ion Conductive Behavior of Cyclic Organoboron Electrolyte/Lithium Salt Matrices; <u>Prerna Joshi</u>, Raman Vedarajan, Noriyoshi Matsumi in *61st Symposium on Macromolecules* in Nagoya, Japan, September 19-21, 2012.